III-Nitride Nanocrystal Based Green and Ultraviolet Optoelectronics

by

Yuanpeng Wu

A dissertation submitted in partial fulfillment
of the requirements for the degree of
Doctor of Philosophy
(Electrical and Computer Engineering)
in the University of Michigan
2020

Doctoral Committee:

Professor Zetian Mi, Chair
Assistant Professor Elaheh Ahmadi
Associate Professor Emmanouil Kioupakis
Associate Professor Pei-Cheng Ku

Yuanpeng Wu

ypwu@umich.edu

ORCID iD: 0000-0002-3605-2887

Dedication

Dedicated to my family.

Acknowledgements

First, I would like to thank my advisor Professor Zetian Mi for the constant support and tremendous resources he provided throughout my entire PhD life. Prof. Mi's hard work and excellent leadership ensures everyone can focus on the research in a collaborative and multi-disciplinary environment. His constant enthusiasm and devotion to research always inspired me and directed most of the success of this work. He is always available for any discussions on my research and provides me with lots of innovative ideas which are essential for addressing the problems I faced. Not only the valuable techniques and knowledge I have learnt from him, but also his hard-working attitude, determination, collaborative and creative way of working that have provided me a great mentorship which will benefit me a lot in my future life. I express my sincere gratitude and deepest appreciation for the many hours he spent making sure my research is a success.

I would like to thank my committee members, Professor Emmanouil Kioupakis, Professor Pei-Cheng Ku and Professor Elaheh Ahmadi. I am grateful of their careful review and valuable suggestions, which help improve the quality of this work from the beginning to the end. I also thank many other professors at University of Michigan, in particular, Professor Pallab K. Bhattacharya, Professor Zhaohui Zhong, Professor Wei Lu, Professor L. Jay Guo, Professor Jamie D. Phillips, Professor Becky Peterson, Professor Fred Terry, Professor Mackillo Kira, Professor Heath Hofmann and Professor Zhenya Zhang for the excellent lectures they taught and their valuable suggestions throughout the past five years.

It was great experience to work with all the Mi Group members. I would like to acknowledge Dr. Songrui Zhao, Dr. Sharif Sadaf, Dr. Yong-Ho Ra, Dr. Renjie Wang, Dr. Mehrdad Djavid, Dr. Hasan Chowdhury, Dr. Sheng Chu, Dr. Shizhao Fan, Dr. Binh Le, Dr. Nhung Tran, Dr. Yichen Wang, Dr. Roksana Rashid in McGill University for teaching me epitaxial growth, MBE system maintenance, optical simulation and device fabrication. I am grateful for the valuable knowledge they shared with me during my first year. I thank my fellow group members and collaborators, Dr. Yongjie Wang, Dr. David Arto Laleyan, Dr. Xianhe Liu, Dr. Srinivas Vanka, Dr. Ping Wang, Dr. Yi Sun, Dr. Debabrata Das, Dr. Baowen Zhou, Dr. Tinh Tran, Ayush Pandey, Walter Shin, Chiyo Ahn, Eric Reid, Kishwar Mashooq, Nick Pant, Yongbum Park, Yongjin Ma, Yixin Xiao, Yazhou Zhang, Ronglei Fan, Chan Ho Soh, Ishtiaque Navid, Majid Aalizadeh and Yakshita Malhotra. Their contributions have greatly helped in my work.

I would also like to thank my collaborators, Zihao Deng, Woncheol Lee, Liangqing Cui, Zhen Xu, Matthew Stevenson, Anthony Aiello, Dr. Seth Coe-Sullivan, Dr. Kai Sun, Dr. Arnab Hazari, Professor Pallab K. Bhattacharya, Professor Emmanouil Kioupakis, Professor Theodore Norris, Professor Elaheh Ahmadi and Professor Mackillo Kira from the University of Michigan. The research work and the resulting research papers published throughout this thesis are results of an efficient and productive collaboration that was only possible because of you professionals.

I would like to thank all staff of the Lurie Nanofabrication Facility at the University of Michigan for their support in and out of the cleanroom. I am grateful for all the help provided by Dennis Schweiger, Sandrine Martin, Pilar Herrera-Fierro, Brian Armstrong, Nadine Wang, David Sebastian, Anthony Sebastian, Matthew Oonk, Terre Briggs, Vishva Ray, Steven Sostrom, Katharine Beach, Samuel Edward Kevin Owen and Shawn Wright. I am also grateful to Dr. Haiping Sun, Dr. Allen Hunter and Dr. Kai Sun, Deanna Wendel and Bobby Kerns from Michigan

Center for Materials Characterization. Their mentorship and support have helped me successfully characterize different materials and devices mentioned in this work. Special thanks to Dr. Kai Sun for the training and help on FIB sampling and STEM characterization on some valuable co-work. I thank Jessi Cebulski, Lisa Vogel, Anne Rhoades, Kristen Thornton, Fran Doman and Elissa Trumbull. Their administrative supports have helped me throughout my graduate school career.

I am thankful to all my friends in Ann Arbor who enriched my graduate life and brought me many happiness. I thank Yongjie who is also my long-time roommate and I am really appreciated for all the helps he provided me. I thank Zhe Liu, Ping Wang, Yi Sun for the relaxing and fun moments. I thank Kam, Ashley and many others for the good times we shared. I will cherish all those wonderful memories, and I am always looking forward to our next gathering in a shining afternoon.

Finally, I thank my wife Dr. Shuaifeng Guo and my parents, parents-in-law, grandparents and elder sister for their unconditional support and love throughout my PhD life, which encouraged and motivated me to complete this dissertation work.

This dissertation work would not be successfully completed without the support, help, encouragement, and supervision from all the people above. I really want to express my sincere appreciation to every individual supporting my graduate studies.

Preface

This presented research work covers the molecular beam epitaxial growth, material characterization, optical simulation, device fabrication and performance evaluation of low-dimensional III-nitride nanostructures. The manuscripts included in this dissertation are listed below.

1. Yuanpeng Wu, David A. Laleyan, Zihao Deng, Chihyo Ahn, Anthony F. Aiello, Ayush Pandey, Xianhe Liu, Ping Wang, Kai Sun, Elaheh Ahmadi, Yi Sun, Mackillo Kira, Pallab K. Bhattacharya, Emmanouil Kioupakis, and Zetian Mi. Controlling Defect Formation of Nanoscale AlN: Towards Efficient Current Conduction of Ultrawide-Bandgap Semiconductors. *Submitted.* (Chapter III)
2. Yuanpeng Wu, Xianhe Liu, Ping Wang, David Arto Laleyan, Kai Sun, Chiyo Ahn, Mackillo Kira, Emmanouil Kioupakis and Zetian Mi. Monolayer GaN Excitonic Deep Ultraviolet Light Emitting Diodes. *Appl. Phys. Lett.* 116, 013101 (2020). (Chapter IV)
3. Yuanpeng Wu, Yongjie Wang, Kai Sun and Zetian Mi. Molecular Beam Epitaxy and Characterization of AlGaN Nanowire Ultraviolet Light Emitting Diodes on Al Coated Si (001) Substrate. *Journal of Crystal Growth*, 507, 65 (2019). (Chapter V)
4. Yuanpeng Wu, Yongjie Wang, Kai Sun, Anthony Aiello, Pallab Bhattacharya and Zetian Mi. Molecular Beam Epitaxy and Characterization of Mg-doped GaN Epilayers Grown on Si (001) Substrate through Controlled Nanowire Coalescence. *Journal of Crystal Growth*, 498, 109 (2018). (Chapter VI)

5. Xianhe Liu, Yuanpeng Wu, Yakshita Malhotra, Yi Sun, and Zetian Mi. Micrometer Scale InGaN Green Light Emitting Diodes with Ultra-Stable Operation. *Submitted.* (Chapter VII)

Table of Contents

List of Tables

List of Figures

Abstract

Extensive research efforts have been devoted to III-nitride based solid-state lighting since the first demonstration of high-brightness GaN-based blue light emitting diodes (LEDs). Over the past decade, the performance of GaN-based LEDs including external quantum efficiency (EQE), wall-plug efficiency, output power and lifetime has been improved significantly while the cost of GaN substrate has been reduced drastically. Although the development of blue and near ultraviolet (UV) LED is mature, achieving equally excellent performance in other wavelengths based on III-nitrides is still challenging. Especially, the significant efficiency droop in the green wavelength, known as "green gap" and the extremely low EQE in the UV regime, known as "UV threshold", have become two most urgent issues. Green LEDs emit light that is most sensitive to human eye, implicating its importance in a variety of applications such as screen- and projection-based displays. UV light sources have a variety of applications including water and air purification, sterilization/disinfection of medical tools, medical diagnostics, phototherapy, sensing, which make solid-state deep UV (DUV) light sources with compactness, low operating power and long lifetime highly desirable. The deterioration of performance with green LEDs originates from increased indium content of the active region, which could degrade material quality and increase quantum confined Stark effect due to the high polarization fields in *c*-plane InGaN/GaN quantum wells (QWs). Meanwhile, limiting factors in III-nitride UV LEDs include low internal quantum efficiency due to large densities of dislocations, poor carrier injection efficiency and low light extraction efficiency.

In this dissertation, we have investigated the molecular beam epitaxial growth, structural characterization, and electrical and optical properties of low-dimensional III-nitride nanocrystals as potential solutions to above-mentioned issues. Through a combination of theoretical calculation and experimental investigation, we show that defects formation in AlN could be precisely controlled under N-rich epitaxy condition. With further optimized *p*-type doping, AlN nanowire-based LEDs emitting at 210 nm were fabricated. We report DUV excitonic LEDs with the incorporation of monolayer GaN with emission wavelengths of ~238 nm, and exhibit suppressed Auger recombination, negligible efficiency droop and a small turn on voltage ~5 V. To enhance the light extraction efficiency of AlGaN nanowires grown on Si substrate, we demonstrated epitaxy of AlGaN nanowires on Al coated Si(001) substrate wherein Al film functions as a UV light reflective layer to enhance the light extraction efficiency. AlGaN nanowire-based DUV LEDs on Al film were successfully grown and fabricated and measured with a turn-on voltage of 7 V and an electroluminescence emission at 288 nm. Green-emitting InGaN/GaN nanowire LEDs on Si(001) substrate were demonstrated, wherein the active region and *p*-contact layer consist of InGaN/GaN disks-in-nanowires and Mg-doped GaN epilayers. The incorporation of planar *p*-GaN layer significantly reduces the fabrication complexity of nanowire-based devices and improves the robustness of electrical connection, leading to a more stable device operation. We also demonstrated micrometer scale InGaN photonic nanocrystal green LEDs with ultra-stable operation. The emission features a wavelength of ~548 nm and a spectral linewidth of ~4 nm, which is nearly five to ten times narrower than that of conventional InGaN QW LEDs in this wavelength range. Significantly, the device performance, in terms of the emission peak and spectral linewidth, is nearly invariant with injection current. Work presented in this thesis provides

a new approach for achieving high-performance green and DUV LEDs by using III-nitride nanostructures.

Chapter 1 Introduction

1.1 A Brief Overview of Solid-State Lighting

The pursuit of solid-state lighting originates from human's demand on artificial light sources to continue activity when the sunlight is not available. The history of solid-state lighting is more than 140 years old since Edison's first invention of incandescent light bulb in 1879.[1] As is well known, incandescent light bulbs, as shown in Figure 1.1a, emit light through an electrically heated filament, which glows light through thermal radiation when reaching extremely high temperature (*e.g.*, ~2100 °C). Considering that only the visible part of the radiation is wanted for illumination purpose, the efficiency of incandescent light bulb is very low as most of emissions are in the infrared regime as shown in Figure 1.1b. In order to address the energy waste and low lifetime issues, fluorescent light sources, which generate light through mercury discharge, become a prominent technology after 1950s.[2] Despite the higher efficiency and longer lifetime compared with incandescent light bulb, fluorescent light sources suffer parasitic energy losses and pose potential threat to the environment especially when the mercury is burnt out from the lamp.[2] These two issues were addressed with the advent of solid-state light sources, especially in terms of light emitting diodes (LEDs) and lasers. For solid-state lighting, the electricity is directly converted into desired light emission, which significantly reduces the energy losses on power lines and makes solid-state lighting the most energy-efficient and environmental-friendly technology over the past decade.

The beginning of visible-spectrum LEDs dates back to 1960s with the commercialization of GaAsP LED, which emits visible radiation in the red part of the spectrum.[3] Since late 1980s, extensive research efforts have focused on potential semiconductors with wider bandgap for next-generation solid-state lighting. Group II-VI compounds, such as ZnSe, were intensively focused on as (Zn, Mg, Cd, Se, S) alloy-crystal systems are lattice-matched with GaAs substrates.[4] However, after the emergence of high-brightness GaN-based blue LEDs in 1993,[5] progress in solid-state lighting primarily depends on the research development of nitride-based LEDs and lasers.

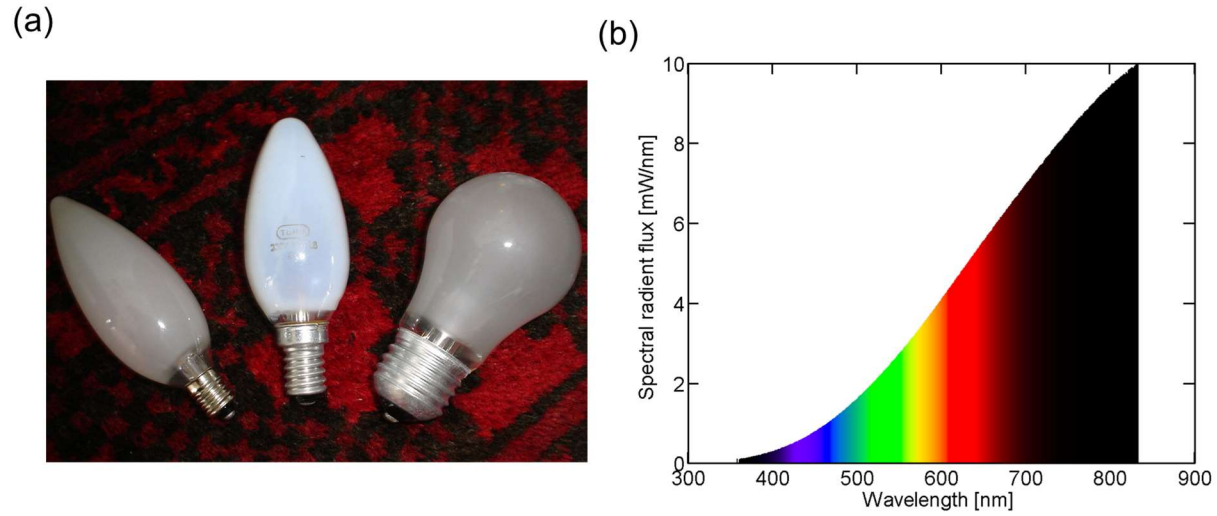

Figure 1.1. (a) 40-watt light bulbs with standard E10, E14 and E27 Edison screw base. (b) Spectral power distribution of a 25 W incandescent light bulb.[1]

Although GaN-based LEDs became widespread in the market shortly after their emergence, their external quantum efficiency (EQE) greatly depends on the emission peak wavelengths. Figure 1.2 shows EQE values of some state-of-the-art LEDs at different peak wavelengths. As can be seen, III-nitride LEDs have EQE of over 80% in the blue regime but the efficiency decreases abruptly at wavelengths of 500-600 nm, which is very well-known as the "green gap" problem in solid state visible spectrum lighting. The existence of green gap limits the

development of next-generation high-resolution and high-efficiency displays, projects, *etc*. Moreover, green LEDs can be used along with red and blue LEDs for RGB color-tunable LED systems that allow a broad color space tunability, which is not possible with phosphor-based white LEDs. Meanwhile, EQE decreases drastically when the emission wavelength is shorter than the corresponding bandgap of GaN (known as the "UV threshold"), which prohibits a wide variety of applications for LEDs emitting in the range of 200-350 nm. Therefore, addressing these problems in order to realize high-performance LEDs over a wide wavelength range is the ultimate goal for researchers of III-nitride-based LEDs and also the focus of this thesis.

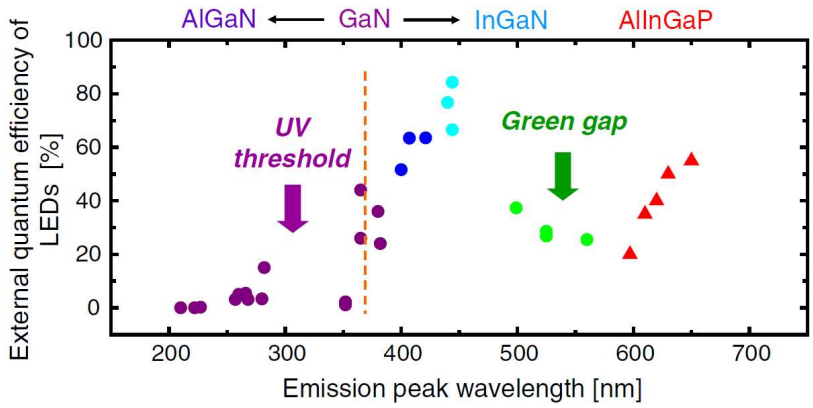

Figure 1.2. Emission efficiency (external quantum efficiency) of LEDs with different wavelengths.[4]

1.2 Green Gap and Efficiency Droop

The existence of the "green gap" in solid state lighting could be attributed to two reasons. First, (Ga, Al)InP-based LED emits light in the red wavelengths, but it cannot cover the entire blue-green-red in visible spectrum due to the bandgap limit of this material system.[3] Secondly, although InGaN LEDs could cover any emission wavelength across the visible spectrum through varying the In composition, the radiative efficiency of planar InGaN active region decreases abruptly with higher In composition. So far, the most used technology for green LEDs is based on *c*-plane InGaN/GaN multi-quantum-well LEDs, as used for blue LEDs but with higher indium

content in the InGaN quantum wells (QWs).[6] However, these planar nitride-based LEDs suffers severe efficiency drop at high injection currents, known as "efficiency droop". It has been reported increasing indium content could lead to decreased material quality and increased quantum confined Stark effect (QCSE) due to the high polarization fields in *c*-plane InGaN/GaN QWs.[6] Researchers at Phillips Lumileds proposed that Auger recombination is the root cause behind the large efficiency droop in nitride LEDs.[7] Meanwhile, carrier leakage from the active region is held accountable for this efficiency droop by some other groups.[8,9]

1.3 Development of Deep-Ultraviolet LED and Current Key Limiting Factors

To date, most of the UV light sources are based on mercury lamps, excimer lamps and deuterium lamps which have many drawbacks including short lifetime, poor stability, toxicity and low efficiency. With the excellent properties including compactness, low operating power and long lifetime, deep ultraviolet (DUV) LEDs and laser diodes (LDs) with wavelengths in the range of 200-350 nm are of great interest for a wide variety of applications. These include water and air purification, sterilization/disinfection of medical tools, medical diagnostics, phototherapy, polymer curing, and sensing as shown in Figure 1.3.[10-17] Notably, peak wavelength at 265 nm in the UV-C band matches well to the absorption spectrum of DNA (deoxyribonucleic acid). In the Raman spectroscopy for chemical and biochemical sensing, using lasers with emission wavelength below 240 nm not only increases the Raman cross-section by orders of magnitude but also greatly eliminates the interference with the fluorescence noise from commonly used bio/chemical agents.[18-20] UV light with wavelength ranging from 207-222 nm has been shown to inactivate bacteria efficiently without harming the skin of mammal. More specifically, UV light of 222 nm can deactivate majority of H1N1 influenza virus in aerosolized form with a small dose of 2 mJ/cm^2.[21] Group III-nitrides, especially Al(Ga)N, have emerged as the most suitable wide

bandgap material for the implementation of DUV LEDs and LDs.[15,17,22] These materials feature a wide tunable emission wavelength range covering the entire UV-A (315-400 nm) and UV-B (280-315 nm) bands and part of the UV-C (100-280 nm) band with the shortest available wavelength of 210 nm with this material system. In addition to the continuously tunable band gap, group III-nitrides have the advantage of some robust physical properties such as high melting point, high thermal conductivity, high mechanical strength, and most importantly, the possibility to achieve both *n*- and *p*-type conductivity which is essential for diode fabrication.[15,23-26]

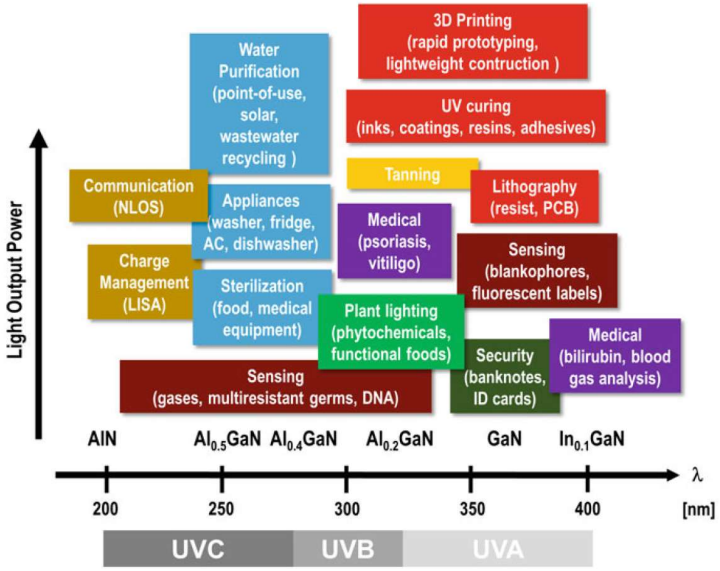

Figure 1.3. Applications of UV (200-400 nm) LEDs.[27]

Over the past decade, extensive research efforts have been dedicated into the development of group III-nitrides-based DUV optoelectronics and recently, due to improvements in the crystalline quality of AlN and high Al-molar fraction AlGaN layers, and the optimization of *p*-type doping in AlGaN and LED structure design, the EQE and output power of AlGaN-based DUV LEDs have increased significantly. An EQE of over 3% and output power of over 1 mW have been reported at 10 mA continuous current injection in a flip-chip DUV LEDs with emission wavelengths between 255 nm and 280 nm in 2010.[28] In 2011, a reasonably high IQE near 70% and EQE of 1.3% at 100 mA continuous wave (CW) current injection with emission wavelength

of 260 nm from psuedomorphic UV LEDs on high quality AlN substrate was reported.[29] A maximum EQE of 10.4% at 20 mA CW injection with an output power of 9.3 mW for 278 nm DUV LEDs was achieved through migration-enhanced metal organic chemical vapor deposition to reduce the threading dislocations (TDs) and utilizing a transparent *p*-type conduction layer, UV reflecting ohmic contacts, and optimized chip encapsulation.[14] Recently, Pandey *et al*. reported AlGaN/GaN/AlGaN tunnel junction LEDs with maximum EQE of 11% at 265 nm emission wavelength.[30] However, compared with the excellent performance achieved in group III-nitride-based LEDs operating at the near UV and blue ranges, the efficiency of DUV LEDs is still rather modest.[11,22] Moreover, EQE decreases drastically with decreasing wavelength in the DUV regime. For emission wavelengths below 250 nm, the EQE is only on the order of 0.1% or 0.01%. There are mainly three factors responsible for the reduced performance for devices emitting in the DUV wavelength region.

1.3.1 The Unavailability of Low-Cost, Lattice and Thermal Expansion Coefficient-Matched and Transparent Substrate Materials

An ideal substrate for the epitaxy of AlGaN-based UV LEDs needs to satisfy several requirements including similar symmetry and closely matched lattice constants, similar thermal expansion coefficient, high thermal conductivity and optical transparency.[11,16] Silicon substrate has the advantages of low cost, large wafer size, high crystalline quality, good electrical conductivity, and feasibility of its removal through chemical etching. However, the large mismatch in lattice constant and thermal expansion coefficient between III-nitrides and silicon leads to excessive tensile strain, resulting in high densities of cracks and dislocations in DUV LED structures.[31] Both 6H-Slicon carbide (SiC) and 4H-SiC exhibit much smaller lattice and thermal misfit with III-nitrides.[32] They also have the advantages of good chemical stability, high

electrical and thermal conductivity, but relatively high cost compared with sapphire and silicon substrates. As shown in Figure 1.4a, GaN substrates have a low lattice mismatch with the AlGaN-based heterostructures grown on them (between 0-24% depending on Al-molar fraction) and excellent physical properties such as high thermal conductivity and mechanical strength. However, for DUV LEDs, GaN has the drawbacks of generation of tensile strain in the AlGaN epilayers with high Al-molar fraction and light absorption and high cost.[11] Moreover, if Si, SiC and GaN substrates are used, it is generally required that the substrates being selectively removed during fabrication of back-emitting DUV LEDs.[11] Sapphire substrate, with its low cost, high transparency and close lattice symmetry as III-nitrides, has been widely utilized for the development of DUV LEDs.[11,15] With low-temperature AlN grown on sapphire substrate as a buffer layer, TD density of subsequently grown AlGaN heterostructures is typically $>10^{10}$ cm^{-2}. Figure 1.4b shows the cross-sectional transmission electron microscopy (TEM) images showing the propagation of the TDs into AlGaN layer. This is detrimental in that a relatively high IQE of DUV LEDs (above 50%) requires a TD density lower than 10^{9} cm^{-2} as shown in Figure 1.4c.[11]

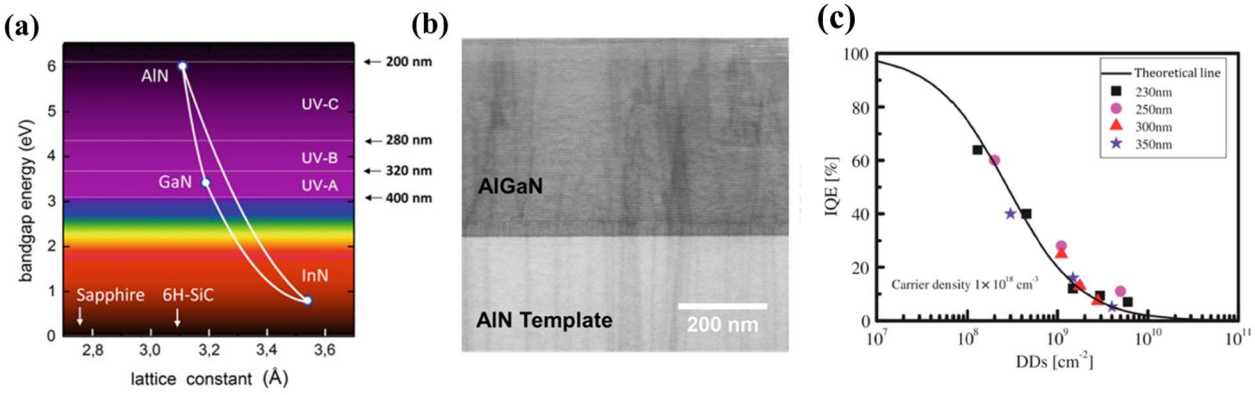

Figure 1.4. (a) Bandgap energies and emission wavelength of InN, GaN, AlN and other III-V and II-VI compound semiconductor materials plotted versus their lattice spacing.[27] (b) Cross-sectional TEM micrograph revealing the behavior of TDs (c) IQE vs. DD under weak excitation with carrier density of 1×10^{18} cm^{-3} in an underlying layer.[11]

1.3.2 Low *p*-Type Conductivity in High Al-molar Fraction AlGaN

The *p*-type conductivity within the AlGaN DUV LEDs strongly affects the device performance. The typical hole concentration of *p*-AlGaN with high Al content (Al > 60%) is as low as 10^{14} cm^{-3},[11,13] which could be attributed to the severe self-compensation by donor-like defects that are produced simultaneously, limited dopant solubility, and increasingly high acceptor activation energy of Mg dopant with increasing Al molar fraction.[10,11] The activation energy reaches ~400 meV for an Al fraction of ~70%, and is as high as 510-630 meV for AlN, as shown in Figure 1.5a.[11] The low *p*-type conductivity directly leads to high resistivity and high turn-on voltage of DUV LEDs, such that the turn-on voltage of AlN *p-i-n* diodes is larger than 20 V as shown in Figure 1.5b. Electron injection efficiency (EIE) of a DUV LED is reduced owing to the leakage of electrons to the *p*-side layers.[11,13] Therefore, numerous efforts have been undertaken to mitigate compensation by decreasing donor defects and increasing solubility of the dopants due to the large activation energy of Mg acceptors, which results in poor hole injection and also detrimental overflow from the active region.[11]

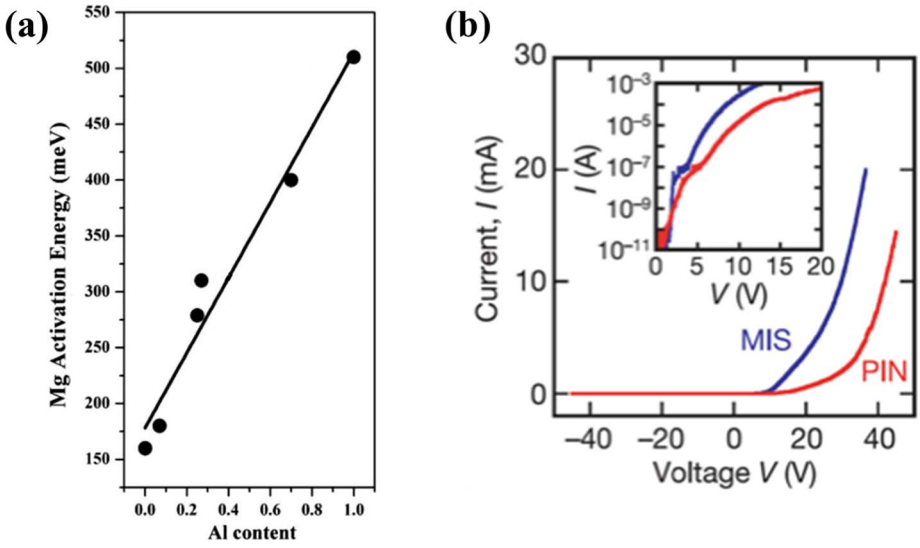

Figure 1.5. (a) Mg activation energy in AlGaN as a function of Al content.[11] (b) *I-V* characteristics of AlN LEDs. The inset shows the semilogarithmic scale plot.[33]

1.3.3. Low Light Extraction Efficiency Caused by Strong Total Internal Reflection and Self-Absorption

As is well known, extensive of progresses in III-nitride-based LEDs were achieved after the realization of efficient *p*-type doping in GaN. However, non-transparent *p*-GaN for emission wavelengths below 365 nm leads to significant self-absorption and a very low light extraction efficiency (LEE) of DUV LEDs.[11] The large valence band offset between *p*-type GaN and high Al composition *p*-AlGaN electron blocking layer prevents efficient hole carrier injection.[11] Moreover, when the Al composition in the AlGaN active region exceeds ~68%, the crystal split-off (CH) subband is positioned at the top of the valence band as shown in Figure 1.5a. The transition between conduction band and CH subband leads to transverse-magnetic (TM) emission with the electrical field polarized along the *c*-axis, which results in a dominant in-plane propagation within the LED device as shown in Figure 1.5b. In order to improve the LEE, series of methods including transparent *p*-AlGaN contact layer, photonic structure for vertical light-propagation and *p*-type electrode with high reflectivity have been studied.[34-36]

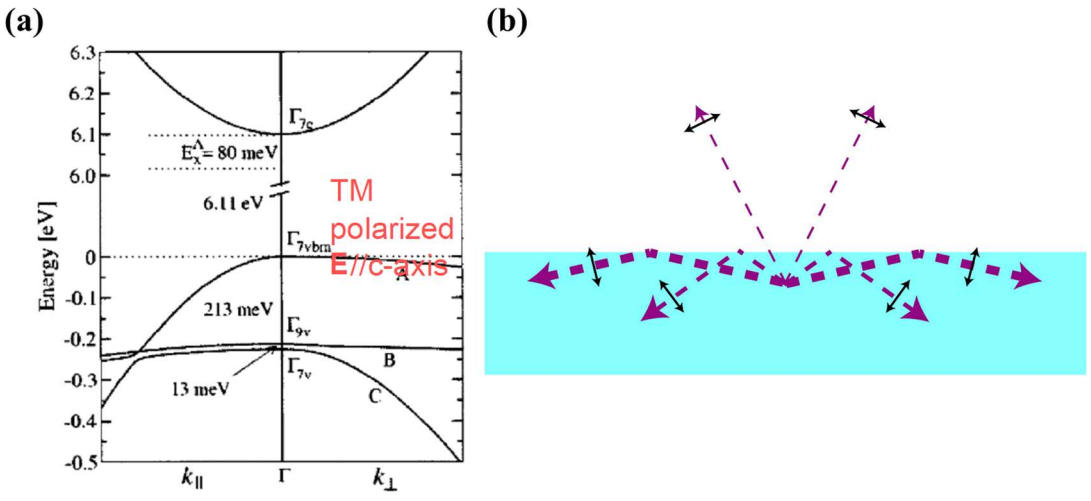

Figure 1.6. (a) Calculated band structure near the Γ point of wurtzite AlN.[37] (b) Schematic of the hindered extraction of TM polarized light from the epilayer structures.[38]

1.4 Advantages of Nanocrystals over Traditional Planar Layers

Nanocrystals, taking the form of nanowires and nanorods, are one-dimensional nanostructures with diameters ranging from tens of nm to a few hundred nm. Due to the efficient lateral strain relaxation related with the large surface to volume ratio, III-nitride nanocrystals feature significantly reduced dislocation density and piezoelectric polarization field compared with conventional planar epilayer structure.[10,17] In addition, recent studies have shown that nearly defect-free III-nitride nanowires can be grown virtually on any substrates. The versatility and reduced dimensions have enabled III-nitride nanocrystals as a new avenue to achieve high-performance optoelectronics.

1.4.1 Reduced Defect Density in Active Region

The growth of nanowires are fairly independent of substrates lattice constant due to their one-dimensional structure which is strain relaxed.[10,39,40] Figure 1.7a shows the SEM image of InGaN/GaN nanowires spontaneously grown on Si substrate. Moreover, the grown nanowires usually have better crystalline quality and optical properties as compared with their planar counterparts grown on lattice mismatched substrate.[10,41] This can be mainly attributed to that the TDs from the substrate will terminate at the sidewall of the grown nanowire as shown in Figure 1.7b, which significantly reduces the defects density, such as TDs and stacking faults (SFs), inside the active region and thereby enhancing the IQE.[10,42-44] Thus, a defect-assisted Auger recombination process, which could cause significant efficiency droop in planar InGaN materials could be minimized in InGaN/GaN nanowire structure. Moreover, nanowire structure can mitigate the polarization field inside the active region through effective strain relaxation. A polarization field of several hundred kV/cm could be obtained in nanowire structure compared with several MV/cm which is common in planar blue QW LEDs.[45] Such low polarization field not only

enhances the overlap between electrons and holes but also enable higher In composition InGaN quantum disks to be inserted in the nanowire.[10,17,46] The diameter and spacing of nanowires can also be controlled by selective area growth as shown in Figure 1.7c.

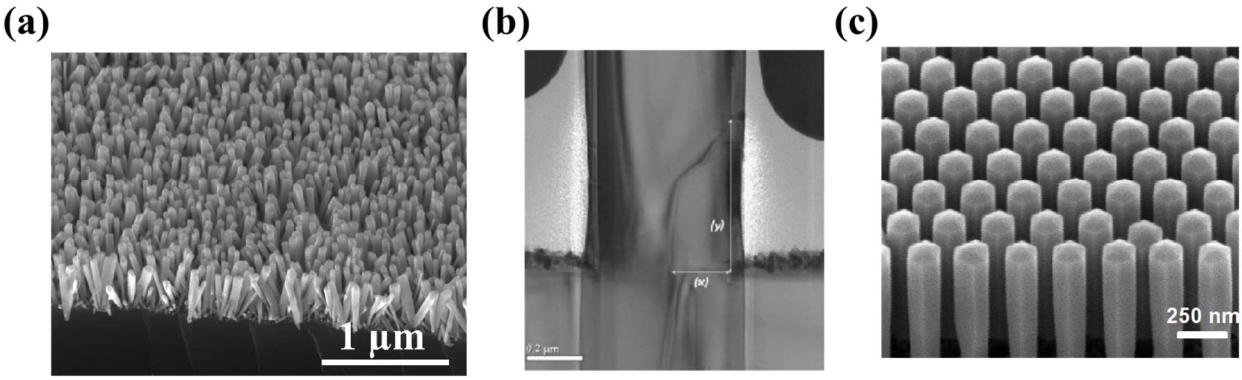

Figure 1.7. (a) A bird's view SEM image of InGaN/GaN nanowires grown on Si substrate. (b) A side view TEM image shows the termination of TDs toward the sidewall of nanowire.[47] (c) A bird's view SEM image of InGaN/GaN nanowires grown on GaN substrate. The dimeter and spacing of the nanowire array are controlled by selective area growth.

1.4.2 Enhanced Mg Incorporation and Hole Concentration

Significantly enhanced Mg dopant incorporation was also observed in AlGaN nanowires, and the free hole concentration was measured in the range of 1×10^{16} cm^{-3} for Mg doped AlN nanowires at room temperature, which is orders of magnitude higher than previously reported values ($\sim1\times10^{12}$ cm^{-3}) in Mg-doped epilayers.[48,49] Detailed first-principle calculation suggests that the Al-substitutional Mg formation energy at the surface is much lower compared with the bulk region positions due to strain relaxation as shown in Figure 1.8a and Figure 1.8b. Therefore, nanowires have much lower Mg formation energy and therefore much higher Mg concentration than bulk material. The expected Mg concentration inside AlN nanowires could reach as high as 10^{20} cm^{-3}. Because the Mg concentration can be very high, Mg energy levels are no longer discrete but rather become broadened impurity band as shown in Figure 1.8c. Consequently, Mg levels that

are closer to the valence band will have a much lower activation energy which further increases hole concentration in AlN nanowire. Also hole carriers can transport inside the Mg-impurity band through hopping effect which further improve the electrical conductivity.[48,49]

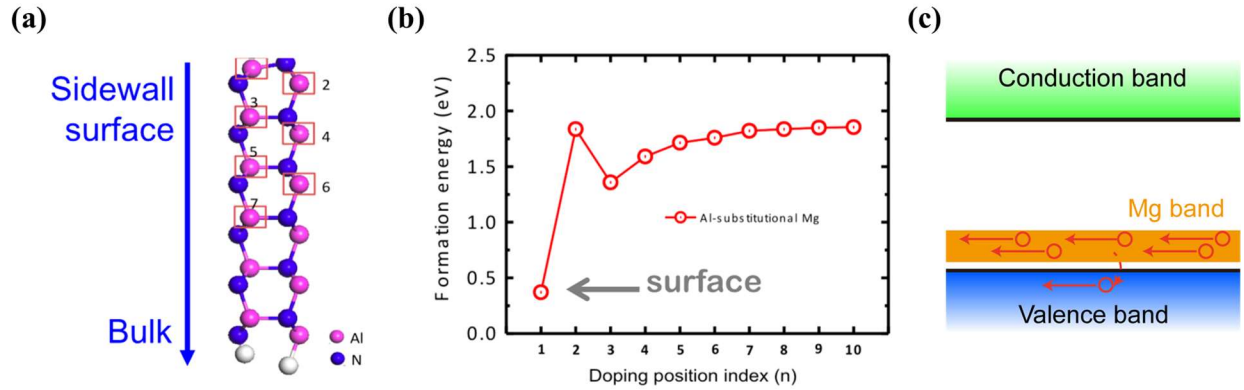

Figure 1.8. (a) Illustration of the AlN structure used for Ab initio calculation.[50] (b) Calculated Mg formation energy of different positions as indicated in (a).[50] (c) Schematic showing reduced Mg activation energy and hole hopping effect.[51]

1.4.3 Enhanced UV Light Extraction Through Scattering Effect

Nanowires-based device benefits from the high material quality and the large surface to volume ratio which makes it easier to extract light.[10,52] This is particularly important in Al-rich DUV LEDs where the TM polarized emission dominates.[11,53,54] It was found that in certain nanowire diameter and spacing ranges, due to the multiple light coupling and scattering process among nanowires, the dominant light emission can be from the nanowire top surface, despite the light is TM polarized, providing a new approach to efficiently extract TM-polarized light from AlN LEDs as shown in Figure 1.9. Detailed finite-differential-time-domain (FDTD) simulation shows for devices with large nanowire diameter and small spacing, the light extraction is more efficient from the side, which is similar to that of conventional *c*-plane planar devices. As the spacing increases, light can also escape from the top surface, which can be mainly attributed to that both the coupling to and scattering from adjacent nanowires occur at the same time.

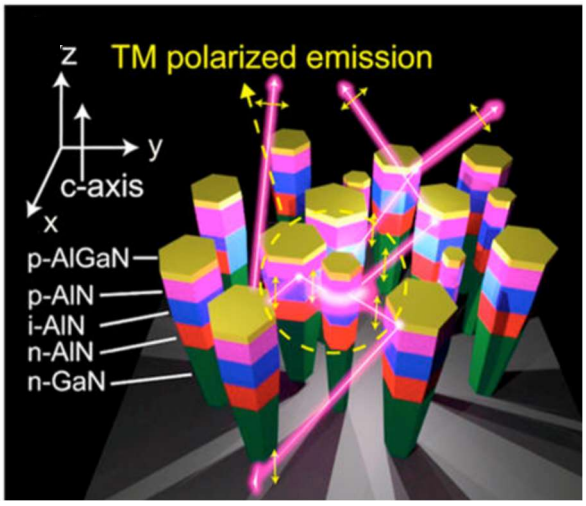

Figure 1.9. Schematic of TM polarized light propagation in AlN nanowire LED.[52]

1.5 Current Status of Nanocrystals-Based LEDs and LDs

Nanocrystals-based LEDs and lasers have attracted a wide range of research interests dedicated to improving the device performance including wavelength tunability, EQE, wall-plug efficiency, output power, *etc*. In 2010, Guo *et al*. first reported wavelength tuning from ultraviolet to red through varying In composition in InGaN/GaN nanowire and achieved white emission LEDs.[55] Nguyen *et al*. further demonstrated controlling electron overflow in InGaN LEDs by using *p*-AlGaN electron blocking layer and obtained nearly zero efficiency droop at injection current up to ~2200 A/cm^2.[56] By using selective area epitaxy, Ra *et al*. demonstrated single nanowire LEDs with emission wavelengths covering nearly the entire visible range through varying nanowire diameters.[57] Regarding nanowire-based LEDs operating in the UV range, Zhao *et al*. conducted a comprehensive growth study and demonstrated DUV LEDs with emission wavelengths tuned from 236 nm to 280 nm by simply changing the substrate temperatures when growing AlGaN nanowire at low nitrogen flow rate.[39] Sadaf *et al*. demonstrated, through incorporating Al tunnel junction, nanowire-based UV LEDs emitting at ~280 nm could achieve an output power >8 mW and a peak external quantum efficiency ~0.4%, which are nearly one to two

orders of magnitude higher than previously reported AlGaN nanowire UV LEDs. AlN nanowire LEDs emitting at 210 nm were first demonstrated by Zhao *et al*.,[50] while the following work showed that the light emissions from AlN LEDs are predominantly from the nanowire top surface, as a results of strong light scattering effect within the nanowire array.[52]

An electrically pumped nanowire array green edge-emitting LDs were firstly demonstrated by Frost *et al*. by fabricating ridge waveguide structure from monolithically grown InGaN/GaN nanowire array on Si substrate.[45] Ra *et al*. demonstrated surface-emitting InGaN/AlGaN nanocrystals-based LDs emitting at ~523 nm with threshold current of ~400 A/cm^2 by operating the LDs at photonic band edge modes.[58] After the first demonstration of AlGaN nanowire-based LDs with 334 nm lasing peak by using Anderson localization,[59] Zhao *et al*. demonstrated nanowire-based LDs operating at 289 nm, 262 nm and 239 nm while the lasing thresholds are 2-3 orders of magnitude smaller than the conventional GaN-based UV lasers.[46,60,61] AlGaN nanocrystals-based LDs with 369.5 nm lasing wavelength and threshold current of 2.1 kA/cm^2 were demonstrated by employing topological high-Q resonance of a defect-free nanowire photonic crystal.[62]

1.6 Overview of the Dissertation

The focus of this dissertation research is on the molecular beam epitaxial (MBE) growth of InGaN and Al(Ga)N nanocrystals and their applications towards high efficiency green and DUV LEDs.

Chapter I introduces the background and development of solid-state light sources with an emphasis on the remaining challenges, including the green gap and efficiency droop in green LEDs and the extremely low EQE in DUV LEDs. Key factors that limit the device performance including dislocation density, doping efficiency and LEE were discussed. Then, in comparison with its

planar counterpart, the advantages of using III-nitride nanocrystals were introduced. Especially, the low dislocation density, significantly improved *p*-type doping and enhanced LEE have enabled III-nitride nanowires as the potential solution for achieving high-performance green and DUV LEDs.

Chapter II first introduces the unique features of molecular beam epitaxy system such as ultrahigh vacuum and abrupt shutter control for pristine interface. Then, the processes of two major nanocrystals synthesis techniques used in this thesis, namely spontaneous formation and selective area epitaxy, were discussed. Several advanced techniques for material characterizations used in this thesis were also briefly discussed.

Chapter III reports a detailed investigation on the effect of nitrogen flow rate, substrate temperature and Mg beam equivalent pressure (BEP) on defect formation and Mg incorporation in *p*-type doped AlN nanowires. Detailed theoretical study in combination with DUV photoluminescence (PL) spectroscopy provide a vital route for synthesizing high quality *p*-AlN nanowires with enhanced Mg-related transitions by utilizing N-rich epitaxy. AlN nanowire LEDs were grown and fabricated. Detailed analysis of the current-voltage characteristics of AlN *p-i-n* diodes suggests that current conduction is dominated by charge-carrier tunneling at room temperature, which is directly related to the activation energy of Mg dopants.

Chapter IV presents molecular beam epitaxy and characterization of DUV LEDs with monolayer GaN as active region. Detailed optical measurements and direct correlation with density functional and many-body perturbation theory suggest that charge carrier recombination occurs predominantly via excitons in the extremely confined monolayer GaN/AlN heterostructures. We have further demonstrated DUV LEDs incorporating single monolayer and double monolayer

GaN, which emit DUV light at ~238 nm and 270 nm, respectively. These unique DUV LEDs exhibit highly stable emission, negligible efficiency droop, and a small turn on voltage ~5 V.

Chapter V demonstrates a novel strategy using AlGaN nanowire grown on Al film for high efficiency DUV emission with significantly improved performance. Monolithically integrated AlGaN nanowire arrays on Al coated Si substrate and DUV LEDs with emission wavelengths ranging from 280-320 nm have been achieved. To our best knowledge, it is the first demonstration of metal nitride nanostructures grown on Al substrate. The Al film underneath the grown AlGaN serves as an efficient DUV light reflector. Moreover, an Al rich AlGaN shell forms surrounding the grown nanowires which reduces the nonradiative surface recombination and further enhances the radiative light emission efficiency.

In Chapter VI, we show that a nanowire coalescence approach of Mg-doped GaN monolithically integrated on Si(001) substrate. The incorporation of planar *p*-GaN contact layer significantly reduces the fabrication complexity of nanowire array-based devices. Controlled *p*-type conduction is further achieved for Mg-doped GaN epilayers, which contributes to forming a more robust electrical connection with the metal contact. We also demonstrated functional InGaN/GaN LEDs on Si(001) substrate, wherein the active region and *p*-contact layer consist of InGaN/GaN disks-in-nanowires and Mg-doped GaN epilayers.

In Chapter VII, we demonstrated micrometer scale InGaN green LEDs with ultra-stable operation. InGaN photonic nanocrystal LEDs with green emission wavelength (~548 nm) exhibit a spectral linewidth ~4 nm, which is nearly five to ten times narrower than that of conventional InGaN QW LEDs in this wavelength range. Significantly, the device performance, in terms of the emission peak and spectral linewidth, is nearly invariant with injection current.

In Chapter VIII, we summarize the main results achieved in previous chapters with a highlight on performance improvement of green and UV LEDs by using III-nitride nanocrystals. Some related future work were also proposed. The first work is based on some preliminary results on the optical design of the two-dimensional nanocrystals photonic crystal surface-emitting laser and further study the wavelength tuning of AlGaN grown by selective area epitaxy and subsequent device fabrication process. The second work focuses on developing UV single photon source through incorporating monolayer GaN in N-polar Al(Ga)N nanowires grown by selective area epitaxy.

Chapter 2 Molecular Beam Epitaxy and Characterization of III-Nitride Nanocrystals

2.1 Introduction

Molecular beam epitaxy has been widely used for the growth/synthesis of high-purity, high-quality semiconductor nanostructures, with atomic level control of the interface and thickness.[63] Compared to conventional metal-organic chemical vapor deposition (MOCVD) technique, molecular beam epitaxy offers advantages of abrupt doping profile and pristine interface for heterostructures.[64] Moreover, the high vacuum during material synthesis can significantly reduce undesired impurity incorporation. The relatively low growth temperature can also enhance indium incorporation. The simple chemistry in the growth process is also ideally suited for the epitaxy of Al-rich rich materials that have been difficult for conventional MOCVD process. In this chapter, we first provide an overview of the MBE systems to grow low-dimensional III-nitride nanostructures, then discuss the state-of-the-art techniques used for charactering crystal structures and optical properties.

2.2 Overview of Plasma-Assisted Molecular Beam Epitaxy

Molecular beam epitaxy distinctly differs from other material growth/deposition system due to its precise flux control for atomic layer growth and abrupt doping profiles.[64] MBE growth has been utilized in various materials systems, including III-nitride, III-V, and II-VI materials. The system discussed and used in this dissertation is a nitrogen plasma-assisted epitaxy system as shown in Figure 2.1. Ultra-high vacuum conditions are maintained with a background vacuum level on the order of 1×10^{-11} Torr. This ensures epitaxially grown materials have far superior optical and electrical properties than previously used vacuum evaporation techniques. Unlike other vacuum evaporation techniques, the substrate heater can be heated to high temperatures (~1000 °C) which is ideal for the epitaxy of large bandgap (*e.g.*, AlN and GaN) materials. Typically, liquid

nitrogen is used to ensure efficient heat dissipation, and some source cells are cooled with chilled water. The MBE used in this dissertation was equipped with different source effusion cells for gallium (Ga), indium (In), aluminum (Al), and nitrogen (N), wherein a nitrogen plasma is derived from an ultra-purity (6N) nitrogen source. In addition, different dopant cells are integrated for *n*-type doping by silicon (Si) or germanium (Ge) and *p*-type doping by magnesium (Mg).

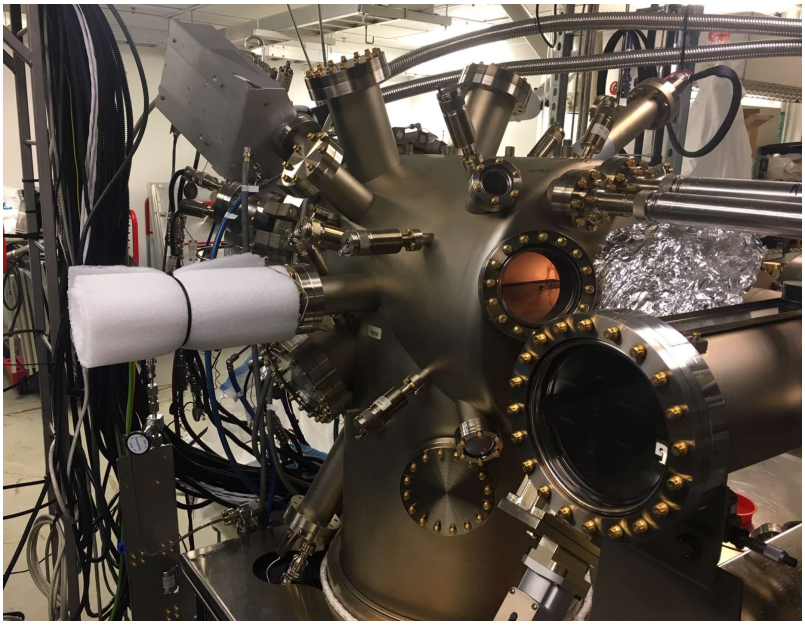

Figure 2.1. Veeco GEN II PAMBE epitaxial system These MBE systems are capable of growing various types of materials. Even within the same material system, there is a considerable amount of diversity regarding structural characteristics. As an example, MBE can epitaxially grow different quantum structures like QWs, nanowires or quantum dots. Each of such nanostructures has unique structural characteristics even if all of them are III-nitride-based.

2.2.1 Spontaneously Grown III-Nitride Nanowires

III-nitride nanowire ensembles that grown spontaneously on foreign substrates have attracted extensive research interests.[65-70] This technique is typically based on commercially available substrates such as Si, Al_2O_3(001) and bulk metals, making this approach cost-effective and simpler in terms of substrate preparation. A prominent example is the spontaneous formation

of GaN nanowires on Si substrate in PAMBE, where dense arrays of single crystalline nanowires form on crystalline as well as amorphous substrates.[71] The growth process can be generally identified as three stages. During the first stage, the impinging Ga flux is fully desorbed, resulting in a negligible Ga incorporation. This stage is known in the literature as the incubation period, during which stable GaN nuclei have not been yet formed on the substrate. The second stage starts with the appearance of GaN-related spots in the RHEED pattern, which signals the formation of stable GaN nuclei. Previous reports have identified these nuclei as spherical cap-shaped three-dimensional islands with critical radius of ~5 nm. Once these nuclei were formed, the subsequent growth will transform the shape toward the final nanowire-like morphology. In the last stage, the nanowires elongate along the *c*-axis. The average diameter of spontaneously grown nanowires depends on the ratio between the impinging Ga and N fluxes.[72] Due to the randomness in the location of nucleation and size of nuclei, the diameter and spacing vary among the self-assembled nanowires as well as the in-plane crystallinity. Therefore, coalescence is an intrinsic characteristic of the self-assembled nanowires, which could lead to formation of SFs and edge dislocations as reported previously.[73]

2.2.2 Selective Area Epitaxy of III-Nitride Nanocrystals

To overcome the fundamental limitations of spontaneously grown nanowires, selective area epitaxy (SAE) has been developed to achieve precise control on the positioning and size of nanocrystals.[57,58] This technique typically involves covering the epitaxial substrate with dielectric masks, such as SiN and SiO_2, or metallic masks such as Al, Ti and Mo, which are patterned by photo-lithography or e-beam lithography depending on the required dimensionality.[57,58,74,75] Figures 2.2a, 2.2b show scanning electron microscope (SEM) images of a patterned Ti mask on the surface of GaN epilayer. SAE could be achieved due to a

higher nucleation probability inside the hole openings, *e.g.*, on the surface of GaN epilayer, compared with on the surface of the mask. Figures 2.2c and 2.2d show the SEM images of nanocrystals with hexagonal cross section grown inside the hole openings. The improved uniformity in nanocrystal morphology significantly enhanced the reproducibility and reliability of nanocrystal-based optoelectronic devices. In addition, arrayed nanocrystals grown by SAE could form a photonic crystal cavity, wherein desired photonic properties can be achieved through varying the design of lattice constant and spacing of the nanocrystals array.

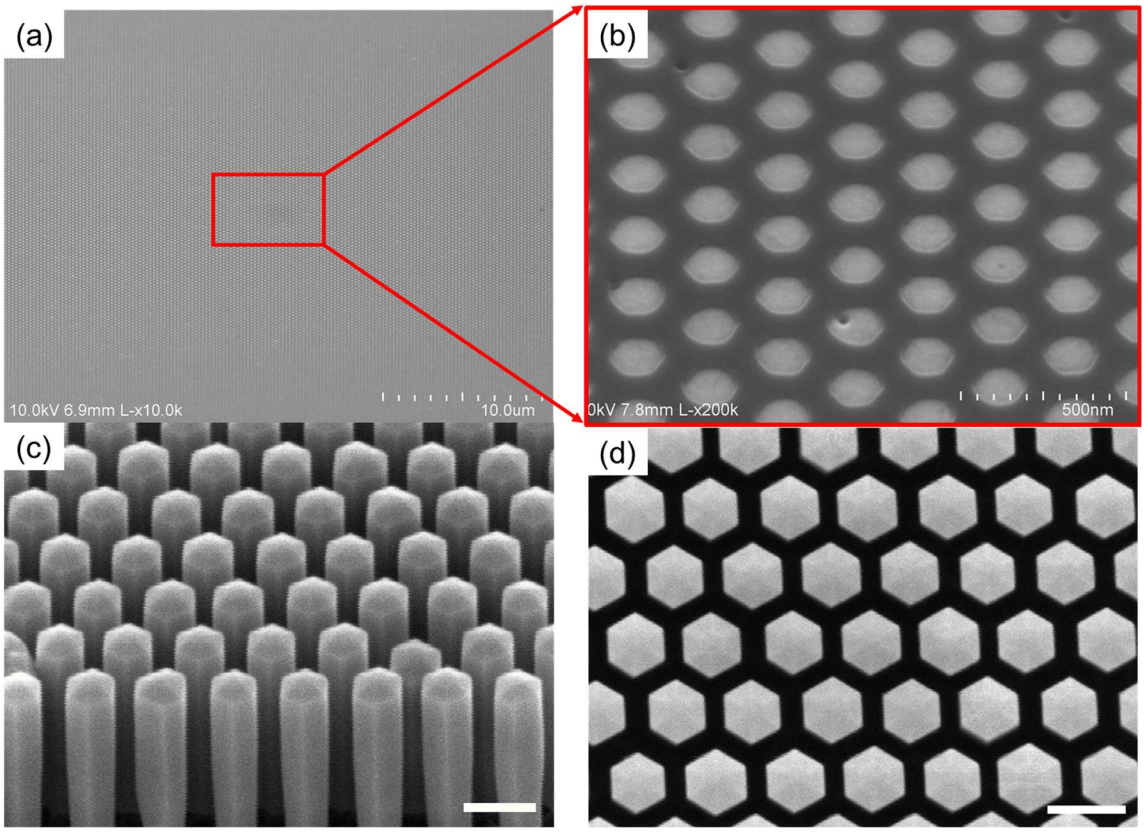

Figure 2.2. (a) Low-magnification SEM image showing Ti masked fabricated on top of GaN epilayer. (b) Magnified SEM image of the region outlined in (a) shows arrayed hexagonal holes. (c) 45º tilted view and (d) top view of GaN nanocrystals grown by SAE. Scale bars: 250 nm.

2.3 Characterization Techniques

2.3.1 Photoluminescence

PL spectroscopy is the measurement of light emission from semiconductor materials after photo-excitation process, which has been widely used to estimate the energy gap of semiconductor materials.[76,77] In this dissertation, room-temperature PL measurements were widely used to estimate the material quality and In/Al composition in nanowire. In addition, PL characterization was used to identify the shallow impurities in semiconductors, wherein the peak positions and linewidths of different peaks indicate the material crystallinity, defects density and interface quality. Time-resolved PL was used performed to give information about the separation and recombination of photoinduced charge carriers, as PL essentially originates from the electron-hole recombination.

Group III-nitride semiconductors have been intensively studied in electronic and optoelectronic devices due to the unique energy band structures. The direct bandgap of ternary alloys, such as AlGaN, can be estimated by using Vegard's law as described by Eqn. (2-1).

$$E_g(Al_xGa_{1-x}N) = x \cdot E_g(AlN) + (1-x) \cdot E_g(AlN) - b \cdot x \cdot (1-x) \quad (2\text{-}1)$$

where b is the bowing parameter and its value typically varies between 1.3 and 1.4.[39] Al compositions can be derived by using Eqn. (2-1), wherein the energy gap of AlGaN nanowires was estimated from the PL measurements.[39]

2.3.2 X-ray Diffraction

Understanding the structural characteristics of these III-nitride nanowires is vital to using them to demonstrate state-of-the-art optoelectronic devices. X-ray diffraction (XRD) has been performed to help determine the crystalline orientation of the as-grown nanocrystals on foreign substrates. XRD measurements were made using Cu Kα radiation in a Bruker-AXS D8-Discover

diffractometer operated at 40 kV and 40 mA. III-nitride nanowires usually grow along the *c*-axis which is perpendicular to the substrate. For nanowires with different alloy composition, the characteristic peak positions are different in XRD spectrum. For example, GaN (0002) peak is located at 34.6 degrees while the AlN peak position is around 36 degrees. Therefore, the AlGaN (0002) peak position is between 34.6 and 36 degrees.

2.3.3 Scanning Electron Microscopy

During SEM characterization, a high-energy electron beam (1-40 keV) is interacting the sample surface to produce secondary electrons, backscattered electrons, and characteristic X-rays for analysis in SEM.[78] Therefore, SEM can image structural morphology and determine elemental compositions, with tunable magnification up to 1000 K, corresponding nanometer resolution. During the SEM characterization, nanowire samples were placed at a 0° and a 45° angle mount in order to obtain top view and bird's view SEM images, respectively.

2.3.4 Transmission Electron Microscopy

TEM has been used to characterize the materials at ultrahigh spatial resolution for morphology, elemental distribution, crystal structure, defects, *etc*. Ultrahigh energy (200-300 keV) electron beam pass through very thin sample specimen and forms images. Conventional TEM using a broad electron beam and scanning transmission electron microscopy (STEM) using a focused electron spot are the two generally used mode for material characterization at atomic microscope. High angle annually dark field (HAADF) STEM imaging collects incoherently scattered electrons at high angles, providing unique contrast which is sensitive to the atomic number or specimen thickness. In this dissertation, HAADF-STEM is mostly used to determine the heterojunction, interface roughness, and morphology of III-nitride nanowires.

2.4 Electrical Measurements and LED Output Power Measurements

2.4.1 Current-Voltage Characteristics and Hall measurements

In order to achieve high performance green and DUV LEDs, the material quality and doping profile of the LED diode are paramount. *I-V* characteristic measurements provide a direct estimate on the diode performance. A direct current (DC) voltage source with its positive terminal connected to the *p*-type contact of the LED and with its negative terminal connected to the *n*-type contact of the material. For III-nitride nanowires grown on Si substrate, the *n* contact is usually the backside of Si substrate which has a Ti(80 nm)/Au(20 nm) coating and bonded to an aluminum plate using conductive epoxy. In the meanwhile, the *p*-contact is usually the top metal deposited by tilted-angle metal deposition. Hall measurements were performed at room temperature on the *p*-GaN film using van der Pauw patterns.

2.4.2 Nanocrystals-based LED Light Output Power Measurement

Due to the strong scattering effects inside the nanocrystal arrays, III-nitride nanocrystals-based LEDs have dominant top emission. Therefore, in this measurement, we put a visible/UV-enhanced detector on top of the light-emitting devices. The detector is mounted to a three-dimensional manipulator which enables the precise position control of the wand detector so that the measured devices (with sizes ranging from 300 μm×300 μm to 1 mm×1 mm) are centered to the detecting window which has a size of 1.5 cm×1.5 cm. It is worthwhile mentioning that this measurement limits the detection of emitted photons. For more accurate power measurements, an integration sphere is required.

2.5 Summary

This chapter provides an overview of the molecular beam epitaxy system, with unique advantages including abrupt doping profile and pristine interface for heterostructures. State-of-the-art characterization techniques, *e.g.*, PL, SEM, XRD, STEM were reviewed for characterizing the energy band structure, crystalline structure, and optical properties of low-dimensional III-nitride nanocrystals. In the last part, we described the electrical measurement of the fabricated nanocrystals-based LEDs and the methods for light output power measurements.

Chapter 3 Controlling Defect Formation of Nanoscale AlN: Towards Efficient Current Conduction of Ultrawide-Bandgap Semiconductors

3.1 Author Contribution and Copyright Disclaimers

The contents of this chapter were submitted to Advanced Electronic Materials in April 2020, for which I retain the right to include it in this thesis/dissertation, provided this thesis/dissertation is not published commercially. The co-authors were David A. Laleyan, Zihao Deng, Chihyo Ahn, Anthony F. Aiello, Ayush Pandey, Xianhe Liu, Ping Wang, Kai Sun, Elaheh Ahmadi, Yi Sun, Mackillo Kira, Pallab K. Bhattacharya, Emmanouil Kioupakis, and Zetian Mi from the University of Michigan. I designed, conducted and authored most of the work. D. A. L., C. A. and P. W. contributed to the material growth process. Z. D. conducted the first-principles density functional theory calculations under supervision of E. K. A. A. conducted TRPL measurements under supervision of P. B. K. S. contributed to STEM characterization. D. A. L and X. L. contributed to the EL measurements. A. P. and Y. S. contributed to device fabrication. E. A. contributed to the electrical calculations. The work was supervised by Z. M., who contributed to the design of the experiments with E. K., M. K., E.A. and P. B. as part of a collaboration. The work was supported by US Army Research Office under Contract W911NF-17-1-0109, University of Michigan College of Engineering Blue Sky Research Program, University of Michigan Rackham Graduate Student Research Grants, NSF grant #DMR-0723032 (for the JEOL JEM 3100R05 AEM), and the technical support from the Michigan Center for Materials Characterization.

3.2 Introduction

Ultrawide-bandgap semiconductors, including AlN, BN, and diamond, are critical for applications in next-generation high-power, high-frequency electronics, UV optoelectronics, high-

power photonics, and quantum devices and systems.[33,63,79-86] Progress in these fields, however, has been severely limited by the lack of scalable substrate, the presence of large densities of defects, and the extremely poor current conduction.[10,80,87] Moreover, it has remained challenging to achieve a precise control of impurity incorporation and defect formation in these ultrawide-bandgap semiconductors, severely limiting their structural, electronic, optical, and quantum properties. For example, free hole concentrations of AlN, the material of choice of high-efficiency UV LEDs for water purification and disinfection, can only be measured at ~10^{10} cm^{-3} level at room temperature for epilayer structures,[33,88,89] which is more than *seven* orders of magnitude lower than what is commonly required (~10^{17} – 10^{19} cm^{-3}) for practical optoelectronic and electronic devices. Magnesium (Mg), the common *p*-type dopant of III-nitrides, has a prohibitively large activation energy E_A for AlN,[88,90] schematically shown in Figure 3.1a, which results in negligible doping efficiency at room temperature. Moreover, during the epitaxy of Mg-doped AlN, the Fermi level is shifted towards the valence band edge,[91] significantly reducing the formation energy for nitrogen-vacancy as well as donor-like point defect and impurity incorporation, shown in Figure 3.1a, which compensates the presence of free holes[92,93] and further introduces various defect-related emissions.[89,90] Illustrated in Figure 3.1b is the calculated formation energy for N-vacancy, Al-vacancy, and Al-substitutional Mg dopant incorporation, as a function of Fermi level of AlN. Detailed theoretical calculation process is described in the Appendix A. Sec. 1.

Here we show, both theoretically and experimentally, that such fundamental material issues of AlN can be potentially addressed through nonequilibrium epitaxy of nanostructures. Dislocation-free semiconductor nanostructures not only enhance the performance and functionality of electronic, photonic, and quantum devices and systems, but also open a new

paradigm for controlling the formation of defects and impurity incorporation.[50,55,94-97] During the epitaxy of N-polar AlN nanostructures, N-rich conditions are commonly used.[50,52,80] Illustrated in Figure 3.1c, the formation energy of N-vacancy related defects can be increased by nearly 3 eV under N-rich epitaxy condition, compared to conventional N-poor condition, thereby suppressing N-vacancy related defect formation. Moreover, the formation energy for Al-substitutional Mg-dopant incorporation is drastically reduced by ~2 eV under N-rich epitaxy, shown in Figure 3.1c, which can significantly enhance Mg-dopant incorporation. Experimentally, we have studied optical properties of Mg-doped AlN nanostructures by DUV PL spectroscopy and their dependence on epitaxy conditions. Power-dependent and time-resolved PL measurements suggest that Mg-acceptor-related optical emission originates from transitions between the conduction band and Mg impurity levels, rather than donor-acceptor-pair (DAP) related emission measured in conventional AlN epilayers, indicating suppressed N-vacancy-related defect formation. Detailed current-voltage characteristics analysis of AlN *p-i-n* diodes suggests that current conduction is dominated by charge-carrier (hole) tunneling at room temperature, with the characteristic tunneling energy determined by the activation energy of the Mg dopant. The dispersion of Mg acceptor levels at very high concentrations leads to drastically reduced activation energy for a portion of Mg dopants, evidenced by a reduction of the characteristic tunneling energy from 364 meV to 67 meV. These studies provide a path for achieving efficient current conduction of AlN that is relevant for a broad range of DUV optoelectronic devices, including LEDs, lasers, photodetectors, modulators, as well as high-power and as high-frequency transistors.

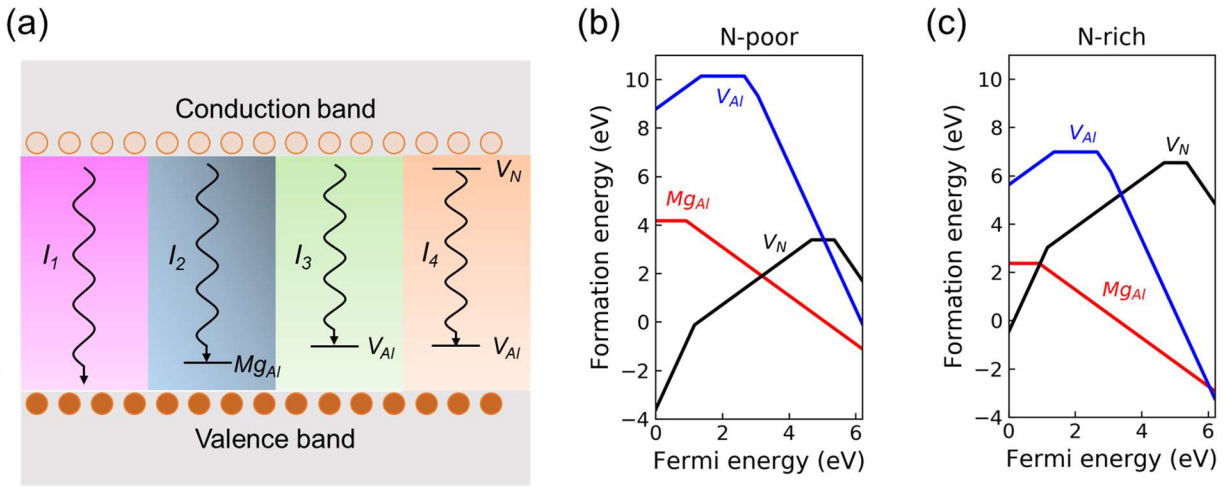

Figure 3.1. (a) Illustration of various transitions in Mg-doped AlN that involve conduction band (CB), valence band (VB), Mg acceptors, Al-vacancy, and N-vacancy related defects. (b, c) Formation energies as a function of Fermi level for the nitrogen vacancy V_N, aluminum vacancy V_{Al}, and Al-substitutional Mg under N-poor and N-rich conditions. Fermi level is set to zero at the valence band maximum. A lower formation energy indicates a high equilibrium concentration of the defects. The formation energy of N-vacancy related defects is increased by nearly 3 eV under N-rich epitaxy condition, compared to conventional N-poor condition, and the formation energy for Al-substitutional Mg-dopant incorporation is decreased by ~2 eV under N-rich epitaxy.

3.2 Molecular Beam Epitaxy and Characterization of AlN Nanowires

In this work, AlN nanostructures were grown on *n*-type Si wafer using a Veeco GEN II molecular beam epitaxy system equipped with a radio frequency plasma-assisted nitrogen source. Shown in Figure 3.2a is the SEM image. The grown nanowires have an average diameter of 50 nm and density of 1.5×10^{10} cm^{-2}, with an estimated filling factor of ~30%. Listed in Table 3.1, AlN samples were grown under different conditions by varying N_2 flow rate, substrate temperature and Mg flux measured as BEP. The detailed growth process is described in the Appendix A. Sec. 2. All the samples were grown under N-rich epitaxy conditions and are largely free of dislocations

and SFs (see Figure A2). For comparison, conventional AlN epilayers generally exhibit poor structural properties when grown under N-rich conditions.[98-100] While the suppression of N-vacancy-related defects may be expected under N-rich epitaxy condition, its impact on the formation of other types of defects, such as Al vacancies, has remained unclear. In this study, we have first investigated the effect of growth temperature and N_2 flow rate on the properties of undoped AlN nanostructures. The studied samples, denoted as A1, A2 and A3, are listed in Table 3.1. Samples in Group A were grown in the temperature range of 810-965 ºC with N_2 flow rates varying between 0.33 and 1 sccm.

Table 3.1: List of three groups of AlN samples presented in this work and their growth conditions including substrate temperature, N_2 flow rate and Mg flux.

#	Growth temperature (°C)	N_2 flow rate (sccm)	Mg flux (Torr)
A1	965	1	N.A.
A2	810	1	N.A.
A3	810	0.3	N.A.
B1	810	0.33	3×10^{-9}
B2	810	0.5	3×10^{-9}
B3	810	1	3×10^{-9}
C1	810	0.4	3×10^{-9}
C2	810	0.4	1×10^{-9}
C3	810	0.4	7×10^{-9}

PL properties of AlN nanowires were measured using a 193 nm ArF excimer laser with a repetition frequency of 200 Hz and pulse duration of ~7 ns as the excitation source. The DUV PL spectra are shown in Figure 3.2b. It is seen that, when grown under a N_2 flow rate of 1 sccm, Sample A1 (growth temperature of 965 ºC) features a single excitonic emission peak at 5.93 eV (denoted as I_1), expected for the excitonic emission of strain-free AlN.[101] An additional and broad Al vacancy related peak at 4.86 eV (denoted as I_3) was observed from Sample A2 (growth temperature of 810 °C), which is consistent with the calculated emission energy between conduction band and singly positive charged Al vacancy state. (see Figure A3a) The comparison of the two spectra indicates that an elevated growth temperature helps suppress Al-vacancy related defect emission (I_3), through enhanced Al adatom diffusion.[68,70,102] In practical device applications, however, a relatively low growth temperature is generally required to enhance Mg dopant incorporation. Shown in Figures 3.1b and 3.1c, the formation energy for vacancies on Al site has a strong dependence on N chemical potentials, or N flux in the experiment. In this regard, Sample A3 was grown at 810 °C but with a relatively low N_2 flow rate of 0.33 sccm, but yet maintaining N-rich epitaxy conditions. Shown in Figure 3.2b, Sample A3 features a strong excitonic emission (I_1) without defect-related emission (I_3), in spite of the low growth temperature. Through these studies, it is evident that some of the commonly seen defects, including Al and N vacancies in AlN can be minimized by optimizing the growth parameters under N-rich epitaxy conditions.

In nanostructures, the complex growth dynamics, including surface adatom migration and desorption, may significantly affect the defect formation and distribution.[103,104] We have experimentally investigated the effect of Mg dopant incorporation on the defect formation. The studied samples (Group B) are listed in Table 3.1 which were grown at the same substrate

temperature of 810 ºC, but with N_2 flow rate varying from 0.33 to 1 sccm. Shown in Figure 3.2c, Mg-acceptor related emission (I_2) was clearly observed for Mg-doped AlN sample grown at a N_2 flow rate of 0.33 sccm, with negligible Al-vacancy related defect emission (I_3). The origin of I_2 can be attributed to transition between conduction band and singly positive charged Mg dopant state. (see Figure A3b) The spectra are normalized to show the intensity ratio among the different peaks and non-normalized spectra can be found in Figure A4a. With increasing N_2 flow rate, Al-vacancy related defect emission (I_3) becomes dominant, compared to Mg-acceptor related emission (I_2) (also see Figure A4b). This observation is consistent with that measured for non-doped AlN, shown in Figure 3.2b.

To achieve efficient current conduction of *p*-type AlN, a large concentration of Mg dopants is required. We have subsequently investigated the effect of Mg concentration on the properties of AlN. Samples in Group C consist of Mg-doped AlN grown under the same substrate temperature of 810 ºC and N_2 flow rate of 0.4 sccm but with Mg BEP varied from 1×10^{-9} to 7×10^{-9} Torr. The growth parameters were chosen such that I_2 emission dominates the PL spectra, which facilitates measurements with large variations of excitation power. Shown in Figure 3.2d, Mg-acceptor related emission (I_2) intensity shows an increasing trend with Mg concentration, followed by a decrease for high Mg BEP (~7×10^{-9} Torr). This suggests enhanced defect formation at very high Mg concentrations, including the increased formation of Al-vacancy related defects, since the incorporated Mg dopants may get desorbed during the growth process as a result of weak Mg-N bond which leaves vacancies on the cation site[105]. This is further verified by the monotonic increase of Al-vacancy-related defect emission (I_3) with increasing Mg concentration, shown in Figure 3.2d.

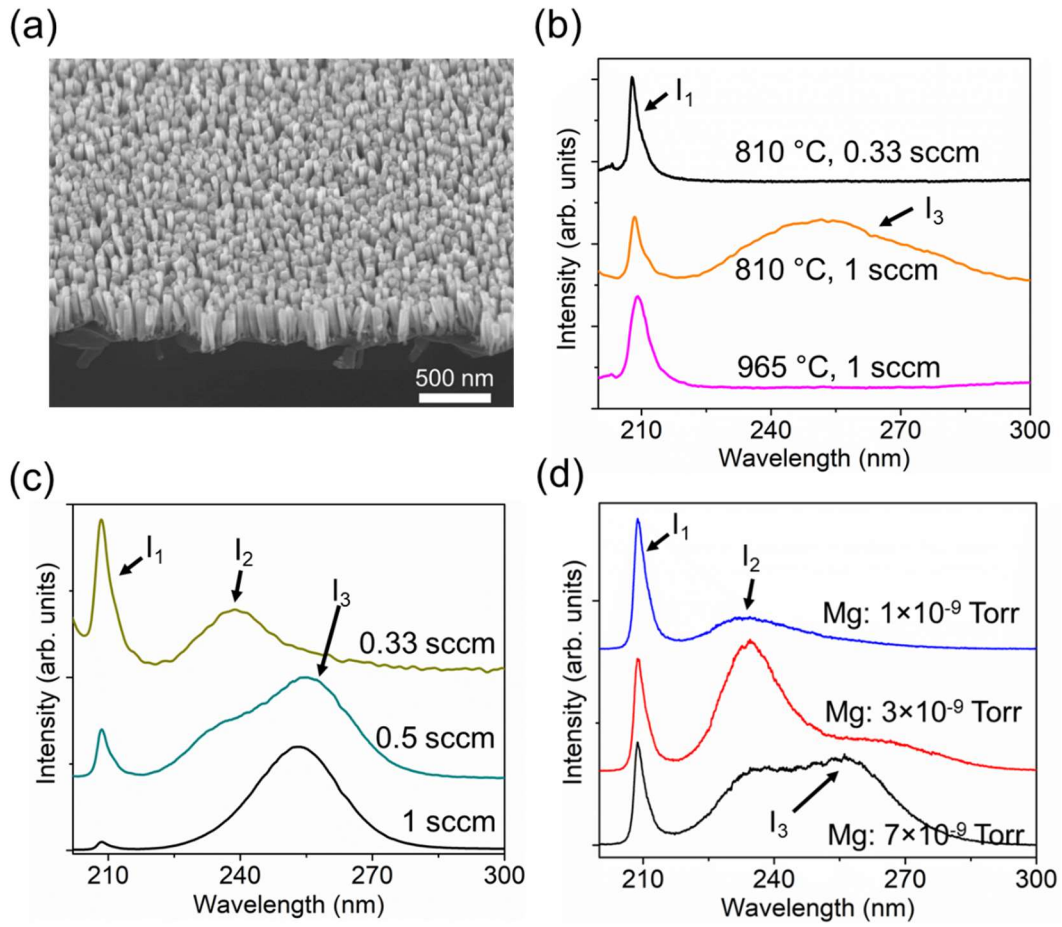

Figure 3.2. (a) SEM image of AlN nanowires grown under 0.33 sccm nitrogen flow rate and substrate temperature of 810 °C. Scale bar, 500 nm. (b) Normalized room-temperature PL spectra of undoped samples from Group A. Variations of the growth temperature and nitrogen flow rate are shown in the figure. (c) Normalized PL spectra of Mg-doped samples from Group B. All samples were grown at temperature of 810 °C and Mg BEP of 3×10^{-9} Torr while the nitrogen flow rate was varied among different samples. (d) Normalized room-temperature PL spectra of Mg-doped samples from Group C. All samples were grown at a substrate temperature of 810 ºC and N_2 flow rate of 0.4 sccm while Mg BEP was varied from 1×10^{-9} to 7×10^{-9} Torr.

To further elucidate the nature of I_2 and I_3 emissions, power-dependent and time-resolved PL measurements were performed on the sample grown under a substrate temperature of 865 ºC, N_2 flow rate of 1 sccm and Mg BEP of 7×10^{-9} Torr. The Mg concentration is estimated ~5×10^{19} cm^{-3}, or higher, based on secondary-ion mass spectrometry (SIMS) studies (see Figure A5). The

PL spectra were analyzed with multiple Gaussian profiles as shown in Figure A6. With increasing excitation power, I_2 shifts from 5.28 to 5.21 eV, and I_3 shifts from 4.86 to 4.8 eV, shown in Figure 3.3a. This redshift cannot be explained by the DAP related transitions reported for AlN epilayers, which were characterized by a blueshift with increasing excitation intensity.[93] The redshift measured in this study is attributed to a combination of laser-induced heating effect and bandgap renormalization,[106] which were observed in GaN/AlN quantum dots[107] and GaN nano-particles.[108] Moreover, DAP emissions generally show a slow decay with typical lifetimes in the μs range,[89] whereas I_2 and I_3 decay fast at 300 K, approaching an exponential law with very short lifetimes of 140 and 360 ps, respectively, shown in Figure 3.3b. Since I_2 and I_3 decay is four orders of magnitude faster than for DAP, both I_2 and I_3 emissions must originate from the transitions involving the conduction band and impurity energy levels inside the bandgap, rather than DAP-related transitions as reported in Mg-doped AlN epilayers,[89,90] which further confirm that the use of N-rich conditions can effectively suppress the formation of donor-related compensating defects. This observation also explains the high hole concentrations (up to 6×10^{17} cm^{-3}) measured at 300 K in Mg-doped AlN nanowires grown under N-rich conditions,[48] whereas hole concentrations ~2.5×10^{15} cm^{-3} were measured in Mg-doped AlN epilayers in spite of the very high measurement temperature (850 K) and the very large Mg concentration (10^{20} cm^{-3}).[89]

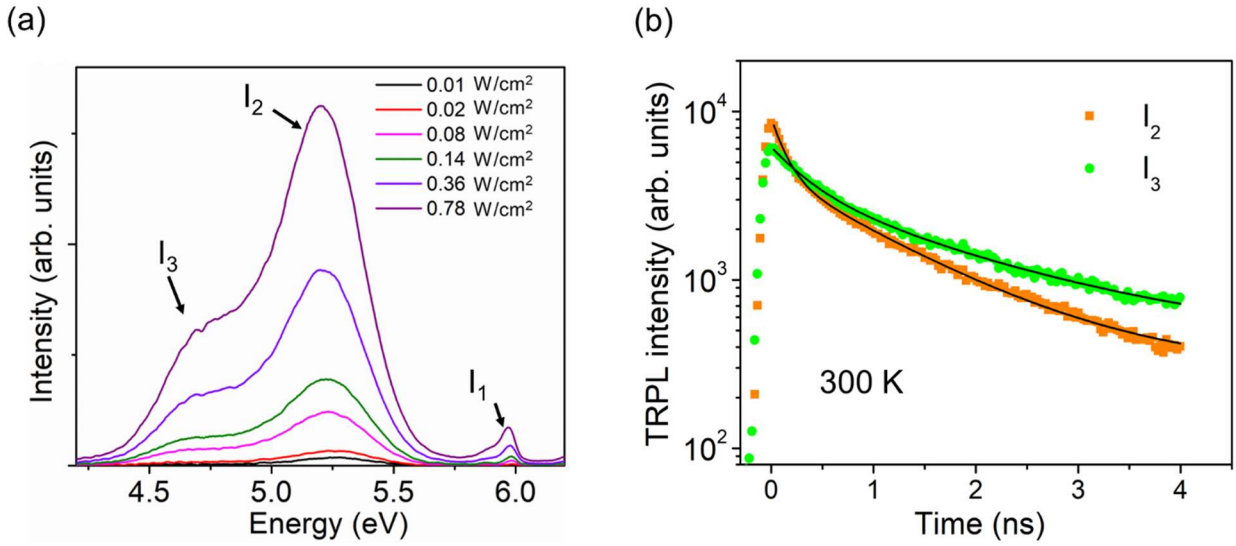

Figure 3.3. (a) PL spectra of Mg-doped AlN nanowires measured under different excitation powers. The sample was grown under a substrate temperature of 865 ºC, N_2 flow rate of 1 sccm and Mg BEP of 7×10^{-9} Torr. (b) Time-resolved PL transients of I_2 and I_3. The black curves are fitting results using a single exponential decay.

3.3 Electrical Properties and Charge Carrier Dynamics of AlN Nanowire LEDs

Previously reported planar *c*-plane AlN LEDs had a turn-on voltage ~30 V.[33] With optimized growth conditions, we have subsequently investigated the electrical characteristics of AlN nanowire LEDs. Schematic illustration of the device structure and growth conditions are shown in Figure A7a. The Si doping concentration in *n*-AlN is ~1.5×10^{19} cm^{-3} and Mg concentration in *p*-AlN is estimated in the range of 1×10^{19} to 6×10^{19} cm^{-3}. It's worth noting that introducing Si doping in AlN could shift the fermi level toward conduction band, resulting in a reduced formation energy of Al vacancy in AlN, as shown in Figure 1c. Therefore, we intentionally grew *n*-AlN and the subsequent unintentioanlly doped AlN at a relatively high substrate temperature of 875 °C to minimize Al-vacancy related defects. Figure 3.4a shows typical room-temperature *I-V* characteristics of as-fabricated AlN nanowire LEDs, which has a small reverse leakage current ~10 nA at -5 V and strong emission at ~210 nm (see Figure A7b). Under forward

bias, the electrical characteristics exhibit three different trends. Region I is characterized by the presence of a carrier-injection barrier $\emptyset_{b1}$ of 2.2 eV related to the large conduction band offset between GaN and AlN (further confirmed and described in Figure A8). In Region II, the obtained minimum ideality factor is 4.6 at 2.4 V, but increases drastically with increasing voltage. In Region III, the device shows a turn-on voltage ~5 V, which is significantly smaller compared with previously reported planar AlN diodes[33] and is largely determined by the energy bandgap of AlN. With further increasing voltage, injection current is limited by parasitic ohmic potential drop across the diodes. We measured the *I-V* characteristics of AlN LEDs with different Mg doping concentrations. The obtained minimum ideality factor shows a decreasing trend from 14.9 to 3.6 with increasing Mg doping concentrations from approximately 1×10^{19} to 6×10^{19} cm^{-3} (see Table 3.2 in Appendix A) This observation rules out the possibility that the large ideality factors of AlN LEDs are the results of sum of the ideality factors of several rectifying junctions as proposed by Shah *et al*.[109]

We further performed temperature-dependent *I-V* measurements. Illustrated in Figure 3.4b, the measured currents between 2.5 and 3.5 V show a monotonic increasing trend with increasing temperature. The dashed black lines in Figure 3.4b indicate the slopes of forward *I-V*, which are largely invariant from room temperature to 200 °C, and hence the ideality factor, extracted by $n = \frac{kT}{q}\left[\frac{dV}{d(lnI)}\right]$, shows a strong temperature dependence. Previous reports attributed temperature-independent slopes of (log*I*)-vs.-*V* plots to the involvement of charge carrier tunneling.[109-111] The total forward current *J* of the *p-i-n* diode can be expressed as the sum of diffusion component J_D in the neutral region (both *p* and *n* layers) and the tunneling current J_T in the depletion region,

$$J = J_{D0}\left[\exp\left(\frac{qV_A}{kT}\right) - 1\right] + J_{T0}\left[\exp\left(\frac{qV_A}{E_T}\right) - 1\right] \qquad (3\text{-}1)$$

where V_A is the voltage applied through the AlN *p-i-n* diode, and E_T is the characteristic tunneling energy.[112,113] Here other factors such as radiative and nonradiative carrier recombination that could lead to larger ideality factors are ignored. Using Eqn. (3-1), E_T of 364 meV is obtained for the AlN LED with a Mg concentration of ~1×10^{19} cm^{-3}. E_T values on this order have been attributed to deep-level-assisted electron (hole) tunneling,[112] such as the deep Mg acceptor levels in AlN, which are in the range of 500-600 meV. In this study, it is observed that E_T decreases to 67 meV for the AlN LED with a Mg concentration of ~6×10^{19} cm^{-3}. Very high Mg impurity concentrations in AlN can result in the formation of an impurity band, schematically shown in Figure 3.4c, instead of localized impurity levels, due to impurity-impurity interactions.[48,49,91] With increasing Mg concentration, the dispersion of Mg acceptor energy levels can lead to reduced ionization energy for a portion of Mg dopants, illustrated in the right panel of Figure 3.4c. This is consistent with the observation of a reduction of the characteristic tunneling energy from 364 meV to 67 meV with increasing Mg concentrations from ~1×10^{19} cm^{-3} to 6×10^{19} cm^{-3}. At elevated temperatures, hole concentrations in the impurity band is increased, and diffusion current becomes more dominant, which leads to a reduction of the ideality factor, shown in Figure 3.4d. A more detailed analysis of the hole tunneling process is described in Appendix A. Section 10. The derived E_T value of 67 meV suggests that the ionization energy of Mg dopants can be effectively reduced by nearly one order of magnitude for AlN nanostructures grown under N-rich epitaxy conditions, compared to that of conventional planar AlN, thereby leading to AlN LEDs with excellent electrical performance.

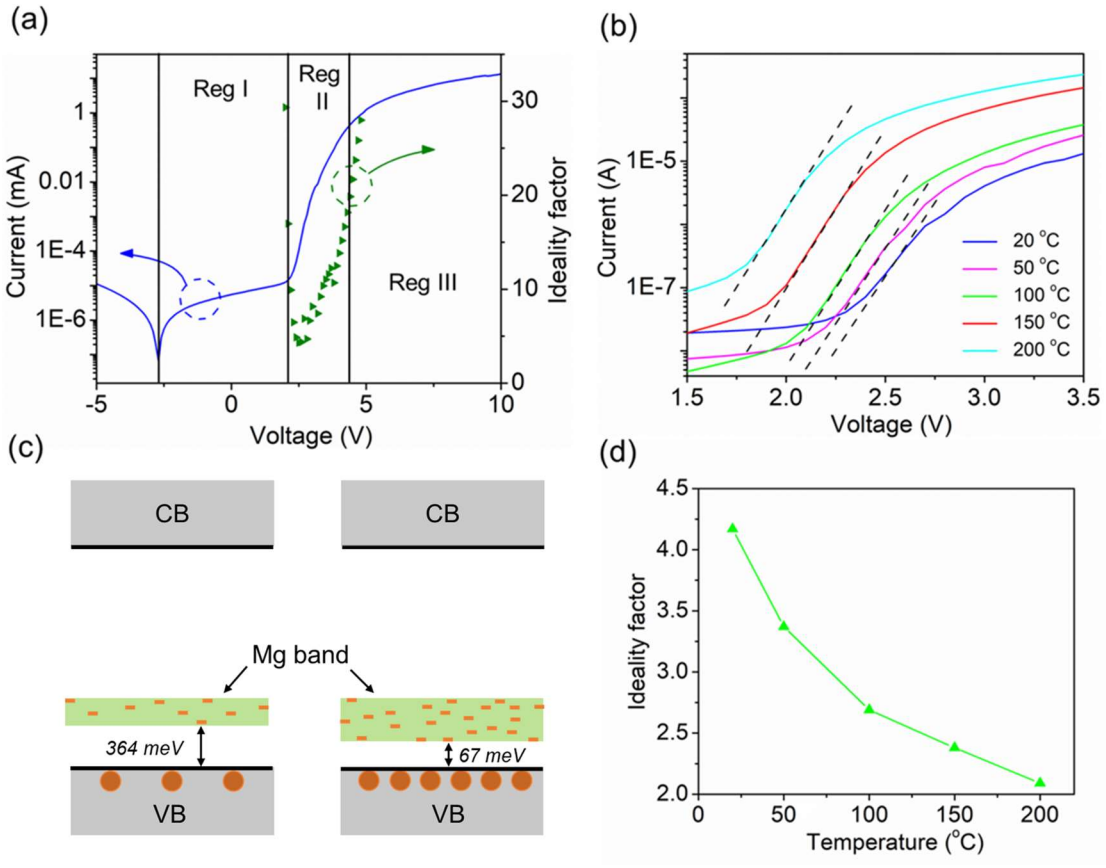

Figure 3.4. (a) *I-V* characteristics of AlN nanowire LEDs measured at room temperature, wherein three regions with different slopes can be identified. (b) Temperature-dependent *I-V* characteristics of AlN nanowire LEDs measured in the temperature range of 20-200 °C. (c) Illustration of the Mg acceptor energy levels under relatively low (left) and high (right) doping concentrations. The dispersion of Mg acceptor energy levels under very high concentrations can lead to significantly reduced activation energy (right). (d) Variations of the minimum ideality factors vs. measurement temperature.

3.4 Conclusion

In summary, through a combined theoretical and experimental study, we show that N-rich epitaxy provides a viable path for achieving efficient *p*-type conduction of AlN that was not previously possible. The benefits of growing AlN nanostructures under N-rich conditions include: i) suppression of N-vacancy related compensating defect formation, and ii) significant enhancement of Al-substitutional Mg-dopant incorporation. Detailed optical measurements show

that Mg-related optical emission originates from conduction-band to Mg-acceptor energy levels, rather than DAP-related transition, further confirming the suppressed donor-related defect formation under N-rich conditions. Analysis of the current-voltage characteristics of AlN *p-i-n* diodes suggests that current conduction is dominated by charge carrier (hole) tunneling at room temperature. The characteristic tunneling energy is largely determined by the activation energy of the Mg dopant. At very high Mg concentrations, the dispersion of Mg acceptors leads to drastically reduced activation energy, evidenced by the small tunneling barrier energy of 67 meV. As such, efficient current conduction can be achieved for Mg-doped AlN when grown under N-rich conditions. This study may also offer a path to address the poor current conduction of other ultra-wide bandgap semiconductors.

Chapter 4 Monolayer GaN Excitonic DUV LEDs

4.1 Author Contribution and Copyright Disclaimers

The contents of this chapter were published in AIP Publishing's Applied Physics Letters in January 2020,[79] for which I retain the right to include it in this thesis/dissertation, provided this thesis/dissertation is not published commercially. The co-authors were Xianhe Liu, Ping Wang, David Arto Laleyan, Kai Sun, Yi Sun, Chihyo Ahn, Mackillo Kira, Emmanouil Kioupakis and Zetian Mi from the University of Michigan. I designed, conducted and authored most of the experimental work. X. L. contributed to the EL measurements. P. W., D. A. L. and C. A. contributed to the material growth process. K. S. contributed to STEM characterization. Y. S. contributed to device fabrication. E. K. conducted the theoretical calculations. The work was supervised by Z. M., who contributed to the design of the experiments with E. K. and M. K. as part of a collaboration. The work was supported by US Army Research Office under Contract # W911NF19P0025, University of Michigan College of Engineering Blue Sky Research Program, and NSF grant #DMR-0723032 (for the JEOL JEM 3100R05 AEM), and the technical support from the Michigan Center for Materials Characterization.

4.2 Introduction

The development of III-nitride UV LEDs is of key importance for a broad range of applications, such as sterilization, water purification, medical treatment, and Raman spectroscopy.[11,114-116] AlGaN QWs with a high Al content have been extensively investigated as active regions for DUV LEDs with wavelengths ranging from 222 nm to 350 nm.[117,118] To date, however, the efficiency of AlGaN DUV LEDs is significantly below than that of GaN-based blue LEDs. For example, for LEDs operating at wavelengths of <240 nm, the reported EQE is well below 1%.[38] Some of the major factors limiting the performance of DUV LEDs include low

quantum efficiency due to the large densities of defects and dislocations in planar AlGaN QW LED heterostructures,[32] poor charge carrier (hole) injection efficiency due to the inefficient *p*-type conduction associated with the very large ionization energy of Mg dopants,[119] and low light extraction efficiency caused by the light absorption and optical polarization.[53,54] Specifically, when the Al composition in the AlGaN active region exceeds ~68%, the crystal split-off (CH) subband is positioned at the top of the valence band. The hole population in the CH subband leads to TM optical transition, which is polarized along the *c*-axis (growth direction) and therefore prevents efficient light extraction in a conventional planar LED device. Other factors, such as electron overflow, Auger recombination, and heating effect may also contribute significantly to the low efficiency of DUV LEDs. Extensive studies, including the use of bandgap engineering, tunnel junction,[36,120] nanostructures[121], AlN substrates,[26,122] nano-patterned substrate,[123,124] and high temperature annealing[125,126] have been performed to address these critical challenges.

Recent studies have shown that monolayer GaN embedded in AlN matrix can exhibit transverse electric (TE), instead of TM, polarized emission in DUV wavelengths.[127-129] The extreme quantum-confinement also promises very large exciton binding energy (up to ~230 meV) and stable excitonic emission in a monolayer GaN LED, due to the strong Coulombic interaction, which can greatly minimize the effect of nonradiative Shockley-Read-Hall recombination. Moreover, due to the enhanced radiative recombination (smaller carrier lifetime), charge carrier densities in the device active region will be significantly smaller than a conventional LED device under otherwise identical injection current, thereby drastically reducing nonradiative Auger recombination ($\propto n^3$) and electron overflow of a DUV LED. To date, however, such a large exciton binding energy in monolayer GaN was not measured, which is likely limited by the epitaxy of

conventional planar AlGaN heterostructures on sapphire, which often have significant surface/interface roughness and large densities of defects and dislocations.[130] III-nitride nanocrystals, including nanowires and nanorods have attracted significant interests,[131] which are largely free of dislocations, due to the efficient surface strain relaxation. To date, however, the controlled epitaxy of monolayer GaN in AlN nanocrystals has remained elusive. In a recent study by Sarwar *et al*., significant thickness fluctuations were observed in monolayer GaN embedded in AlN nanowires, leading to optical emission varying from ~240 nm to 320 nm.

In this chapter, we report on a detailed investigation of the epitaxy and characterization of monolayer GaN formed in N-polar AlN nanowire arrays by using PAMBE. With the use of growth interruption and migration enhanced epitaxy, we demonstrate the controlled formation of monolayer GaN in an AlN matrix. DUV emission from ~4.9 eV to 5.25 eV was measured by varying AlN barrier thickness. Direct correlation with the calculated electronic and optical bandgap of monolayer GaN suggests the excitonic binding energy for monolayer GaN embedded in an AlN matrix is ~200 meV. The predominant excitonic emission is also consistent with the measured linear increase of light intensity with excitation power. We have further demonstrated large-area LEDs with the incorporation of single monolayer and double monolayer GaN active region, which exhibit strong emission at 238 nm and 270 nm, respectively.

4.3 Epitaxial Growth of Nanowires with Monolayer Thin GaN

In this study, DUV LED quantum heterostructures, schematically shown in Figure 4.1a, were grown on *n*-type Si wafer using a Veeco GEN II MBE system equipped with a radio frequency plasma-assisted nitrogen source. Prior to loading into the MBE system, the Si wafer was cleaned in buffered hydrofluoric acid solution. Si-doped GaN nanowires with a length of ~100 nm were first grown directly on Si substrate, which serve as a template for the subsequent epitaxy of

AlN/GaN quantum heterostructures. Si-doped AlN nanowires (~150 nm) were grown at a substrate temperature of 875 ºC. Three periods of GaN/AlN quantum heterostructures were grown at the same substrate temperature of 875 ºC, wherein the thickness of GaN quantum disk was either one or two monolayer and the AlN barrier thickness was ~10 nm. The growth rate was ~0.1 ML/s. The growth was performed under N-rich conditions, and the nominal Ga/N ratio was ~0.29 and Al/N ratio was ~0.26 during the active region growth. Because of the strong preference of Al incorporation over Ga, an Al-free surface is essential for the controlled formation of monolayer GaN in the AlN matrix. Therefore, at the end of each AlN barrier growth, the Al shutter was closed for 10 mins, with only the nitrogen shutter open to help consume extra Al adatoms at the growth front. Then the Ga shutter was opened briefly, which was immediately capped by AlN. The thickness of the GaN quantum disks was varied from one to two monolayers by varying the Ga shutter opening time. Subsequently a ~40 nm Mg-doped *p*-AlN hole-injection layer and ~3 nm *p*-GaN contact layer were grown. Figure 4.1b shows a typical SEM image of the as-grown nanowire heterostructures, which feature a high density of 2×10^{10} cm^{-2} and relatively uniform height. The nanowires are vertically aligned to the substrate and have N-polarity based on previous studies.

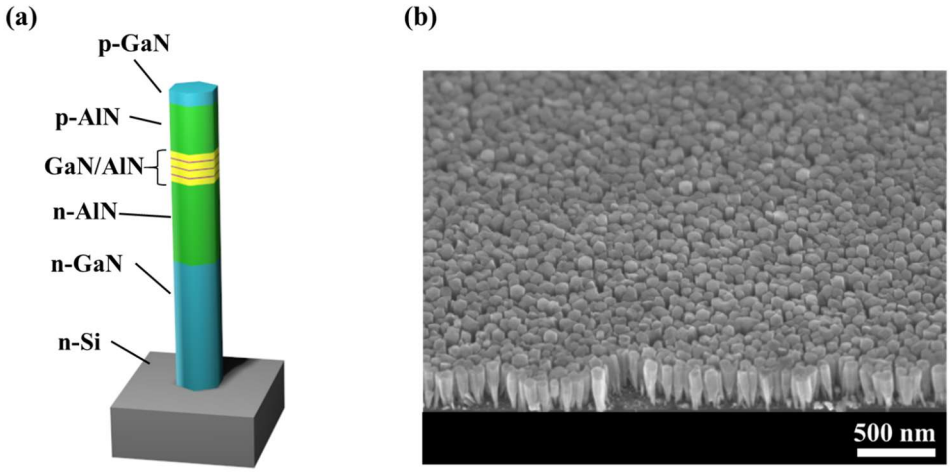

Figure 4.1. (a) Schematic illustration of DUV LED heterostructure with the incorporation of monolayer GaN active region. (b) A SEM image of the grown sample.[79]

4.4 Structural and Photoluminescence Characterization of Ultrathin GaN/AlN

For TEM studies, GaN/AlN nanowires were mechanically removed from the substrate and dispersed on a lacy carbon film mesh Cu TEM grid. Transmission electron micrographs were collected using a JEOL JEM3100R05 TEM with double aberration correctors operated in STEM mode with settings defining a probes size smaller than 0.1 nm for HAADF imaging with a detector collection inner angle ~79 mrad. Shown in Figures 4.2a and 4.2b are the HAADF-STEM images of the single and double monolayer GaN samples, respectively, which confirmed the formation of monolayer GaN on the *c*-plane of the AlN nanowire. A sharp interface was observed between the GaN monolayer and the bottom AlN barrier, while there was slight interdiffusion between the GaN monolayer and the top AlN barrier, which could be caused by the non-optimum Ga deposition time for nanowires with different sizes.

PL properties of monolayer GaN/AlN heterostructures were measured using a 193 nm ArF excimer laser as the excitation source at room temperature. Shown in Figure 4.2c, distinct emission peaks at 238 nm and 270 nm were measured for samples with single and double monolayer GaN, respectively, which are in good agreement with previous theoretical calculations. It is noticed that there is significant inhomogeneous broadening (full-width-at-half-maximum ~20 nm), which is largely due to the size dispersion of AlN nanowires and the resulting variations in strain distribution and associated adatom interdiffusion. Significantly reduced spectral broadening is expected with the use of SAE to precisely control the size of AlN nanowires.[132] While identifying genuine exciton contributions directly from PL spectra requires a sophisticated quantitative analysis,[133] temporally and spectrally integrated PL determines the total number of

radiatively recombined electron-hole pairs,[106] which can be used to determine the ratio of radiative and nonradiative Auger recombination. Shown in Figure 4.2d, the temporarily and spectrally integrated PL intensity (I_{PL}) from monolayer GaN is found to linearly increase with the excitation intensity (I_0), *i.e.,* $I_{PL} \propto I_0$. This implies that the number of generated charge carriers ($\propto I_0$) is equal to radiatively recombined ones ($\propto I_{PL}$).[106] Since Auger recombination would invalidate this balance, the linear relationship between I_{PL} and I_0 suggests strong suppression of Auger recombination under the presented measurement conditions, as expected for exciton-dominated systems.

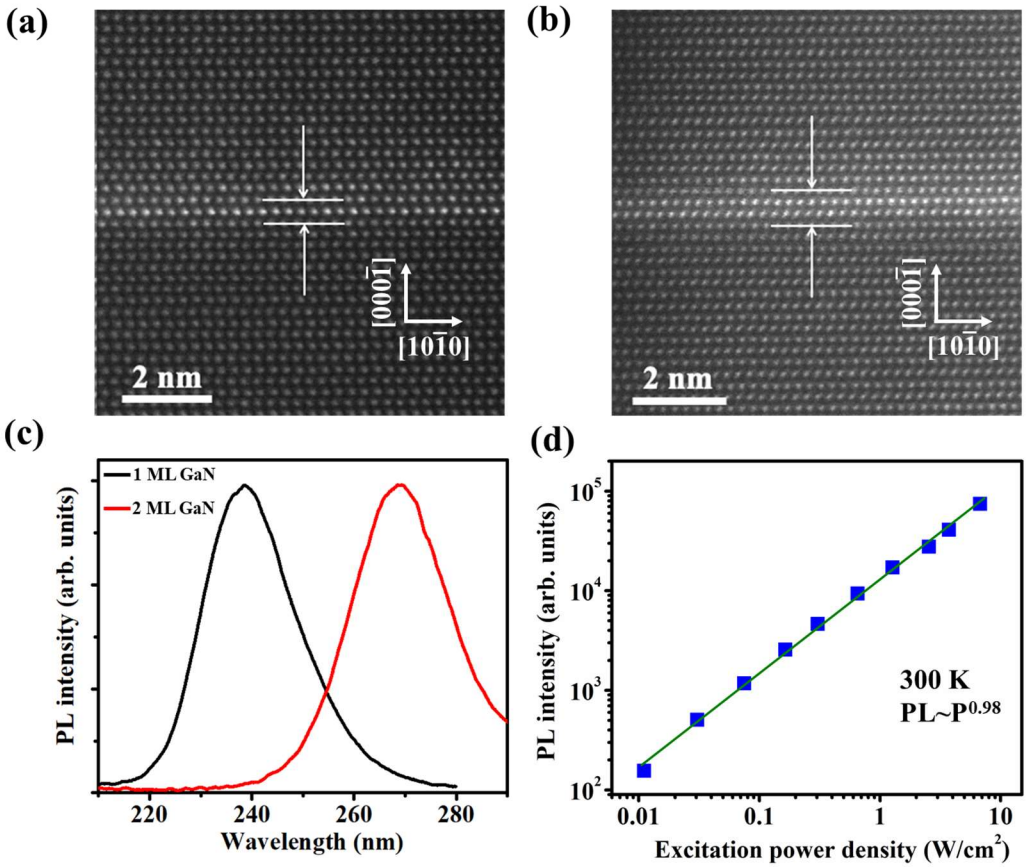

Figure 4.2. STEM-HAADF images of (a) one monolayer GaN and (b) two monolayer GaN embedded in AlN matrix. (c) Normalized PL spectra for one monolayer (black) and two monolayer (red) GaN measured at room temperature. (c) Variations of the integrated PL intensity with excitation power for the sample containing monolayer GaN active region.[79]

4.5 First Principle Calculation and Electroluminescence of Monolayer GaN Based LEDs

Next, we compare our experimental data to previous theoretical predictions[134] from first-principles calculations based on density functional and many-body perturbation theory, which yield accurate electronic and optical properties of materials. The theoretical electronic and optical gaps of 1 ML GaN/AlN heterostructures with AlN barrier 1-9 MLs thick are shown in Figure 4.3b. Increasing the thickness of AlN barrier, the electronic gap increases to 5.44 eV and the optical gap increases to 5.2 eV for 1 ML GaN/9 MLs AlN due to increased quantum confinement inside the GaN QDs.[129] Thicker AlN barriers increase the electronic gap and optical gap only slightly above this value. At the other extreme, the structure of alternating GaN and AlN single MLs has an optical gap of 4.66 eV. We also obtained experimental PL peak positions for a series of GaN/AlN heterostructures with monolayer-thick GaN and varying AlN barrier thickness. The observed peak positions (Figure 4.3a) are in good agreement with the calculated optical gaps, in contrast to previous reports for planar ML GaN structures in which the PL photon energies are closer to the electronic gaps.[129] This further confirms that the emission in our PL measurements has exitonic nature with binding energy of ~200 meV. It's worth mentioning the PL emission obtained from previously reported Ga-polarity monolayer GaN/AlN heterostructure showed peak photon energies closer to the electronic band, indicating the obtained emission in planar structure is non-exitonic.[129] Previous study have shown that the interface between GaN and AlN is usually diffusive due to the negative polarization charge when the surface has Ga-polarity, which is common for commercial GaN on sapphire substrate.[135] In contrast, the spontaneously grown nanowires on Si substrate have N-polarity,[136] generating a positive polarization and abrupt interface between the GaN/AlN, which essential for providing extreme quantum confinement of electron hole pairs.[135] The strain field in ML GaN/AlN heterostructure and its spatial variation

could lead to a confinement along the lateral direction of the nanowire, which, together with variations in the nanowire size, explains the large linewidth measured for the excitonic emission.[137]

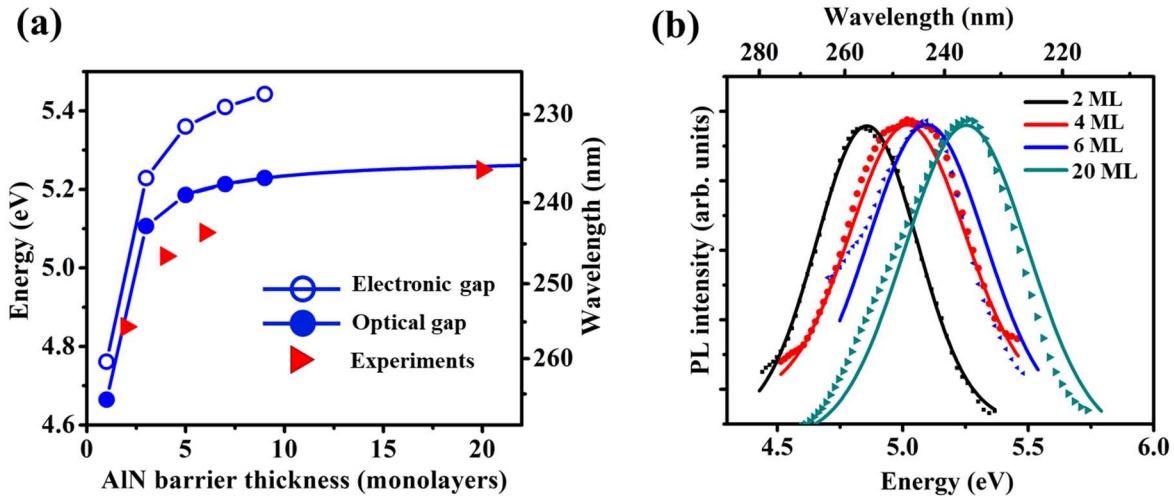

Figure 4.3. (a) Electronic and optical gaps of monolayer GaN as a function of the AlN barrier thickness. Experimentally measured PL peaks at 300 K are indicated with red triangles. Lines connected to and extrapolated from the theory data points are guides to eye. (b) Normalized PL spectra of monolayer GaN with different AlN barrier thicknesses measured at room temperature. The solid lines are fittings to experimental data.[79]

4.6 GaN Monolayer-based DUV LEDs

Figure 4.4a shows the schematic of DUV LEDs, which were fabricated by standard optical lithography and contact metallization techniques. First of all, e-beam evaporation of Ti (80 nm)/Au (20 nm) was deposited on the backside of Si substrate as the *n*-metal contact. The top metal layers of Ni (10 nm)/Au (10 nm) were deposited using a tilting angle deposition technique to define the device areas.[40] We note that no filling materials were used to avoid the absorption of UV photons. Ti (20 nm)/Al (300 nm)/Au (20 nm) metal grid contacts were also deposited on the device top surface to facilitate current spreading. The device mesa sizes are in the range of 300 μm by 300 μm to 1 mm by 1 mm. Figure 4.4b shows the current-voltage characteristics of the fabricated devices with turn-on voltages of ~5 V, which is lower than the ones reported in GaN monolayer-

based planar DUV LEDs due to enhanced Mg doping in the *p*-AlN and reduced monolayer periods.[127] The leakage current of the devices is on the order of a few hundred nA for a reverse bias of -10 V as shown in Figure 4.4b inset, indicating efficient doping and also a low density of dislocations inside the materials. Previously, it has been demonstrated that the formation energy of Al-substitutional Mg acceptors is drastically reduced in AlN nanostructures, compared to epilayers, due to the efficient surface stress relaxation.[38] Consequently, a portion of Mg acceptors has significantly reduced activation energy. As shown Figure 4.4b, the current density can reach over 50 A/cm^2 at 10 V at room temperature.

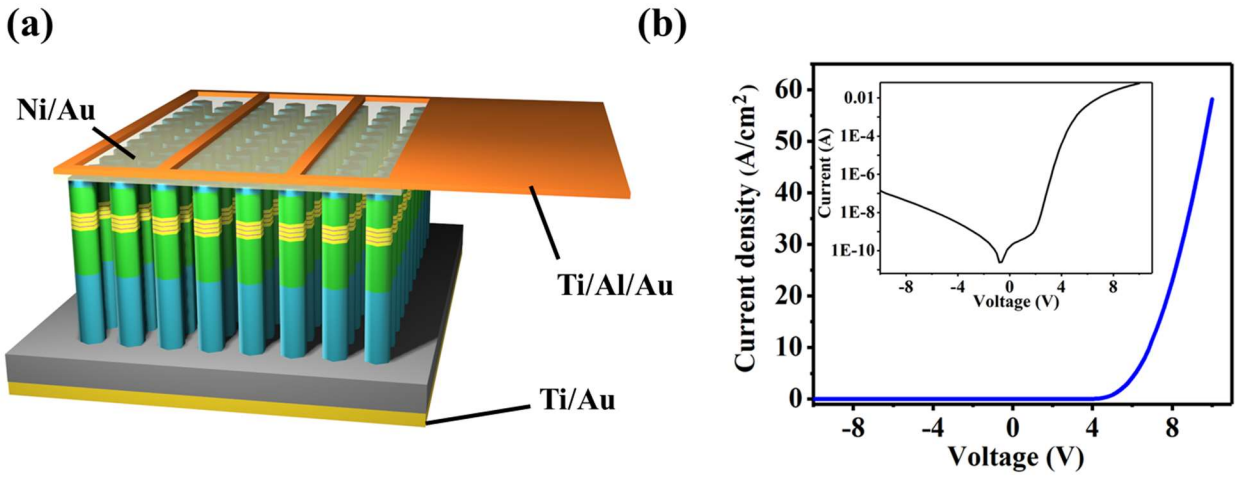

Figure 4.4. Schematic illustration of the fabricated large area monolayer GaN DUV LED. (b) *I-V* characteristics measured at room temperature. Inset: logarithmic scale.[79]

Figure 4.5a shows the electroluminescence (EL) spectra for the LEDs incorporating single and double monolayer GaN active regions, with peak emission at ~238 nm and 270 nm, respectively, which are consistent with the PL measurements shown in Figure 4.2c. EL spectra for the monolayer GaN DUV LED device measured under different injection currents are further shown in Figure 4.5b. The peak positions remain nearly constant vs. current, shown in Figure 4.5c, which can be attributed to the negligible quantum-confined Stark effect, due to the extreme

quantum-confinement of electrons and holes in an atomically thin active region, despite of the large polarization field between GaN and AlN. It is also seen that the integrated EL intensity increases near-linearly with current, showing negligible efficiency droop, suggesting suppression of Auger recombination. In monolayer GaN LEDs, because the strong exciton binding energy enhances radiative decay[106] and quenches scattering,[138] the radiative carrier lifetime is reduced and thus Auger recombination. As a consequence, Auger recombination induced droop in DUV devices can be suppressed in strongly excitonic systems.

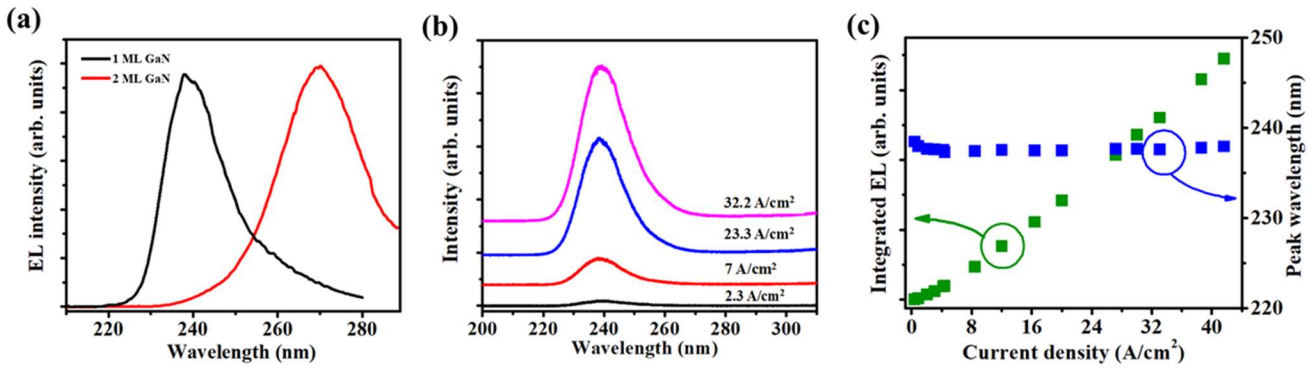

Figure 4.5. (a) EL spectra measured from one monolayer (black) and two monolayer (red) GaN LEDs, respectively. (b) EL spectra measured under injection currents from 2.3 A/cm^2 to 32.2 A/cm^2 for the monolayer GaN LED. (c) Variations of the integrated EL intensity (green) and peak position (blue) vs. injection current. The measured device size is 300 μm × 300 μm.[79]

4.7 Summary

In conclusion, we have demonstrated controlled epitaxy of monolayer GaN in an AlN matrix. Our experimental studies and direct correlation with first-principles calculations based on density functional and many-body perturbation theory provide strong evidence that monolayer GaN can exhibit a very large exciton binding energy of ~200 meV. The emission wavelengths can be further tuned by varying the thicknesses of GaN and/or AlN barrier. We have further

demonstrated DUV LEDs with the incorporation of single and double monolayer GaN, which operate at ~238 nm and 270 nm, respectively. These unique DUV LEDs exhibit highly stable emission and negligible efficiency droop. Future studies include the controlled epitaxy of monolayer GaN in AlN nanocrystals grown by SAE to significantly reduce the inhomogeneous broadening and to achieve DUV LEDs with high power operation.

Chapter 5 High Performance Al-rich AlGaN Nanowires-based LEDs on Al Coated Si (001) Substrate

5.1 Author Contribution and Copyright Disclaimers

The contents of this chapter were published in Elsevier's Journal of Crystal Growth in February 2019,[87] for which I retain the right to include it in this thesis/dissertation, provided this thesis/dissertation is not published commercially. The co-authors were Yongjie Wang, Kai Sun, and Zetian Mi from the University of Michigan. I designed, conducted and authored most of the work. Y. Wang contributed to the material growth process. K. S. contributed to the STEM characterization. The work was supervised by Z. M., who contributed to the design of the experiments. This work was supported by National Science Foundation with award Grant DMR-1807984.

5.2 Introduction

DUV LEDs and LDs with wavelengths in the range of 200-350 nm are of great interest for a wide variety of applications including water and air purification, sterilization/disinfection, medical diagnostics, phototherapy, polymer curing, and sensing.[10] Among all the wide bandgap semiconductors, group III-nitrides (GaN, AlN, InN and their ternary and quaternary alloys) are deemed as the most suitable material family for the implementation of DUV LEDs and LDs.[32,59,118,139-142] Extensive efforts have been devoted to improving device performance in the past decades, and previously reported AlGaN based QW DUV LEDs often exhibit an EQE of less than 10%.[35,143-145] There are mainly three factors limiting the performance of DUV LEDs. First of all, typical TD density of AlGaN heterostructures grown on sapphire is ~10^9 cm^{-2}, or higher, resulting in an IQE of less than 50%.[146,147] Secondly, the large Mg activation energy in Al-rich AlGaN severely limits the available hole concentration, resulting in a low carrier

injection efficiency.[13] Thirdly, LEE of the dominating TM polarized emission in Al-rich AlGaN planar structure has been limited to 10% or less.[148,149] Very recently, through migration-enhanced metal organic chemical vapor deposition to reduce the TDs and by utilizing UV reflecting ohmic contacts and optimized chip encapsulation, an EQE of 20% at 20 mA CW injection for 275 nm DUV LEDs was achieved.[34]

AlGaN nanowires have emerged as a promising alternative to its planar counterparts in circumventing the above-mentioned challenges.[17,50,150] Dislocation-free nanowires can be achieved on lattice-mismatched substrate due to the efficient surface strain relaxation.[41,42,44,151] It has been shown that nanowires can be monolithically integrated on low cost substrate including Si,[43,61] SiO_2[152] and Ti.[153,154] Tran *et al* performed detailed investigation of MBE growth of Mg-doped AlN nanowires and obtained hole concentration up to ~6×10^{17} cm^{-3}, which is orders of magnitude higher compared with the reported values (~10^{12} cm^{-3}) in Mg-doped AlN epilayers. The significantly enhanced Mg incorporation was attributed to efficient hole hopping conduction in the Mg impurity band. Liu *et al* showed that a maximum LEE >90% can, in principle, be achieved for TM-polarized emission for AlGaN nanowire LEDs on reflective substrate.[155] To date, however, most of the reported nanowire based DUV devices are grown directly grown on Si substrate which is opaque to any UV emission and severely reduces the LEE.

A particular interest has been seen in growing nanowire structure on metals, and it has been envisioned that LEDs on metallic substrate have the advantages of excellent electrical and thermal conductivity.[156-158] Zhao *et al* reported growth of disks-in-nanowires on Ti coated bulk polycrystalline-Mo substrate. Janjua *et al* demonstrated AlGaN nanowire based UV devices grown on a Ti coated *n*-type Si substrate. The device shows a UV emission wavelength of 337 nm and

it's believed that the incorporation of Ti layer improved current injection and heat dissipation. Prantie *et al* demonstrated that the incorporation of a thin metal layer could significantly reduce the junction temperature by 44 °C which further contributed to enhanced power and reliability of AlGaN devices.

Although Ti film can reflect ~35% light at 337 nm, the reflectivity plunges when moving to emission wavelengths shorter than 300 nm. Al has been widely adopted in UV reflectors with an over 85% reflectivity for emission wavelengths in the range of 250-300 nm. Moreover, Al has a thermal conductivity of 202 W/(m•K) while Ti has 22 W/(m•K) at room temperature, making it an ideal metal for enhancing the performance of DUV LEDs. However, due to its disadvantageous low melting temperature of 660 °C, to our best knowledge there have been no reports of AlGaN nanowires growth on Al film.

In this context, we have demonstrated epitaxial growth of AlGaN nanowires on Al coated Si substrate. A two-step growth method was utilized to realize high quality AlGaN nanowires vertically oriented on the substrate. The as-grown nanowires feature diameters of >200 nm and relatively uniform height distribution. AlGaN nanowires with emission wavelengths across nearly the entire UV-A and UV-B bands have been successfully achieved by varying Al/Ga BEP ratio and growth temperature. Detailed STEM characterization shows that the AlGaN nanowires were nearly free of TDs and SFs. The fabricated AlGaN nanowire LED devices have excellent rectification characteristics with a turn-on voltage of 7 V. A single peak EL emission at 288 nm was obtained. An EQE of ~0.04% was obtained at 20 A/cm^2 current injection which is at least one order of magnitude higher than the previous reports of AlGaN *p-i-n* nanowire based LEDs,[159] except one most recent report wherein tunnel injection was utilized to enhance the device performance.[40] Significantly improved EQE is expected by optimizing the growth of AlGaN

nanowire arrays directly on Al template and by eliminating light absorption through the Ni/Au *p*-contact metal on top of the AlGaN nanowire array.

5.3 Epitaxial Growth and Emission Wavelength Tuning of Al-rich AlGaN Nanowires on Al Coated Si(001) Substrate

Al film with a thickness of 300 nm was first deposited on the Si(001) substrate at a rate of 2 Å/s. Ellipsometry measurements show that the Al coated substrate has an over 85% reflectivity in the wavelength range of 250-400 nm at various incident angles. The Al template was cleaned using buffered hydrofluoride solution prior loading into the MBE chamber. A two-step growth method was adopted to realize vertically aligned AlGaN nanowires on Al template. GaN with a thickness of ~250 nm was firstly grown at a relatively low temperature (LT) of 600 °C as a buffer layer which is crucial in controlling the out-of-plane orientation of the nanowires as shown later. The formation of AlN layer underneath the GaN buffer is also expected during this step as shown later. During the second step, while keeping the same Ga BEP of 1.5×10^{-7} Torr, nitrogen flow of 1 sccm, plasma forward power of 350 W and a relatively high temperature (HT) of 780 °C was utilized to induce the formation of GaN nanowires homo-epitaxially on top of the LT-GaN layer. Figure 5.1a shows the schematic of the AlGaN/GaN nanowire segments on such LT-GaN. The corresponding bird-view SEM image is shown in Figure 5.1c. It can be observed that the obtained HT-GaN/AlGaN nanowire segments are nearly vertically grown on the substrate with a relatively uniform height distribution. The density of the nanowire ensembles is ~1×10^{9} cm^{-2} with diameters in the range of 200-350 nm, which are ~5-10 times larger than those grown on bare Si substrate under similar conditions.[160] The discrepancy can be attributed to the larger nucleation island size at the initial stage of HT-GaN nanowire growth as shown later. Direct growth of the nanowires on Al coated Si substrate without LT-GaN insertion was also investigated. As illustrated in Figures

5.1b and 5.1d, the obtained nanowire array features random out-of-plane tilting to the substrate. Moreover, the Al film thickness was reduced significantly to less than 20 nm while uniformity was also severely jeopardized. The random orientation could be attributed to the variation of nucleation sites on unstable Al film surface which undergoes severe adatom desorption at high growth temperature.

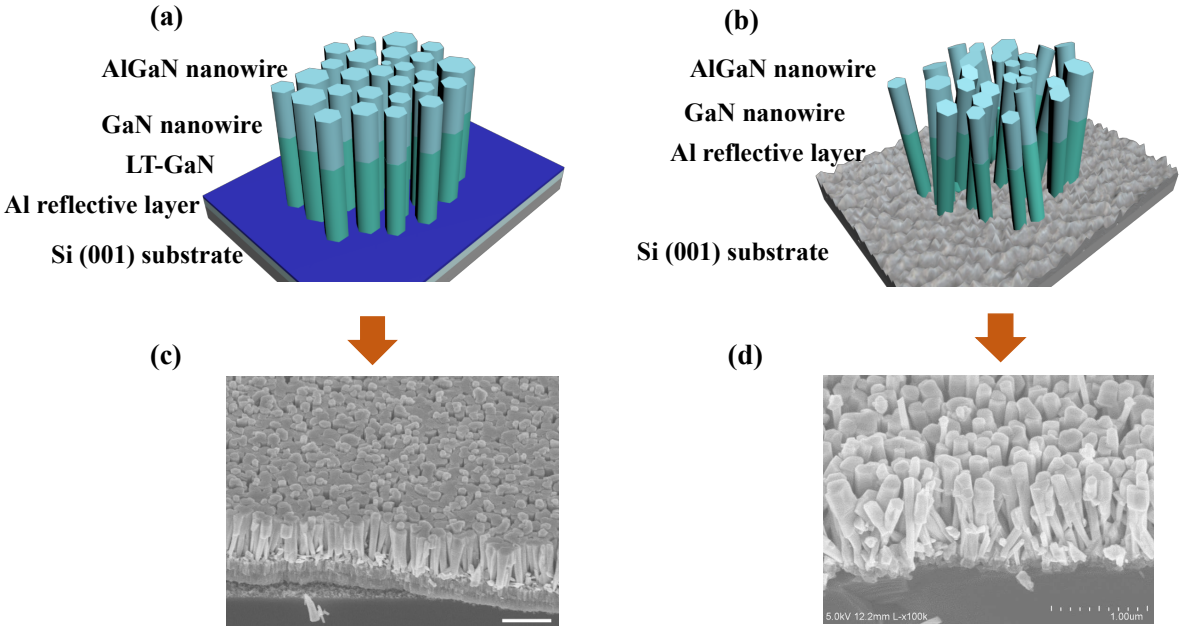

Figure 5.1. (a) Schematic of AlGaN nanowires grown on a LT-GaN buffer on Al-coated Si substrate. (b) Schematic of direct growth of AlGaN nanowires on Al-coated Si substrate. (c) SEM image of GaN/AlGaN nanowires vertically integrated on Al-coated Si. (d) SEM image of randomly tilted AlGaN nanowires grown directly on Al-coated Si substrate. The SEM images were taken with a 45° tilting angle.[87]

Subsequently, AlGaN nanowires were grown on the GaN nanowire template. The nitrogen flow rate was decreased to 0.4 sccm to enhance Al migration which was found to be essential to improve crystal quality.[39] A series of AlGaN samples were grown with the same Al BEP of 2.5×10^{-8} Torr while the Ga BEP was varied between 1×10^{-7} and 3.5×10^{-8} Torr in order to tune the emission wavelengths. As indicated by the blue, red and black curves in Figure 5.2, the PL spectra

exhibit a consistent blueshift with decreasing Ga BEP, and the full-width-at-half-maximum (FWHM) are ~20 nm. In order to achieve shorter wavelengths, the growth temperature for AlGaN nanowires was further raised to enhance Al adatom migration and Ga adatom desorption. AlGaN nanowire arrays with an emission wavelength of 288 nm, corresponding to Al composition of ~40% in the UV-B region was obtained at a growth temperature of 820 °C.

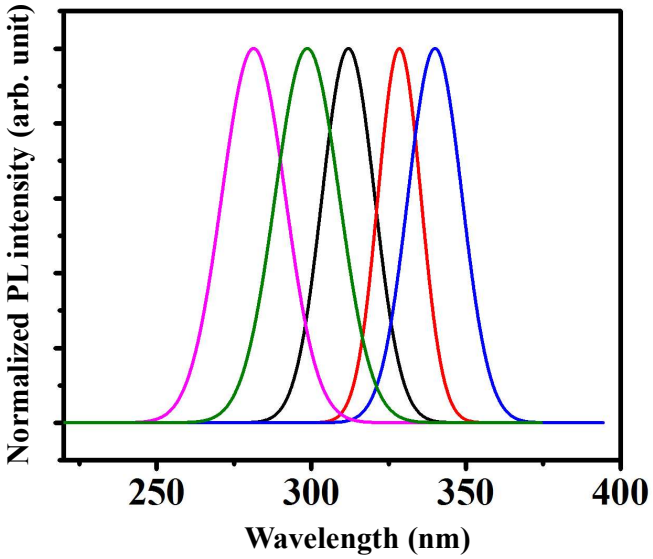

Figure 5.2. Normalized PL spectra of samples grown under different Ga BEP and substrate temperatures with a nitrogen flow rate of 0.4 sccm. The blue, red and black curves correspond to samples grown with Ga BEP of 8×10^{-8}, 6×10^{-8} and 3.5×10^{-8} Torr, respectively at a substrate temperature of 780 °C. The green and magenta curves correspond to samples grown at a substrate temperature of 800 °C and 820 °C, respectively, with Ga BEP ~3.5×10^{-8} Torr and Al BEP ~2×10^{-8} Torr.[87]

5.4 Structural Characterization of Al-rich AlGaN NW on Al Coated Si

We have subsequently investigated structural properties of AlGaN nanowires grown on Al template. A cross-sectional specimen of the grown AlGaN/GaN nanowires with an emission wavelength of 288 nm was prepared by using an in-situ lift-out method performed using a FEI Helios 650 FIB/SEM dual beam system. Structural properties of the sample were studied using a

JEOL JEM-3100R05 analytical electron microscope with double Cs-correctors operated at 300 keV. Figure 5.3a shows the typical cross-sectional STEM bright field (BF) image of the GaN/AlGaN nanowires grown on Al coated Si substrate, wherein individual layers of the heterostructure can be clearly distinguished in the light of the varying image contrast. The GaN/AlGaN nanowires feature a large diameter of 200-350 nm and are nearly vertically aligned to the substrate. High resolution (HR) HAADF image of the red outlined region in Figure 5.3b confirms the AlGaN segment is nearly free of TDs and SFs. Fast Fourier transform (FFT) (shown in Figure 5.3d) of Figure 5.3b confirms that the nanowire grows along *c*-axis with sidewalls being *m*-planes. Figure 5.3c shows the STEM-HAADF image of the yellow-boxed region in Figure 5.3a, and the contrast variation along the lateral dimension indicates the presence of core-shell structure. Energy dispersive X-ray spectroscopy (EDAX) line profile analysis was further performed along line 1-2. Shown in Figure 5.3e, the Ga composition peak intensity increases toward the center of nanowire. In contrast, Al signals show a clear peak in the sidewall region and drop toward the center of the nanowire. This provides unambiguous evidence for the formation of a core-shell heterostructure, with the presence of an Al-rich AlGaN shell surrounding the AlGaN core. Such a core-shell heterostructure has also been observed in previous studies. The formation of Al-rich AlGaN shell provides effective carrier confinement in the nanowire LED active region and suppresses nonradiative surface recombination.[25] Figure 5.3f further shows a STEM-HAADF image of the interface between the nanowires and LT-GaN layer, which features a columnar morphology. Nucleation islands with sizes of ~75 nm were formed on top of the columns as pointed by the red arrows. These nucleation islands are significantly larger than their counterpart grown on Si substrate where a typical diameter of ~10 nm was reported,[68,161] resulting in a large diameter of the subsequent GaN/AlGaN nanowire. SFs were observed in the LT-GaN buffer

as shown in Figure 5.3g, while the HT-GaN nanowires were nearly free of TDs and SFs (Figure 5.3h).

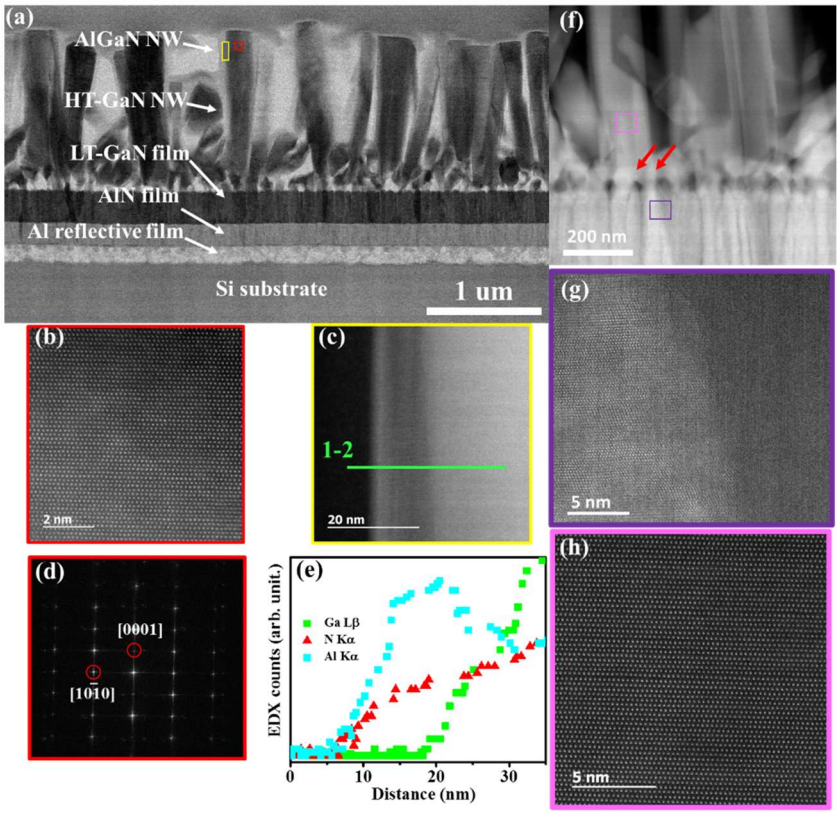

Figure 5.3. (a) Low magnification cross-sectional STEM BF image of AlGaN/GaN nanowires on Al coated Si (001) substrate. (b, c) HAADF-STEM images of red and yellow boxed region of the AlGaN nanowire region. (d) FFT image of (b) shows that the AlGaN/GaN nanowire grows along the *c*-axis direction. (e) EDAX line profile analysis along the lateral dimension of the AlGaN segment. (f) STEM-HAADF image of the interface between nanowires and LT-GaN layer. The red arrows point to the nucleation islands. (g) STEM-HAADF image of the purple-boxed region shows the out-of-plane crystallographic orientation of each column is aligned along the *c*-axis. (h) STEM-HAADF image of the magenta-boxed region in (f).[87]

5.5 Electroluminescence Measurement Results

The device schematic is shown in Figure 5.4a, which consists of ~150 nm Al reflective layer on Si(001) substrate followed by ~250 nm Ge-doped LT-GaN layer. Ge-doped HT-GaN

nanowire template was grown on top of the GaN buffer layer. Then *n*-AlGaN, i-AlGaN and *p*-AlGaN segments of 100 nm, 60 nm and 100 nm were grown sequentially on top of the HT-GaN nanowire template. The Ge concentration of *n*-AlGaN is ~5×10^{19} cm^{-3}, and the Mg concentration of *p*-AlGaN is ~1×10^{20} cm^{-3}. On top of the *p*-AlGaN segments, 5 nm of *p*-GaN contact layer was grown with Mg concentration ~5×10^{19} cm^{-3}. The fabrication of AlGaN nanowire DUV LEDs involves the use of standard lithography, plasma etching and contact metallization techniques. Ni (10 nm)/Au (10 nm) was deposited on top of the nanowire array using a tilted angle deposition to serve as *p*-metal contact. It's worthwhile mentioning that no filling materials were used to avoid the absorption of UV photons. Device mesa with various sizes was then patterned by photolithography and plasma etching using Cl_2/BCl_3/Ar. Al(100 nm)/Au(50 nm) was deposited on Ge-doped LT-GaN layer to serve as *n*-metal contact. *I-V* characteristics of the AlGaN *p-i-n* structures were measured under CW biasing condition. The devices showed a typical turn-on voltage of 7 V. The device specific resistance estimated from the linear region of the forward *I-V* characteristics (between 8 and 10 V) was ~35 ohm for AlGaN nanowire UV LEDs, shown in Figure 5.4b. The optical image of the device under 20 A/cm^2 injection current was shown in Figure 5.4b inset. EL from a device with an areal size of 300 μm by 300 μm was measured under different injection current densities. It can be observed that the peak emission wavelength is 288 nm which matches very well with the PL measurement results. The peak position is invariant of the injection current, shown in Figure 5.4c. The FWHM of the EL peak is ~17 nm. The measured EQE at room temperature under CW operation was shown in Figure 5.4d. It can be seen that the EQE first increases with injection current and reaches a maximum value of ~0.04 % at around 20 A/cm^2 before decreasing with further increasing current. It's worth noting that the obtained EQE of as-fabricated devices is severely limited by the following factors. First, a large portion of the emitted

light was absorbed by the Ni/Au *p*-contact layer atop AlGaN nanowires. Our previous finite-FDTD simulation showed that Ni/Au of ~25 nm could result in a low LEE of ~0.4%. In order to avoid DUV light absorption by the absorptive *p*-metal, nanowire coalescence could be introduced so that metal contact can be deposited around the edge of the devices. Secondly, the decreasing EQE with increasing current indicates the existence of electron overflow from the active region. Therefore, electron blocking layers with sufficient high barrier height are required to achieve a high carrier injection efficiency. Thirdly, the present GaN buffer absorbs UV emission shorter than 365 nm and an AlGaN buffer layer is required to achieve significantly enhanced EQE.

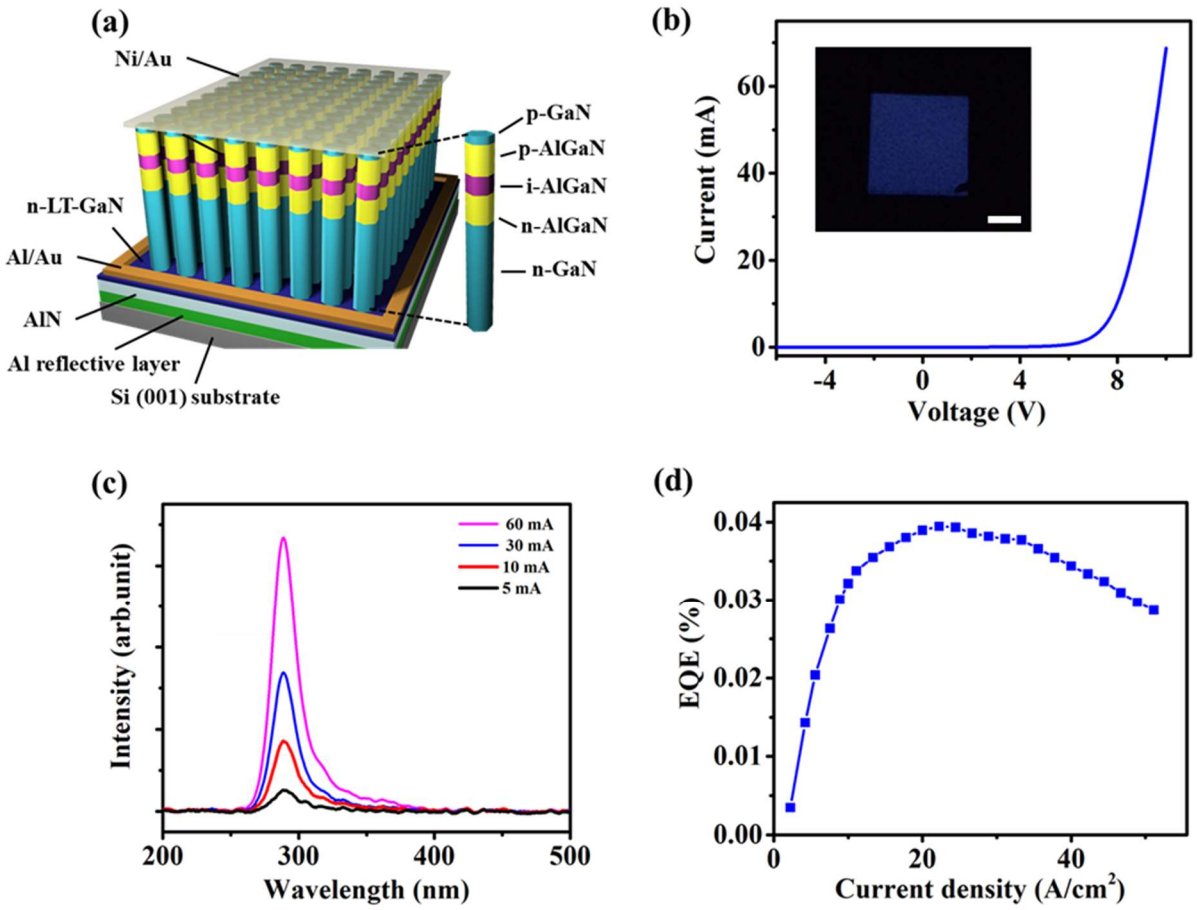

Figure 5.4. Characteristics of AlGaN nanowire LEDs. (a) Schematic of AlGaN nanowire based DUV LED on Al coated Si (001) substrate. (b) *I-V* characteristics of AlGaN nanowire LEDs emitting at 288 nm, with the inset showing the optical image of LED under an injection current of 20 A/cm^2. Inset scale bar: 100 μm. (c) EL spectra measured from AlGaN nanowire LEDs with different injection currents. (d) The measured EQE vs. injection current of a device emitting at 288 nm.[87]

5.6 Summary

In conclusion, we have demonstrated epitaxial growth of AlGaN nanowire heterostructures on Al coated Si substrate. We have shown that the utilization of LT-GaN buffer layer can overcome the out-of-plane tilting issue and lead to the formation of nanowires vertically oriented to the substrate. The as-grown nanowires feature diameters of >200 nm and uniform height distribution. AlGaN nanowires with PL wavelengths from 340 nm-288 nm have been successfully achieved by varying Al/Ga BEP ratio and growth temperature. Detailed structural characterizations suggest that the AlGaN nanowires are largely free of TDs and SFs. We have further demonstrated functional AlGaN nanowire LEDs on Al coated Si(001) substrate which exhibit relatively good *I-V* characteristics. A single peak EL emission at 288 nm was obtained under different current injections. EQE of ~0.04% was obtained at 20 A/cm^2 injection current. Further improved EQE is expected by removing the absorptive Ni/Au *p*-contact metal on top of the AlGaN nanowire array, reducing electron overflow by introducing electron blocking layers, and replacing GaN buffer with Al-rich AlGaN buffer layer.

Chapter 6 Mg-doped GaN Epilayers Grown on Si(001) Substrate Through Controlled Nanowire Coalescence

6.1 Author Contribution and Copyright Disclaimers

The contents of this chapter were published in Elsevier's Journal of Crystal Growth in September 2018,[160] for which I retain the right to include it in this thesis/dissertation, provided this thesis/dissertation is not published commercially. The co-authors were Yongjie Wang, Kai Sun, Anthony Aiello, Pallab Bhattacharya, and Zetian Mi from the University of Michigan. I designed, conducted and authored most of the work. Y. Wang contributed to the material growth process. K. S. contributed to the STEM characterization. A. A. contributed to the PL measurements. The work was supervised by Z. M., who contributed to the design of the experiments with P. B. as part of a collaboration. The STEM characterization was performed with technical support from the University of Michigan Center for Materials Characterization. This work was supported by US Army Research Office with award W911NF-17-1-0109, the University of Michigan College of Engineering, and NSF grant #DMR-0723032 (for the JEOL JEM 3100R05 AEM).

6.2 Introduction

III-nitride based semiconductors have been the subject of extensive research and development in recent years, largely driven by their application in LEDs and LDs and in high power and high frequency electronics.[17] For these applications, the realization of high quality GaN epilayers on large area Si substrates will contribute significantly to a reduction in cost, which are also compatible with existing processing lines commonly used in the electronics industry. However, direct growth of GaN epilayers on Si generally leads to the presence of very high densities of TDs as well as SFs due to the large lattice and thermal expansion coefficient

mismatches, which severely limit the device performance and reliability.[162-166] The GaN film crystalline quality was found to be improved using Al-rich buffer layers.[164] Nevertheless, the resistive Al-rich layer eliminates the possibility of vertically contacted LEDs fabricated on conducting Si and the potential integration of electronic and optical devices. A particular interest has been seen in growing GaN epilayers through lateral epitaxial overgrowth (LEO) and spontaneous coalescence of GaN nanowires which can be formed directly on Si with a low density of extended defects.[167-172] As GaN nanowires feature an extended 1D geometry, the LEO requires tuning the growth conditions so that the axial growth mode is suppressed while in-plane 2D expansion is promoted.

Li *et al*. demonstrated inducing GaN LEO through deactivating Ni catalyst on top of the nanowire array at higher growth temperature,[172] while Yeom *et al*. divided the LEO process into four steps with gradually increased trimethylgallium flux and growth temperature.[173] Averett *et al*. performed GaN LEO using PAMBE by switching growth parameters to a metal rich condition following nanowire growth.[171] Similar strategy was also adopted by Dogan *et al*. and they further noticed that the nanowire templates with a higher coalescence degree led to smaller grain size in the overgrown GaN.[174,175] Sekiguchi *et al*. studied the effect of Be doping in the overgrown GaN cladding layer and found that higher Be cell temperature generated a better surface flatness.[176] Despite the efforts and progress being made on GaN LEO using nanowire array,[177] several critical issues remain to be addressed before the realization of high performance optoelectronic devices. First of all, the incorporation of foreign metal catalyst during nanowire growth may cause impurity contamination during the GaN LEO. Secondly, overgrowth of the GaN film tends to proceed by filling the gaps in between the nanowires and the morphology features a fluid-like surface, especially when LEO is performed under metal rich condition.

Thirdly, there has been no demonstration of *p*-type conductivity of GaN epilayer formed through nanowire coalescence directly on Si substrate, which is essentially required in optoelectronic devices including LEDs, lasers and photodiodes.

In this chapter, we present a detailed investigation of GaN LEO using plasma-assisted MBE under nitrogen rich conditions, demonstrating a controlled lateral/axial nanowire growth rate by varying growth temperature. The axial/lateral growth ratio of nearly dislocation-free GaN nanowires on Si(001) can be modulated by nearly two orders of magnitude. As such, the transition from GaN nanowire arrays to coalesced GaN epilayers can be obtained through a relatively thin (~150 nm) intermediate layer, which leads to the subsequent formation of crack-free GaN epilayers on Si(001) substrate. Detailed STEM studies suggest that the resulting GaN epilayers are nearly free of dislocations and SFs. Controlled *p*-type conduction is further achieved for Mg-doped GaN epilayers. Hole concentrations in the range of 5×10^{16} - 5.6×10^{17} cm^{-3} were measured at room temperature, with mobility values ~ 3 $cm^2/V\cdot s$. Moreover, we have demonstrated a functional InGaN/GaN LEDs on Si(001) substrate, wherein the active region and *p*-contact layer consist of InGaN/GaN disk-in-nanowires (DINW) and Mg-doped GaN epilayers, respectively. The devices exhibited a turn on voltage of 2.7 V and strong emission at 525 nm. These studies offer a new path for potentially achieving high performance GaN-based optoelectronic devices on low cost, large area Si substrates.

6.3 Epitaxial Growth of Mg-doped GaN Epilayers on Si(001) Substrate

To evaluate the effects of the growth temperature on the radial growth rate of nanowires, we performed a series of two-step experiments. The first step is identical for all samples and consists of the synthesis of a vertically aligned GaN nanowire template, which has a height of 360 nm, with an areal density of 2×10^{10} cm^{-2} and an average diameter of 35 nm on Si(001) substrate,

illustrated in Figures 6.1a and 6.1e. During the second step, in order to induce lateral GaN growth following the growth of vertically aligned GaN nanowire template, the growth temperature is reduced and varied among the samples between 570 °C and 790 °C while the Ga and N flux are kept the same. The overgrowth duration for all the investigated samples was set to 15 mins. In contrast to the one-step growth experiment, this approach allows us to elucidate the influence of growth temperature on the axial and radial growth rate. Cross-sectional and plan-view SEM images of samples with the overgrowth temperature at 790 °C, 680 °C and 570 °C are shown in Figures 6.1b and 6.1f, 6.1c and 6.1g, 6.1d and 6.1h, respectively. It is observed that, with decreasing growth temperature, the nanowire length decreases, accompanied with an increase in the diameter, indicating that an opposing trend exists between the axial and lateral growth modes with decreasing temperature. Variations of the lateral growth rate vs. growth temperature are plotted in Figure 6.2. Specifically, at 790 °C, the nanowire primarily grows along the *c*-axis with an axial growth rate of 6 nm/min while the nanowire diameter remains nearly constant. At the lowest growth temperature of 570 °C, the axial growth rate reduces to 3.5 nm/min, close to the impinging Ga flux rate of 3.3 nm/min, while the lateral growth rate increases to 1.8 nm/min, a value comparable to the axial growth rate. The controlled scaling behavior can be well explained by taking into account the temperature-dependent Ga adatom diffusion, desorption and incorporation on both the top and side facets of nanowires.[66,70,178,179] At a high growth temperature, Ga adatoms feature a large diffusion length L of 40-45 nm.[70,180] Ga atoms impinging on the nanowire sidewall at distances to nanowire top facet less than L will be collected by the nanowire tip, resulting in an axial growth rate larger than the Ga impinging flux rate. On the other hand, Ga adatoms that impinge on the nanowire side facets with a distance to the top surface larger than L are thermally desorbed, leading to a negligible lateral expansion and a

primary one-dimensional axial growth mode. At a reduced growth temperature, however, both the thermal desorption and lateral migration of impingent Ga adatoms on the nanowire side facets are reduced, which lead to significantly enhanced lateral growth rate and simultaneously, a suppressed axial growth rate.

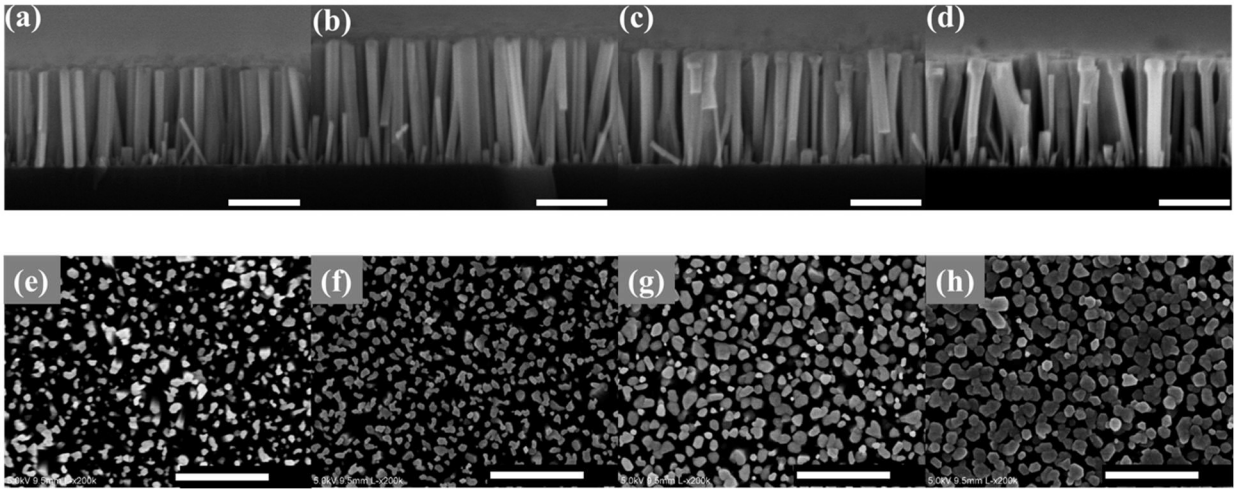

Figure 6.1. Cross-sectional and plan-view SEM images, respectively, of the GaN nanowire template grown at 790 ºC (a/e) and the overgrown nanowires at 790 ºC (b/f), 680 ºC (c/g) and 570 ºC (d/h). All the scale bars are 500 nm.[160]

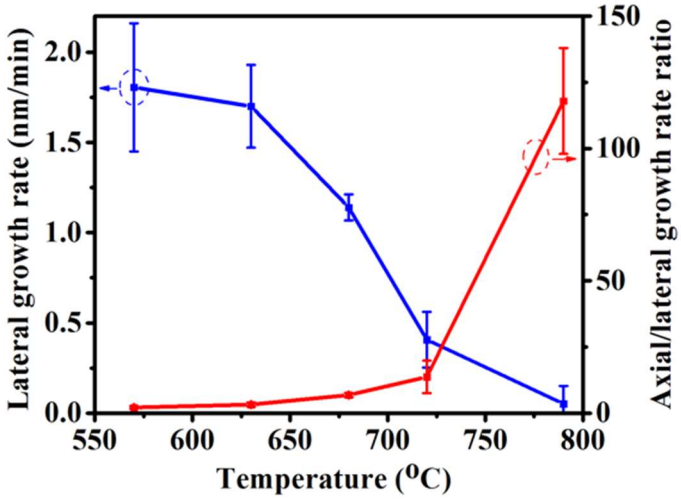

Figure 6.2. Temperature dependence of lateral growth rate (left axis) and axial/lateral growth rate ratio (right axis) of the overgrown GaN. The dots represent the experimental data, the solid blue and red lines are guidance to eye.[160]

6.4 Structural Characterization of Mg-doped GaN Epilayers on Si(001) Substrate

Figure 6.3a shows the cross-sectional SEM image of a planar GaN film after LEO duration of 4 hours at 630 °C. It can be observed that a fully coalesced, crack-free planar GaN epilayer of ~800 nm is formed atop the GaN nanowire template. The transition region between the GaN nanowires and planar GaN film features a small thickness of ~150 nm. The morphology is in sharp contrast with previously reported results where epilayer overgrowth proceeds by filling in the gaps between the nanowires under a metal rich growth condition. The bird's eye view SEM image (Figure 5.3b) of the fully coalesced GaN epilayer features a relatively flat surface where crystal grain mosaicity can be observed. The mechanism of the grain formation is discussed later.

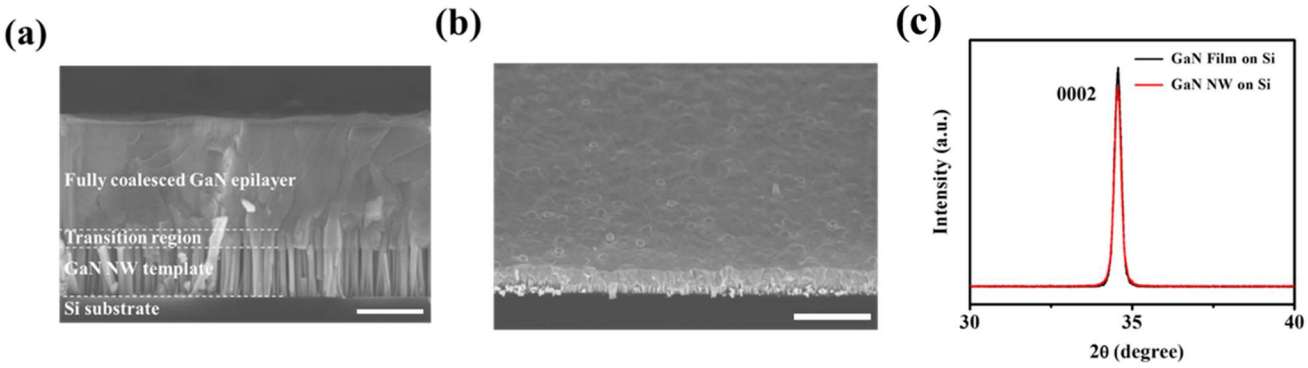

Figure 6.3 (a) A cross-sectional SEM image of overgrown GaN epilayer on GaN nanowire on Si (001) substrate. Scale bar: 500 nm. (b) Bird's-eye-view SEM image of overgrown GaN epilayer on GaN nanowire on Si (001) substrate. Scale bar: 2.5 µm. (c) XRD rocking curves of 600 nm GaN nanowire grown at 790 ºC on (001) Si substrate and 800 nm thick coalesced GaN grown at 630 ºC on Si.[160]

A cross-sectional specimen of the grown planar GaN epilayer was further prepared by using an in-situ lift-out method performed using a FEI Helios 650 FIB/SEM dual beam system. Structural properties of the sample were studied using a JEOL JEM-3100R05 analytical electron

microscope with double Cs-correctors operated at 300 keV. Selected area electron diffraction (SAED) patterns were taken in TEM mode, and both HAADF and BF images were taken in STEM mode simultaneously from same sample regions. Figure 6.4(a) shows the typical low magnification cross-sectional STEM-BF image of a fully coalesced GaN epilayer on top of GaN nanowires grown under nitrogen rich condition, wherein a sharp interface between the nanowire template and overgrown layers is further confirmed. The GaN nanowires feature a high uniformity in height and diameter and are also vertically aligned with the Si(001) substrate. Such GaN nanowires are nearly free of dislocations.[181] The variations in contrast from one region to another in the image indicate that the grown GaN epilayer atop GaN nanowire features multiple domains as pointed by the red arrows, indicating the existence of crystal grain mosaicity. A detailed examination of the epilayer microstructure was further performed by atom-resolved STEM imaging. Shown in Figures 6.4b and 6.4d are two high-resolution (HR) HAADF images taken at two adjacent boxed regions outlined as orange and red, respectively, in Figure 6.4a. No TDs or SFs were observed within each domain in the GaN epilayer. FFT power spectrum (shown in Figure 6.4c) of Figure 6.4b, as well as SAED pattern (Figure 6.4e) taken from the same region of Figure 6.4d confirms that the GaN film grows along the [0001] direction. The boundary (magenta boxed region) between the two adjacent domains was also studied by HR-STEM HAADF imaging (Figure 6.4f). It can be observed that while the $<11\bar{2}0>$ zone axis of the right domain is resolved, the left domain appears as totally featureless, indicating in-plane crystallographic orientation varies across the boundary. Therefore, the origin of domain formation can be attributed to in-plane crystallographic misalignment between the two adjacent domains. Figure 6.4g further shows a HR-HAADF image taken from the transition region with only a few edge dislocations observed, which manifest a drastically decreased density as the growth evolves

into fully coalesced GaN epilayer. Shown in Figure 6.4h is the inverse FFT image of Figure 6.4g, which clearly shows that the periodicity of the edge dislocation increases as the epitaxy proceeds along the [0001] direction, showing a self-crystallographic alignment effect.

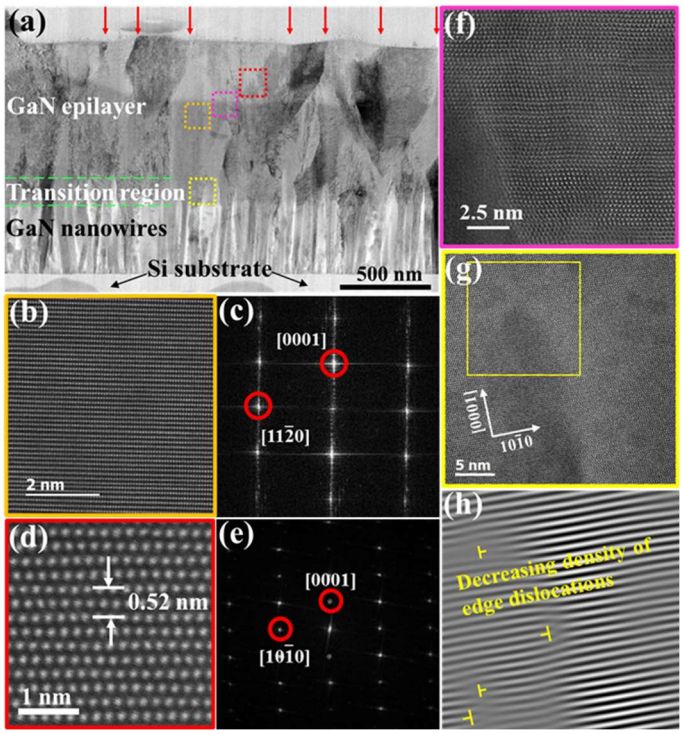

Figure 6.4. (a) Low magnification cross-sectional STEM BF image of overgrown GaN epilayer on GaN nanowire on Si (001) substrate. The red arrows point to the coalescence boundaries. (b, d, f) HR-STEM images of orange, red and magenta boxed region in the fully coalesced GaN epilayer. (c) FFT image of (b), and (e) SAED pattern of (d) show that the GaN epilayer grows along the *c*-axis direction. (g) HR-HAADF image from the yellow boxed region in the transition zone showing a reducing edge dislocation density along the growth direction. (h) Fourier-filtered HR-HAADF image corresponding to the $(10\bar{1}0)$ plane showing the increased dislocation periodicity as the epitaxy proceeds along the $[0001]$ direction.[160]

6.5 Photoluminescence, Hall Measurement and Electroluminescence Measurement Results

For practical device applications, it is essential to demonstrate efficient *p*-type conduction in the coalesced GaN layers on Si(001) substrate. Schematic shown in Figure 6.5a is the coalesced

p-GaN epilayers for Hall effect measurement, which consists of 400 nm thick non-doped GaN nanowire grown on Si(001) substrate, a 250 nm thick non-doped GaN transition region, and a 750 nm thick Mg-doped GaN epilayer. We confirmed that the non-doped GaN transition layer had a high resistivity of 2×10^8 Ω·cm, suggesting a very low background carrier concentration which can be attributed to the reduced density of donor-related defects and high crystalline quality.[182,183] The Mg-doped GaN epilayers were grown at 630 ºC with Mg cell temperatures varied in the range of 240-320 °C. Hall measurements were performed at room temperature on the *p*-GaN film using van der Pauw patterns. The metal contacts consist of Ni (20 nm)/Au (100 nm) deposited by e-beam evaporator and were annealed at 550 ºC in N_2 ambient for 1 min to form ohmic contact. Shown in Table I, the hole concentrations first show an increasing trend with increasing Mg cell temperature and reach a maximum value of 5.6×10^{17} cm^{-3} for Mg cell temperature 290 °C. Further increasing Mg cell temperature to 320 °C, however, results in a reduced hole concentration to 2×10^{16} cm^{-3}, which is likely due to the formation of compensation defects at high doping concentrations.[184,185] To our knowledge, this is the first report on the demonstration of controlled *p*-type conduction for Mg-doped GaN epilayers through nanowire coalescence on Si substrate. Figure 6.5b shows the room temperature PL obtained from the *p*-GaN epilayer with the highest hole concentration. The inset of Figure 6.5b is the cross-sectional SEM image of the corresponding sample in which the three layers are clearly identified. The emission features a dominant 3.2 eV peak which can be attributed to the isolated Mg acceptors related free to bound recombination (Mg^0, e) in line with previous reports.[186,187] Some additional equally spaced (~0.13 eV) peaks are also observed, which matches the Fabry-Perot mode originating from the reflection between the *p*-GaN/air interface and the planar GaN/nanowire interface.

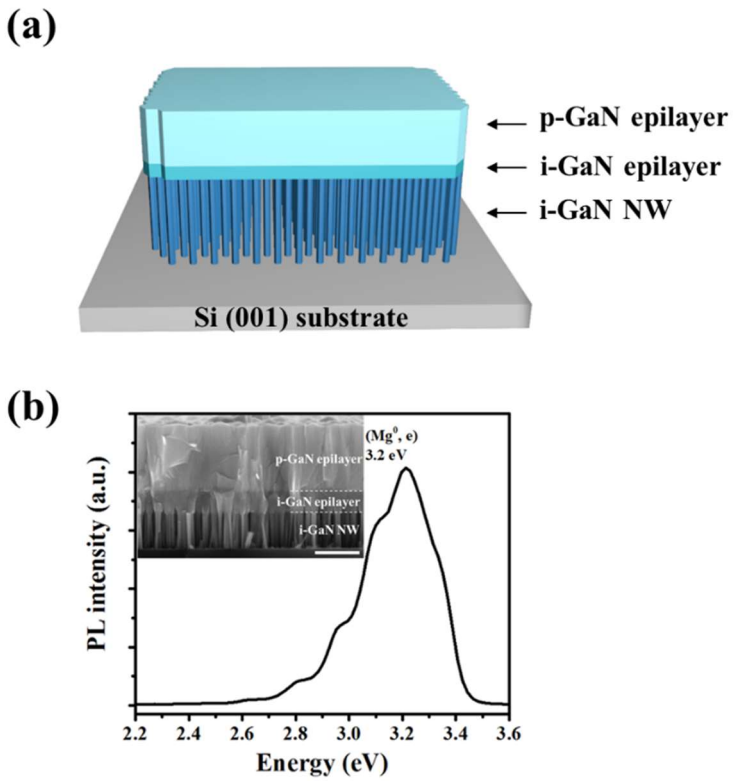

Figure 6.5. (a) Schematic consists of *p*-GaN epilayer, non-doped GaN transition layer and non-doped GaN nanowire on Si (001) substrate. (b) Measured PL spectrum from Mg-doped GaN with hole concentration of 5.6×10^{17} cm^{-3} at 300 K. The inset shows a cross-sectional SEM image of the corresponding sample with 750 nm thick *p*-GaN epilayer, 250 nm thick non-doped GaN epilayer and 400 nm thick non-doped GaN nanowire on Si (001) substrate.[160]

6.6 InGaN/GaN Nanowire LEDs with Coalesced *p*-GaN as Hole Injection Layer

Finally, with the use of coalesced GaN epilayer, we have demonstrated a functional nanowire LED on Si (001). The device heterostructure consist of *p* (planar GaN)-*i* ($10\times In_{0.34}Ga_{0.66}N$/GaN DINW array)-*n* (GaN nanowire), shown in the inset of Figure 6.6.[188,189] The *p*-GaN film was grown under the same conditions as described above. The device area of 300×300 μm^2 was defined through standard lithography followed by mesa etching. The *p*-ohmic contact on the top planar GaN layer was formed with Ni/Au and the *n*-ohmic contact was formed on the silicon substrate using Al. The measured current voltage characteristics are shown in Figure 6.6, which exhibit a sharp turn on voltage of 2.75 V. A small leakage current ~50 nA is measured under 3 V reverse bias. The device exhibit strong emission in the green spectrum.

The measured electro-luminescence spectrum under an injection current density 117 A/cm^2 is shown in the lower inset of Figure 6.6. It is worth noting that compared with previously reported conventional nanowire based LED on Si substrate, the incorporation of planar *p*-GaN contact layer significantly reduces the fabrication complexity of nanowire array based devices.[190-192] Furthermore, the planar *p*-GaN epilayer also contributes to forming a more robust electrical connection with the metal contact, leading to more stable device operation.

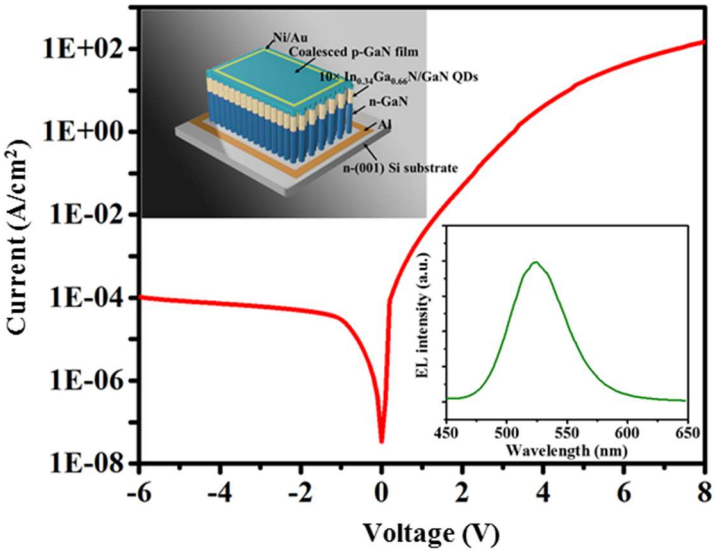

Figure 6.6. *I-V* characteristics of the *p*(planar GaN)-*i* (10×$In_{0.34}Ga_{0.66}N$/GaN DINW array)-*n*(GaN nanowire) on *n*-type(001) Si. The insets show the device schematic and EL of the fabricated *p-i-n* LED at room temperature under an injection current density of 117 A/cm^2.[160]

6.7 Summary

In conclusion, we have demonstrated controlled *p*-type conduction of GaN epilayers grown on Si(001) substrate through nanowire coalescence. We have shown that the axial/lateral growth rate ratio can be drastically modulated by varying the growth temperature. This controlled scaling behavior leads to the formation of high quality, nearly dislocation-free, fully coalesced planar GaN epilayer obtained on top of the nanowire array. Detailed STEM studies further confirm the GaN epilayer on Si(001) substrate is nearly free of TDs and SFs while its in-plane crystallographic

orientation varies from region to region. The highest obtained hole concentration is 5.6×10^{17} cm^{-3} at room temperature, with hole mobility ~3 $cm^2/V\cdot s$. The realization of relatively efficient *p*-type conduction of coalesced GaN epilayers is further confirmed by the demonstration of a GaN-based nanowire LED on Si substrate, wherein a Mg-doped GaN coalesced epilayer serves as the *p*-contact layer. This work provides a cost-effective approach for realizing high performance GaN-based devices on large area Si substrate.

Chapter 7 Micrometer Scale InGaN Green Light Emitting Diodes with Ultra-Stable Operation

7.1 Author Contribution and Copyright Disclaimers

The contents of this chapter were submitted to AIP Publishing's Applied Physics Letters in March 2020, for which I retain the right to include it in this thesis/dissertation, provided this thesis/dissertation is not published commercially. The co-authors were Xianhe Liu, Yakshita Malhotra, Yi Sun, and Zetian Mi from the University of Michigan. I designed and conducted part of the work. X. L. conducted theoretical simulation and contributed to the device fabrication and EL measurements. X. L. and Y. M. contributed to the PL measurements. X. L., Y. M. and Y. S. contributed to the material growth process and related substrate preparation. The work was supervised by Z. M., who contributed to the design of the experiments. The work was supported by NS Nanotech Inc. The authors are also thankful for the discussions with Dr. Matthew Stevenson and Mr. Seth Coe-Sullivan from NS Nanotech Inc.

7.2 Introduction

High efficiency, high brightness LEDs with sizes on the order of micrometer scale are highly desired for a broad range of applications, including ultrahigh resolution mobile displays, virtual/mixed/augmented reality, and biomedical sensing and imaging, to name just a few.[193-204] In this regard, the development of GaN-based micro LEDs has attracted significant interest in the past decade. To date, however, it has remained challenging to realize high efficiency LEDs on the micrometer scale using conventional organic, or inorganic materials. While GaN-based large area blue QW LEDs can exhibit high efficiency emission, the efficiency degrades drastically with reducing device size, which has been limited, to a large extent, by the surface recombination and poor *p*-type conduction induced by top-down etching.[205-207] Moreover, to achieve green

emission, relatively high indium compositions are required in the QW active region, which increases the formation of defects, dislocations, and phase separation, resulting in weak and broad emission and therefore poor device efficiency and color quality.[208-210] The performance of InGaN-based QW LEDs also suffers severely from quantum-confined Stark effect, particularly in the green spectrum, due to the strain-induced polarization field, which leads to unstable operation, *e.g.,* significant shift in the emission wavelengths with increasing current.[211,212] Organic LEDs, on the other hand, suffer from poor stability, low brightness and drastically reduced efficiency with decreasing size.[213]

Recent advances of III-nitride nanocrystals provide distinct opportunities to realize micrometer scale light emitters with high efficiency and highly stable operation.[197,214-219] Due to the efficient surface strain relaxation, such nanostructures are largely free of dislocations.[220-224] While considerable efforts have been devoted to nanowire LEDs with a lateral *p-i-n* configuration by metal-organic chemical vapor deposition (MOCVD),[225-232] recent studies suggested that nanowire LEDs employing a vertical *p-i-n* configuration can significantly simplify the device fabrication process.[17,218,233] The emission wavelengths can be tuned across nearly the entire visible spectrum by varying indium compositions in the quantum dots embedded in the nanowire structure.[197,234] Surface recombination, a major limiting factor for the efficiency of nano and microscale LEDs, can be largely suppressed by employing a unique core-shell structure surrounding the device active region.[235,236] Significantly, highly stable and efficient photoluminescence emission, which is insusceptible to temperature-dependent bandgap and quantum-confined Stark effects commonly seen in wurtzite InGaN structures, was observed in InGaN nanowire structures by employing the scalable band-edge modes in InGaN nanowire

photonic crystals.[237] To date, however, the realization of such devices on the micrometer scale under direct electrical injection has remained elusive despite a report on large area devices.

In this work, we report on the demonstration of InGaN photonic nanocrystal tunnel junction surface-emitting green LEDs, which are designed to operate at the Γ point of the photonic band structure. The device active region has an areal size of ~3 μm^2. The EL spectra exhibit a very narrow linewidth of ~4 nm, which is nearly five to ten times smaller than that of conventional InGaN QWs operating in this wavelength range. Significantly, the device shows highly stable emission. There are virtually no variations of the emission peak with increasing current density, suggesting the insusceptibility to quantum-confined Stark effect if there is. There are virtually no variations of the emission peak with increasing current density, suggesting the absence of quantum-confined Stark effect. The external quantum efficiency exhibits a sharp rise with increasing current and reaches a maximum at ~5 A/cm^2, which is comparable to conventional blue QW LEDs. A relatively small (~30%) efficiency droop was measured at an injection current density over 200 A/cm^2 at room temperature. Such small size, ultra-stable LEDs are ideally suited for near-eye display applications.

7.3 Optical Design of InGaN Photonic Nanocrystal LEDs

The optical design of InGaN photonic nanocrystal LEDs is first described. Schematically shown in Figure 7.1a, the nanocrystal array is arranged in a triangular lattice, with the lateral size and lattice constant of the nanocrystals denoted as *d* and *a*, respectively. Shown in Figure 7.1b is the energy band diagram calculated using two-dimensional (2D) finite-element method for nanocrystal array with *d* =298 nm and *a* =280 nm. In this work, the InGaN photonic nanocrystal LEDs are designed to operate at the Γ point of the 4^{th} band (the blue curve in Figure 7.1b) photonic band structure where the in-plane wavevector is zero. As such, the overall wavevector is along the

vertical direction of the photonic nanocrystal array, which leads to direct surface emission. Furthermore, the group velocity is significantly reduced at the Γ point, resulting in long interaction time for the optical field and the active medium. Strong resonance at the corresponding wavelength can therefore be expected, which can lead to significantly reduced spectral linewidth. The normalized frequency of the Γ point of the 4th band is ~ 0.504, which corresponds to a wavelength of ~555 nm for the lattice constant 280 nm. Since the emission is largely governed by the optical resonance of the photonic nanocrystal, rather than the semiconductor active medium itself, light emission of such LEDs is expected to be highly stable and relatively invariant with temperature and injection current.

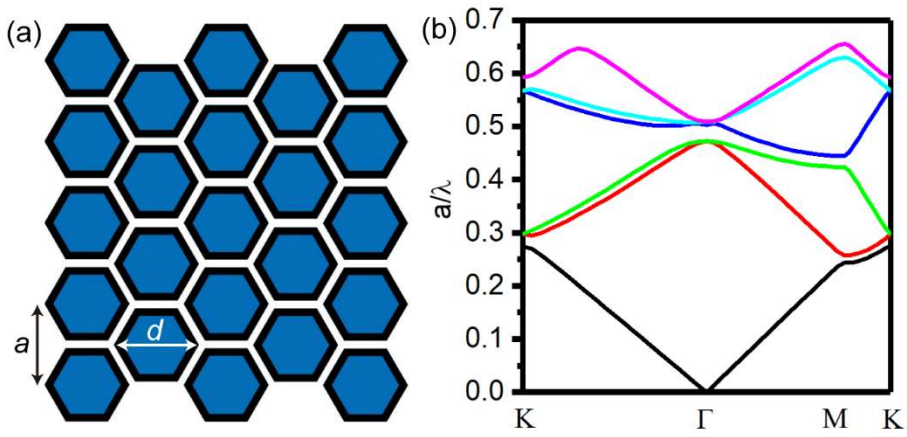

Figure 7.1. (a) Schematic for a triangular lattice photonic crystal with a lattice constant a and a lateral size of d. (b) The band structure of a triangular lattice photonic crystal with a lattice constant a=280 nm and a lateral size d=298nm.

7.4 Epitaxy and Characterization of InGaN Photonic Nanocrystal LEDs

Experimentally, the technique of SAE was used to grow InGaN photonic nanocrystal LED structures. The growth was performed on n^+-GaN template on sapphire substrate using a Veeco GEN 930 MBE system equipped with a radio frequency plasma-assisted nitrogen source. Shown in Figure 7.2a, the LED structure consists of ~450 nm n^+-GaN layer, six vertically aligned

InGaN/AlGaN quantum dots, 60 nm p^{+}-AlGaN cladding layer, p^{++}-GaN/n^{++}-GaN tunnel junction, 60 nm *n*-GaN layer and n^{++}-GaN contact layer. Si and Mg were used as the n and *p*-type dopant, respectively. The use of AlGaN, instead of GaN barrier during the growth of quantum dot active region promotes the formation of an Al-rich AlGaN shell structure surrounding the active region, which can significantly reduce surface recombination. In this study, the average Al composition is estimated to be ~5%.[214,236] Prior to the growth process, nano-patterned substrates were prepared for the SAE of nanocrystals to facilitate the formation of highly regular nanocrystal arrays. Firstly, a thin (~10 nm) Ti layer was deposited as the growth mask on GaN-on-sapphire substrate. E-beam lithography and reactive ion etching techniques were used to define openings on the Ti mask. Under optimum growth conditions, nanocrystals were only formed in the opening apertures, with no epitaxy taking place on the Ti mask layer. The resultant nanocrystal arrays are shown in Figure 7.2b, which exhibit very high uniformity in position and dimension. Photoluminescence spectrum is collected using a fiber placed exactly on top of the sample at a distance of one inch and the acceptance angle is estimated to be ~1.13°. With careful control over the spacing between nanocrystals and the lattice constant, strong resonance in the green spectrum is observed from the PL of an InGaN photonic nanocrystal array with a lattice constant of 280 nm and a spacing of around 20 nm, shown in Figure 7.2c. Too thin layer above the active region can prevent the observation of such strong resonant peak, which is considered to be due to poor optical confinement in the vertical direction or poor optical isolation from the scattering loss at the non-flat nanocrystal/air boundary.

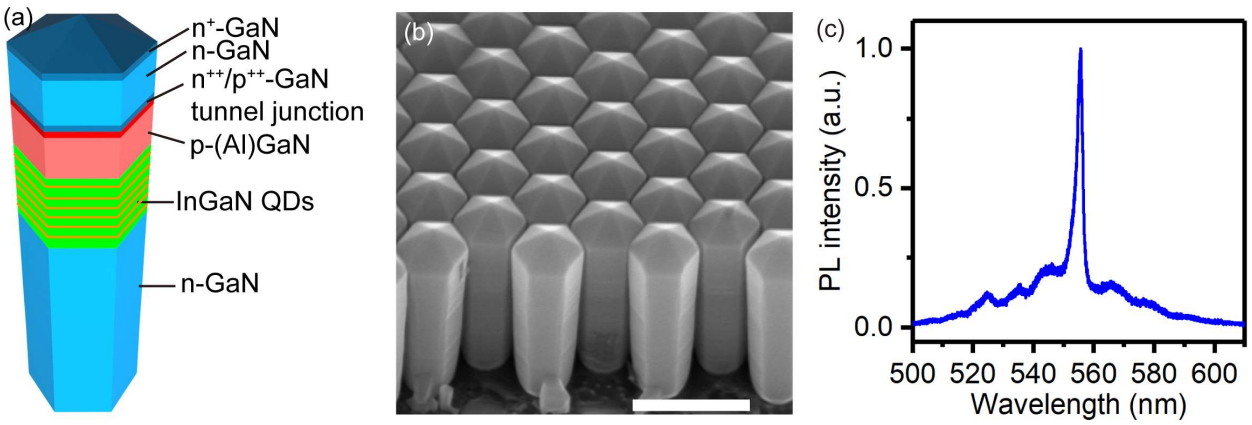

Figure 7.2. (a) Schematic of the InGaN dot-in-nanowire tunnel junction LED heterostructure. (b) SEM image of an InGaN photonic nanocrystal array. The scale bar represents 500 nm. (c) PL spectrum for an InGaN photonic nanocrystal array measured at room temperature, showing a pronounced emission peak corresponding to the resonance wavelength of the Γ point in the photonic band structure.

7.5 Fabrication of InGaN Photonic Nanocrystal LEDs

Microscale LEDs were subsequently fabricated using the photonic nanocrystal arrays grown by SAE. The device schematic is shown in Figure 7.3a. The fabrication process is similar to that of conventional planar QW LEDs. A 300 nm thick silicon dioxide layer was firstly deposited by plasma-enhanced chemical vapor deposition for surface passivation and isolation. Photolithography and wet chemical etching were performed to create openings in the silicon dioxide layer, which defines the device active area for current injection. A metal stack consisting of 5 nm Ti and 5 nm Au was deposited by e-beam evaporation. Subsequently, a 180 nm thick indium tin oxide layer was deposited by sputtering. A metal stack of 5 nm Ti and 5 nm Au was also deposited on the *n*-type GaN template as the *n*-contact metal. An annealing was then performed at 400℃ for one minute under nitrogen ambient. Finally, a thick metal layer was deposited by e-beam evaporation as the contact pad to facilitate electrical probing and measurements. The current-voltage (*I-V*) characteristics are shown in Figure 7.3b. The device has a turn-on voltage ~4 V, with negligibly small reverse bias leakage. The current density can readily

reach 100 A/cm^2 at ~7 V without any degradation of the *I-V* characteristics. The electrical performance can be further improved by optimizing the doping and fabrication process. Shown in the inset of Figure 7.3b is the image of an LED taken under room light, showing strong green light emission.

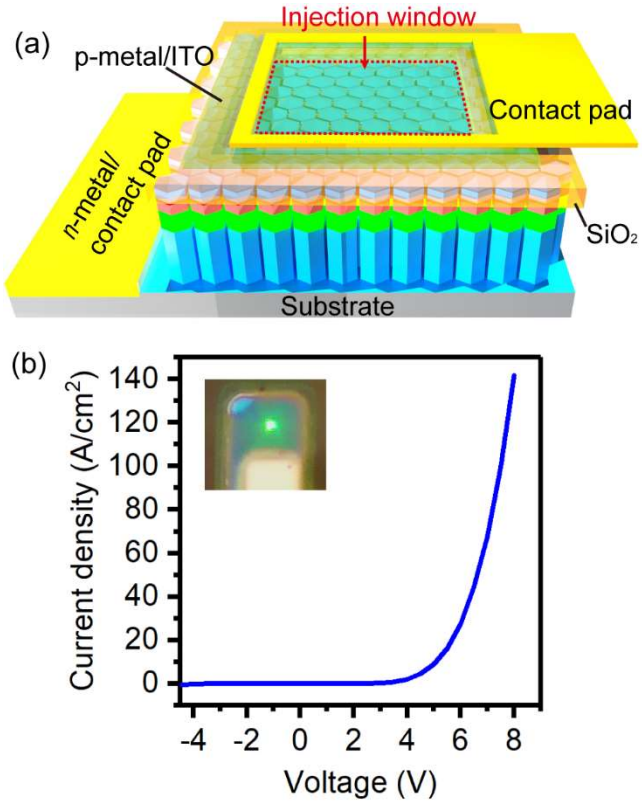

Figure 7.3. (a) Schematic of a fabricated microscale LED (not drawn to scale). (b) *I-V* characteristics of InGaN photonic nanocrystal LED. Inset: image of a microscale LED under room light, showing strong green emission.

7.6 Output characteristics of InGaN Photonic Nanocrystal LEDs

The output characteristics of InGaN photonic nanocrystal LEDs were further measured in detail. The electroluminescence (EL) spectra were measured using fiber in the same way as photoluminescence for current densities varying from 0.5 A/cm^2 to over 200 A/cm^2, shown in Fig. 4(a). The EL spectra were measured for current densities varying from 0.5 A/cm^2 to over 200 A/cm^2, shown in Figure 7.4a. The emission spectra exhibit a pronounced peak emission at ~548

nm. The spectral linewidths are measured to be ~4 nm, which is nearly five to ten times smaller than those of conventional InGaN QW LEDs in this wavelength range. Moreover, it is seen that the emission peak does not show any noticeable shift or broadening with increasing current. Such distinct emission characteristics have not been measured in any conventional planar InGaN QW LEDs in this wavelength range. The relative EQE, defined as the integrated EL intensity divided by current density, is shown in Figure 7.4b. The relative EQE shows a sharp increase with injection current density and reaches a maximum at ~5 A/cm^2, which exhibits a trend that is comparable to conventional high efficiency blue LEDs.[196] The sharp rise of EQE with injection current suggests a very small Shockley-Read-Hall recombination coefficient, which is attributed to the significantly reduced defect formation in nanocrystals and suppressed nonradiative surface recombination with the use of core-shell dot-in-nanowire active region. The efficiency droop is moderate, with only ~30% drop in the EQE at a current density of more than 200 A/cm^2. Such moderate efficiency droop also suggests a small Auger recombination coefficient in nearly defect-free InGaN nanocrystals.

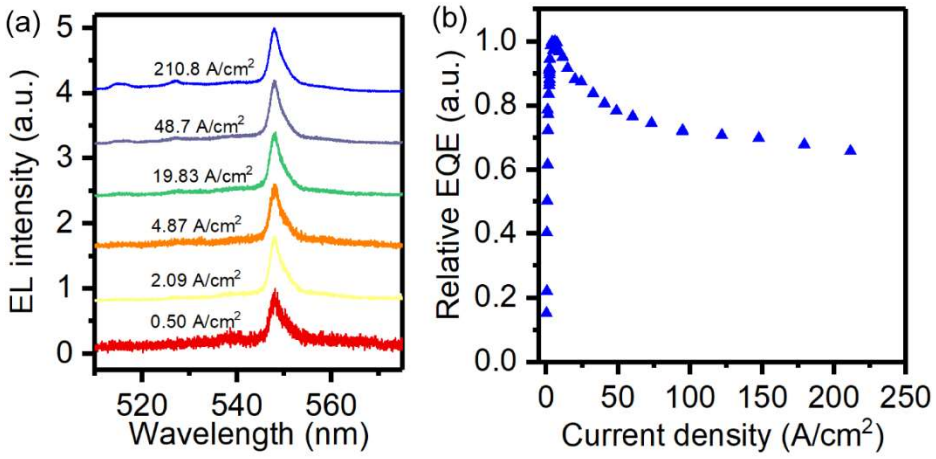

Figure 7.4. (a) EL spectra of InGaN photonic nanocrystal LED measured under varying injection current at room temperature. (b) Variations of relative EQE vs. injection current density.

More detailed analysis on the emission properties of InGaN photonic nanocrystal LEDs were further performed. Shown in Fig. 5(a), the peak position remains extremely stable within a range of 0.13 nm centered at ~548 nm as the injection current density increases from 0.5 A/cm^2 to 211 A/cm^2. Shown in Figure 7.5a, the peak position remains extremely stable at ~548 nm as the injection current density increases from 0.5 A/cm^2 to 211 A/cm^2. Significantly, the spectral linewidths are nearly invariant with injection current. Variations of the full-width-at-half-maximum (FWHM) of the EL spectra are shown in Figure 7.5b. The FWHM only varies between 3 nm and ~3.7 nm as the injection current density increases from 0.5 A/cm^2 to 211 A/cm^2. It is worthwhile mentioning that these measurements were performed at room temperature without any active cooling. For comparison, conventional InGaN QW light emitters in this wavelength range suffer severely from quantum-confined Stark effect, which exhibits significant blue-shift in the emission with increasing current, accompanied with a large spectral broadening due to band filling effect. The extraordinary stability of InGaN photonic nanocrystal LEDs is attributed to the reduced strain distribution of InGaN dot-in-nanowire structures and, more importantly, the strong resonance at the Γ point of the photonic band structure, which largely governs the emission characteristics and is only determined by the geometry of photonic nanocrystals. These studies further suggest that InGaN photonic nanocrystals grown by MBE are extremely stable even under harsh operating conditions. Such ultra-stable small size LEDs without the use of any active cooling is highly desired for near-eye display applications. It is also worth pointing out that the FWHM depends on the acceptance angle of the collected emission because the emissions at other wavelengths, which is at other angles, are not suppressed. Large acceptance angle inevitably collects light at other wavelengths emitted at various oblique angles, which makes the overall spectrum broader.

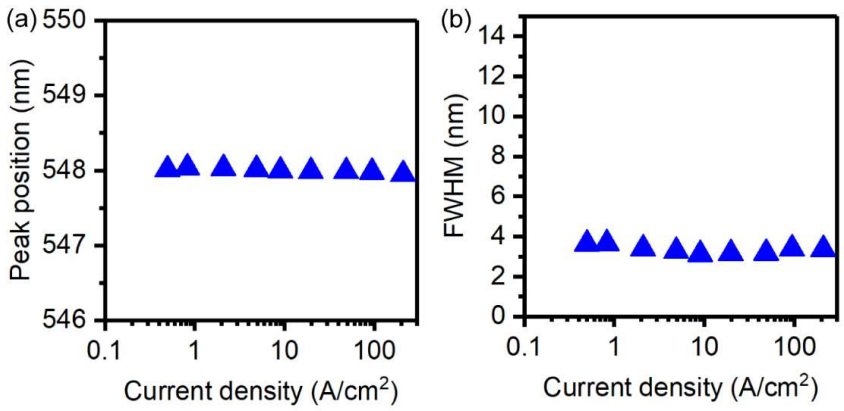

Figure 7.5. Variations of (a) peak position and (b) FWHM with injection current density.

The far-field angular distribution of the emission was studied by collecting EL emission with a fiber mounted on a rotation stage. The distance between the fiber and the LED is one inch. The angular resolution is 2°. The EL intensity at each emission/collection angle was calculated by integrating over a spectral range from 543 nm to 553 nm. Shown in Figure 7.6 is the angular distribution of the EL intensity. It is seen that the emission is mainly distributed along the vertical direction, with a divergence angle ~10 degrees. This small divergence angle does not come from reflection by metal layers in surrounding regions since they are on a non-flat SiO2 layer conformally deposited on nanocrystals and thus non-flat and nonideal for directional reflection. Such optics-free, highly directional emission is directly related to the surface-emission mode at the Γ point of InGaN photonic nanocrystal structures described earlier, which can greatly simplify the design and reduce the cost of next-generation ultrahigh resolution display devices and systems.

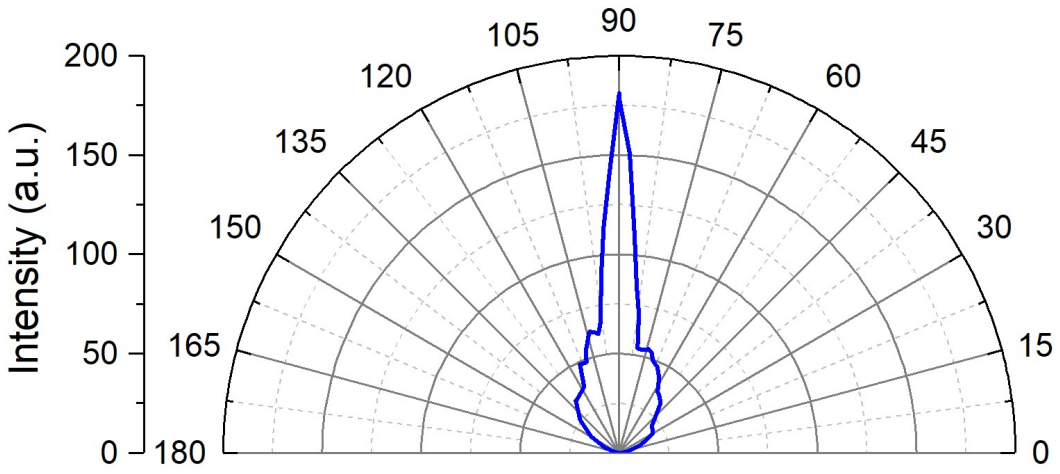

Figure 7.6. Far-field angular distribution of EL intensity.

7.7 Summary

In conclusion, we have demonstrated microscale green LEDs utilizing InGaN photonic nanocrystals. By exploiting the unique resonance properties of the photonic band structure, we show that such microscale devices can exhibit distinct emission characteristics, including a spectral linewidth that is five to ten times narrower than that of conventional InGaN QW LEDs, ultra-stable operation with the absence of QCSE commonly seen in QW devices in this wavelength range, and highly directional emission. Moreover, the micrometer size LEDs exhibit a small efficiency droop under high injection current. This study offers a new approach for achieving high efficiency, high brightness light emitters for next generation displays and for applications in the emerging virtual/mixed/augmented reality devices and systems.

Chapter 8 Conclusion and Future Work

8.1 Summary of Present Work

This thesis focuses on addressing some challenges in current green and UV LEDs by using III-nitride nanocrystals. III-nitride nanowires were synthesized through self-assembly and SAE on commercial Al_2O_3(001) and Si(111)/(001) substrates. InGaN with ~34% In composition was used for green emission and AlGaN with different Al compositions were used for UV-B and UV-C emissions. Chapter 3 to Chapter 6 focus on nanowires grown spontaneously on Si(111)/(001) or Al-coated Si(001) substrates. A series of growths with different III/V ratios, substrate temperatures have been performed and the optical and electrical properties of the as-grown materials have been systematically characterized by various of techniques including XRD, SEM, STEM, PL, *I-V*, EL, *etc*. The effects of different growth parameters on nanowire array morphology, defect formation and doping levels have been studied, which are paramount for high-performance optoelectronic devices. In Chapter 7 and 8, the SAE technique involving pre-masked substrate were discussed, which provides more precise manipulation on nanocrystal array properties including uniformity, density and light emitting properties. We show that nanocrystals grown by SAE with pre-designed lattice constant and spacing can form a two-dimensional photonic crystal, wherein the in-plane light propagation and the out-plane coupling properties including light extraction efficiency and directionality can be readily varied.

Chapter III focuses on controlling the large densities of defects and the extremely poor current conduction issues in AlN which is a ultrawide bandgap material and has tremendous promise for high-efficiency DUV optoelectronics and high-power/frequency electronics. Through a combined theoretical and experimental study, it is shown that such a critical challenge can be addressed for AlN by utilizing N-rich epitaxy. Under N-rich conditions, the *p*-type Al-substitutional Mg-dopant formation energy is significantly reduced by 2 eV, whereas the formation

energy for N-vacancy related compensating defects is increased by ~3 eV, both of which are essential to achieve high hole concentrations of AlN. Detailed analysis of the *I-V* characteristics of AlN *p-i-n* diodes suggests that current conduction is dominated by charge-carrier tunneling at room temperature, which is directly related to the activation energy of Mg dopants. At high Mg concentrations, the dispersion of Mg acceptor energy levels leads to drastically reduced activation energy for a portion of Mg dopants, evidenced by the small tunneling energy of 67 meV, which explains the efficient current conduction and the very small turn-on voltage (~5 V) for the diodes made of nanoscale AlN. This work shows that nanostructures can overcome the dopability challenges of ultrawide-bandgap semiconductors and increase the efficiency of devices.

Chapter IV reports on the molecular beam epitaxy and characterization of monolayer GaN embedded in N-polar AlN nanowire structures. DUV emission from 4.85 to 5.25 eV is measured by varying AlN barrier thickness. Detailed optical measurements and direct correlation with first-principles calculations based on density functional and many-body perturbation theory suggest that charge carrier recombination occurs predominantly via excitons in the extremely confined monolayer GaN/AlN heterostructures, with exciton binding energy exceeding 200 meV. We have further demonstrated DUV LEDs incorporating single monolayer and double monolayer GaN, which emits light at 238 nm and 270 nm, respectively. These unique DUV LEDs exhibit highly stable emission and a small turn on voltage around 5 V.

Chapter V demonstrated the epitaxial growth of AlGaN nanowires on Al coated Si(001) substrate. The as-grown nanowires feature diameters of >200 nm and relatively uniform height distribution. AlGaN nanowires with emission wavelengths from 340 nm to 288 nm have been successfully achieved by varying Al/Ga BEP ratio and growth temperature. Detailed structural characterization suggests that AlGaN nanowires grown on Al template are free of dislocations. We

have further demonstrated functional AlGaN nanowire DUV LEDs, which exhibit a turn-on voltage of 7 V and a single peak EL emission at 288 nm. The realization of high quality AlGaN nanostructures on reflective Al template provides a promising approach for achieving high efficiency DUV light emitters.

Chapter VI reports on a detailed investigation of MBE and characterization of GaN epilayers on Si(001) substrate through controlled nanowire coalescence. By varying the substrate temperature, the axial/lateral growth ratio of GaN nanowires on Si(001) can be modulated by nearly two orders of magnitude. As such, the transition from GaN nanowire arrays to coalesced GaN epilayers can be obtained through a relatively thin (~150 nm) intermediate layer, which leads to the subsequent formation of crack-free GaN epilayers on Si(001) substrate. Detailed STEM studies suggest that the resulting GaN epilayers are nearly free of dislocations and SFs. Controlled *p*-type conduction is further achieved for Mg-doped GaN epilayers. Hole concentrations of ~5.6×10^{17} cm^{-3} were measured at room temperature, with mobility values of ~3 $cm^2/V\cdot s$. Moreover, we have demonstrated functional InGaN/GaN LEDs on Si(001) substrate, wherein the active region and *p*-contact layer consist of InGaN/GaN disks-in-nanowires and Mg-doped GaN epilayers, respectively. The devices exhibited a turn on voltage of 2.7 V and strong emission at 525 nm.

In Chapter VII, we report on the demonstration of InGaN photonic nanocrystal LEDs, which operate in the green wavelength (~548 nm). The devices are designed to operate at the Γ point of the photonic band structure and exhibit a spectral linewidth ~4 nm, which is nearly five to ten times narrower than that of conventional InGaN QW LEDs in this wavelength range. Significantly, the device performance, in terms of the emission peak and spectral linewidth, is nearly invariant with injection current, suggesting the absence of QCSE commonly seen in InGaN

QWs. The external quantum efficiency is characterized by a sharp rise with increasing current and reaches a maximum at ~5 A/cm^2, which is comparable to conventional blue QWs LEDs. A relatively small (~30%) efficiency droop was measured at an injection current density over 200 A/cm^2 at room temperature without any active cooling.

8.2 Future work

8.2.1 Electrically Driven AlGaN Photonic Crystal Surface Emitting Lasers

UV and DUV light sources are in high demand in daily life, industrial and research area. The UV light at sufficiently short wavelengths can be used as a disinfection method (ultraviolet germicidal irradiation, UVGI) to kill or inactivate microorganisms or pathogens, since it can destroy the nucleic acids in these organisms so that their DNA is disrupted.[238] Therefore, it is useful for sterilization and water/air purification. UV light can accelerate the decomposition of organic compounds, which provides better solutions for environmental pollution and plastic recycling. UV radiation is helpful in the treatment of skin conditions such as psoriasis and vitiligo (UV light therapy).[239] Photography by reflected UV radiation is useful for medical, scientific, and forensic investigations, for the applications of detecting bruising of skin, alterations of documents, or restoration work on paintings. UV photography can also be used in astronomy to identify the chemical compositions of the interstellar medium, the temperature and the compositions of stars.[240] The fluorescence produced by UV illumination can be used in mineralogy, gemology, chemical sensors, fluorescent labelling, biological detectors and so on.[241] High-power UV light can be used for a speed curing process by photochemical reaction that instantly cures inks, adhesives and coatings.[242] UV spectroscopy, along with visible and IR spectroscopy, is routinely used to qualitatively determine the presence of elements and organic compounds by using absorption or transparency of the sample.[240]

However, the primary limitation of current applications is the existing UV and DUV sources. The conventional UV light sources are mercury lamps, Nd:YAG (solid-state) lasers or excimer lasers (for example ArF and Ar_2 lasers). These sources suffer from a low level of performance, poor reliability, significant size, and the emission of toxic substances. Compared with conventional light sources, semiconductor light-emitting devices are an ideal choice due to their reliability, compactness and high efficiency.

Semiconductor light-emitting devices have three configurations: LEDs, LDs with edge emission and surface emission. Compared with other two configurations surface-emitting lasers have various advantages. The emission light is perpendicular to the surface, so it could be integrated into two dimensional arrays. A large number of devices could be integrated on one wafer to give high output power. Circular beam makes it easy to be coupled into the fiber. Besides, it could be tested on wafer level during processing which greatly decreases the manufacturing cost. Compared to edge-emitting lasers, it has low temperature sensitivity due to its single-longitudinal-mode cavity.

The unique characteristics have enabled surface-emitting lasers as preferred optical sources in advanced biomedical sensing, including patient diagnostics, instruments for surgical procedures, and sensors attached directly to the body for monitoring purposes. Surface-emitting lasers operating at wavelengths of the UV-C band are potential enabling devices for small particle detection, high-accuracy medical treatment and high-resolution surface monitoring. For example, living subjects sensed commonly need to be immobilized, anesthetized, and repeatedly positioned. Changes in distance and orientation between the excitation source and subject may adversely affect spatial resolution and sensitivity.[243] Continuous long-term (days to weeks) sensing is impossible. UV surface-emitting lasers are particularly beneficial due to its smaller dimension,

less than or equal to 100 μm, which makes it most useful for in vivo biomedical applications where small size and high flexibility enable improved and less-traumatic access to remote areas of the body.[244] In addition, highly directional UV surface-emitting lasers with small divergence angle and high stability can be used for photodynamic medical therapies requiring minimally invasive treatment, in addition to a range of dermatological treatments, catheters, and other medical laser applications and diagnostic testing.

Despite of the fact that the emission wavelength of III-nitride surface-emitting lasers has completely covered the full visible spectrum, and the quantum cascade lasers based on the principles of electrons conducting intersubband transition in the QWs and the phonon-assisted resonant tunneling have also expanded the achievable wavelength range to the infrared and the terahertz regimes, it is of great challenge to develop the short-wavelength semiconductor lasers, especially the UV-C band semiconductor lasers. Since the first demonstration in 2008, there have been several groups that have reported electrically injected GaN-based surface-emitting lasers, wherein most of the reports have emission wavelengths above 400 nm.[245,246] The development of electrically pumped AlGaN based UV surface-emitting lasers has been limited by two major reasons. One arises from the poor internal quantum efficiency. High-density dislocations ($>10^9/cm^2$) are produced in high Al component AlGaN materials prepared by heteroepitaxy due to the lattice mismatch, which act as nonradiative recombination centers in the AlGaN-based optoelectronic devices, thus inhibiting their IQE. The other is the low carrier injection efficiency (CIE) caused by the low hole concentration in *p*-type AlGaN, which directly degrades the hole-related transport property. Moreover, reports of UV surface-emitting lasers have consisted of hybrid epitaxial dielectric, and dual dielectric DBR designs and from device fabrication point of view, fabricating highly reflective mirrors are challenging.

Two-dimensional AlGaN nanowire photonic crystal is proposed for surface-emitting lasers operation in the UV-B band. Figure 8.1a shows photonic band structure of a bottom-up AlGaN nanowire photonic crystal structure with triangular lattice, which is calculated using plane-wave expansion method. The information on the refractive indices of the AlGaN nanowires was obtained from AlGaN epilayer with identically Al composition which is measured independently by spectroscopic ellipsometer. The designed photonic crystal pattern has lattice constant of 180 nm and hexagonal nanowire diameter of d=150 nm. This photonic crystal structural parameters are chosen, such that the emission band of the optical gain material, coincides with the bandedge mode at Γ_1 point of ~0.57, which features vertical emission and is suitable for surface-emitting operation. The corresponding lasing wavelength is 315 nm which is in the UV-B band. Figure 8.1b shows the TM field intensity profiles of the Γ_1 point bandedge mode. The feedback mechanisms can be explained as $\mathbf{k}+(\mathbf{k}-2\mathbf{G}_i)=0$, which corresponds to the second order distributed feedback mode in the M direction. Under this condition six waves are coupled to form a Block wave. But a pair of counter-propagating waves realizes the major feedback, as indicated the black arrows in Figure 8.1b.

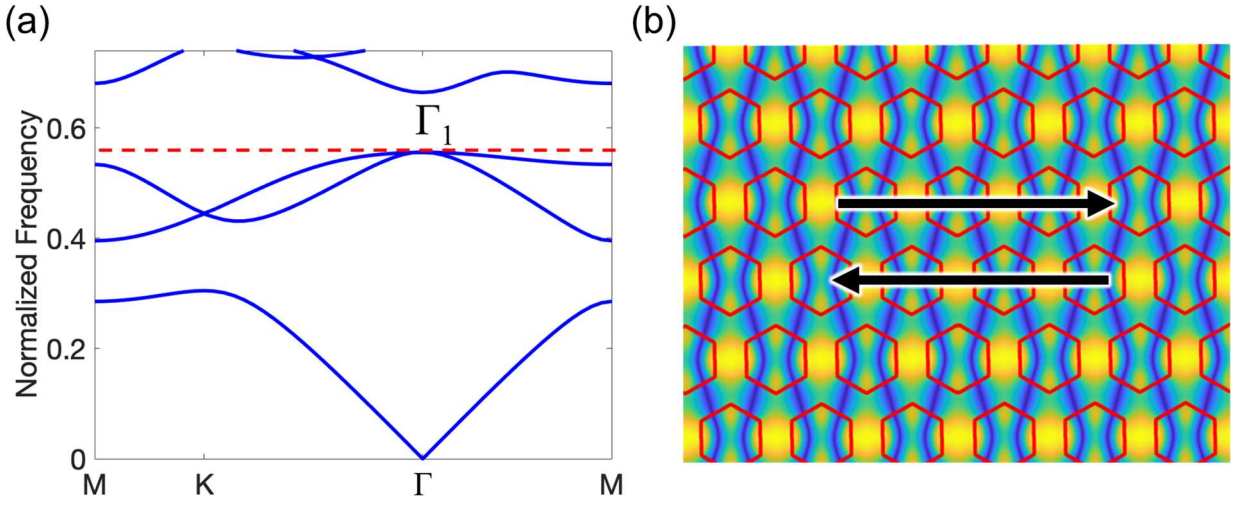

Figure 8.1. (a) Photonic band structure of a two-dimensional triangular nanowire photonic crystal. The lattice constant is 180 nm and the diameter of hexagonal nanowire is 150 nm. (b) Calculated TM field intensity profile of Γ_1 point

bandedge mode. The two black arrows indicate counter-propagation waves as the main distributed feedback mechanism.

In Chapter 2, we have discussed the SAE of GaN nanocrystals. On top of the GaN nanocrystals, we will further grow AlGaN nanocrystals and study the effects of substrate temperature, nitrogen flow rate and Al/Ga flux on the emission wavelength. The optimal Al composition in AlGaN will be tuned to target the emission wavelength that coincide with Γ_1 bandedge mode. Then, detailed PL measurements will be performed on the as-grown AlGaN nanocrystals array with 266 nm laser as an optical excitation. The emission will be spectrally measured through a high-resolution spectrometer. A full *p*-*i*-*n* device structure will be grown with higher Al composition in the *p*-type and *n*-type region, which helps improve carrier confinement in the active region. The schematic of the nanocrystals array is as shown in Figure 8.2.

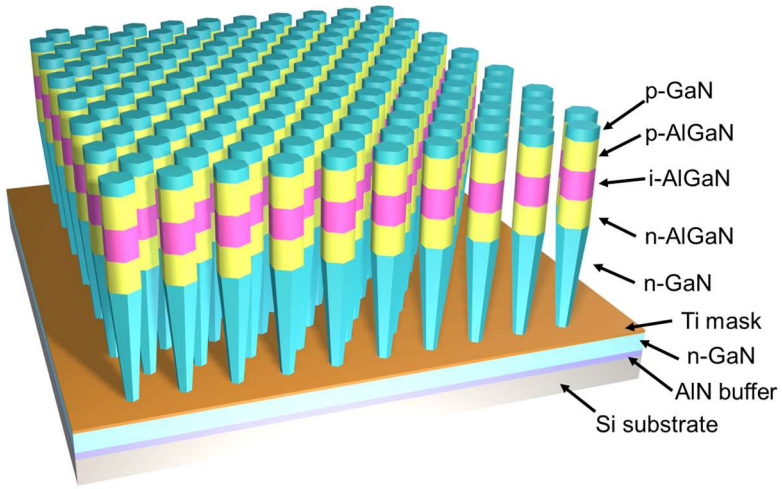

Figure 8.2. Schematic illustration of AlGaN/GaN *p*-*i*-*n* heterostructure arranged in triangular lattice for surface-emitting laser operating in UV-B band.

The proposed device structure is as illustrated in Figure 8.3. The fabrication process will start with Chlorine-based RIE etching into the *n*-type GaN substrate followed by *n*-type

metallization consists of 5 nm Ti and 5 nm Au. 300 nm thick SiO_x layer will be deposited by plasma-enhanced chemical vapor deposition for surface passivation and electrical isolation. Photolithography and wet chemical etching will be performed to defines the size of actual device. Then, 5 nm Ni and 5 nm Au will be deposited by e-beam evaporation at 45° or larger incidence angle to form contact layer on top of the nanowires, which also prevents the metal from reaching the region below *p*-type region which typically causes shortage. Subsequently, a thin indium tin oxide layer (~100 nm) will be deposited by sputtering to further improve current spreading. The *p*-metal will be annealed at 400℃ for one minute under nitrogen ambient. Finally, a thick metal pad consists of 280 nm Ti and 20 nm Au surrounding the current injection window will be deposited by sputtering.

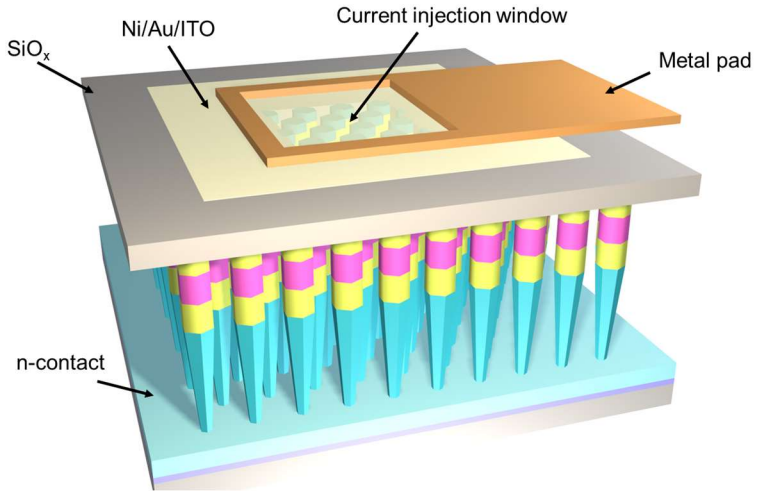

Figure 8.3. Schematic of the proposed UV surface-emitting LD structure.

8.2.2 Narrow-Band UV Single-Photon Emission Through GaN Monolayer in Selectively Grown Nanowires

Single photon sources are crucial system components used in various quantum information processing applications such as quantum key distribution, linear optical quantum computing and

quantum memories.[247] Recently, semiconductor quantum dots/disks have attracted considerable attention due to their outstanding potential for high-speed and integrated all-solid-state single photon sources. In particular, wide bandgap III-nitride quantum dots/disks offer significant advantages because both *n*-type and *p*-type doping are feasible, which enables the possibility of electrically-driven single photon source operated under high-temperature with wavelengths ranging from the UV to the infrared.[248] However, so far, both an in-depth understanding and a precise control over the optoelectronic properties of III-nitride quantum dots/disks have not been demonstrated. III-nitride quantum dots, such as InGaN/GaN quantum dots, synthesized through Stranski-Krastanow (S-K) growth mode, have a typical density range of 10^{8}-10^{11} cm^{-2} and average height of 3-6 nm (Figure 8.4).[249] It is worth noticing that the In composition fluctuation often happens along with size variation of quantum dots. Similar issues have also been observed in quantum disks embedded in spontaneously grown III-nitride nanowires. These variations result in a considerable level of inhomogeneous broadening of the emission line widths, thus hindering both device development and fundamental studies. The variations in the diameter of the nanowires within the array as a result of lack of control on nanowire diameters. This dispersion in nanowire diameter effectively affect the lateral confinement of the embedded GaN monolayer, leading to a broadening in measured PL and EL emission.

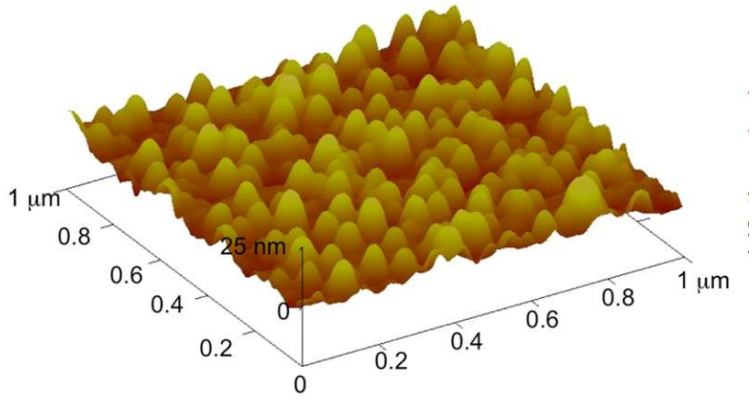

Figure 8.4. Atomic force micrograph of InGaN/GaN quantum dot layer grown by molecular beam epitaxy.[249]

In this regard, we propose exploiting selective area grown N-polar nanowires with embedded GaN monolayer to realize narrow-band UV single-photon emission. There are mainly two advantages. First of all, SAE provide good control of the nonuniformity of nanowire morphology which can significantly reduce the thickness variations of GaN monolayer among the nanowires. Meanwhile, by adopting N-polarity, the GaN monolayer can be synthesized on the *c*-plane on top of the nanowire, avoiding the discontinuity issue when grown on semi-polar planes.

The optical properties of the samples will be investigated by micro-PL with a pulsed 193 nm excimer laser as an excitation source to identify the optimal growth condition that ensures narrow-band single photon emission. Low-temperature micro-PL measurements will also be performed in a liquid helium flow cryostat. The optimized growth condition will be adopted in electrically-driven devices wherein Si doping and Mg doping will be introduced in the electron and hole injection regions, respectively. EL emission will be collected by a UV-transparent optical fiber. Photon autocorrelation measurements will be performed using a Hanbury-Brown Twiss Setup comprised of photomultiplier tubes designed for operation in the UV.

Appendix

Appendix A

Supporting Information for Chapter 3

Section 1. Theoretical computational details

To calculate the defect formation energy in AlN, first-principles density functional theory calculations were performed with the projector-augmented wave method [250,251] as implemented in the Vienna ab initio Simulation Package (VASP).[252] PBE pseudopotentials (PAW_PBE Al_GW and N_GW_new) [253] were used for Al and N, with a plane-wave cutoff energy of 500 eV to converge the total energy to 1 meV/atom. The HSE06 hybrid density functional [254] with a mixing parameter of 0.33 was employed to obtain a band gap of 6.2 eV for AlN, in close agreement with the experiment.[255] Defect calculations were performed for AlN using 96-atom orthorhombic supercells [256] with a 2×2×2 Γ-centered Brillouin-zone-sampling grid. All structures were relaxed by allowing atoms to move until the force on ions is less than 0.02 eV/Å, with spin-polarization included for unpaired electrons. The defect formation energies were calculated by the following equation:

$$E^f(X^q) = E_t(X^q) - E_t(AlN) + \sum_i n_i\mu_i + q(E_F + E_{VBM}) + E_{corr}. \quad \text{(A-1)}$$

$E_t(X^q)$ denotes the total energy of the supercell with a defect X in charge state q and $E_t(AlN)$ is the total energy of the perfect supercell. n_i is the number of atoms that the supercell exchanges with the chemical reservoir and μ_i is the chemical potentials. E_F is the fermi energy referenced to the valence band maximum of the AlN. E_{corr} accounts for the correction to the artificial interaction between charged defect and its image charge. Here, we adopt the approach of Freysoldt *et al*. to evaluate the correction.[257] We assume Mg-rich conditions and μ_{Mg} is bounded by the formation of secondary Mg_3N_2 compound. Our results on defect formation

energies and charge-transition levels in AlN are in good agreement with previous theoretical calculations.[92,258]

Section 2. Detailed epitaxy conditions of AlN nanowires on Si substrate

All samples were grown on *n*-type Si(111) wafer using a Veeco GEN II MBE system equipped with a radio frequency plasma-assisted nitrogen source. AlN(0001) thin films grown under slightly N- and Al-rich conditions at a lower temperature (680 ºC) was used to calibrate the Al and N fluxes in AlN-equivalent growth rate units (nm/min). All samples were grown under $\emptyset_{Al}$=0.87 nm/min. N_2 flow rate of 1 sccm corresponds to 12 nm/min AlN growth rate. Prior to loading into the MBE system, the Si wafer was cleaned using standard solvents and dipped in buffered hydrofluoric acid solution to etch the surface oxide. We performed a series of two step experiments. The first step is identical for all samples and consists of the growth of a GaN nanowire template with $\emptyset_{Ga}$=0.87 nm/min. As shown in Figure A1, the NW template consists of ~100 nm high and well separated nanowires with an areal density of 2×10^{10} cm^{-2} and an average diameter of 50 nm. During the second step, ~150 nm long AlN nanowires were grown at different N_2 flow rates, substrate temperatures and Mg BEPs.

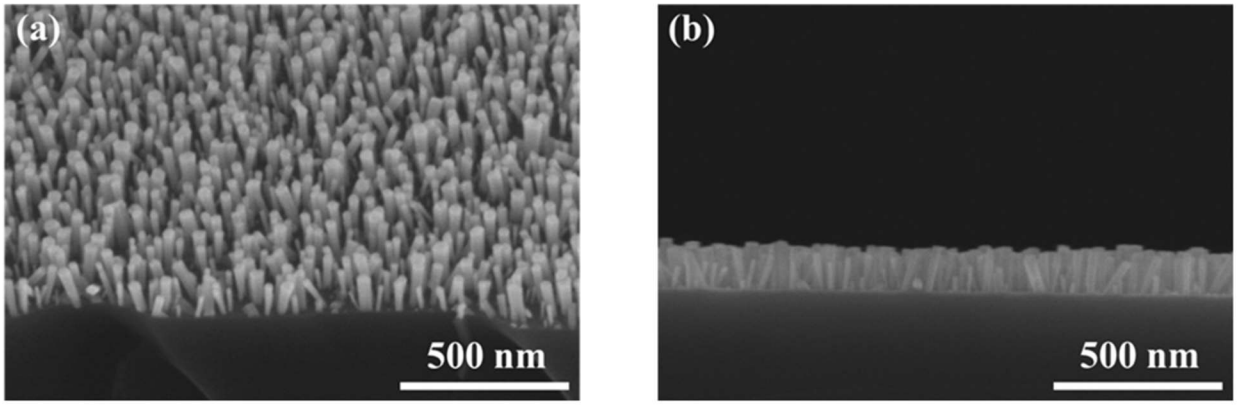

Figure A1. Bird's-eye view (a) and side view (b) secondary electron SEM imaging of GaN nanowire template for subsequent AlN nanowire epitaxy.

Section 3. STEM images of as-grown AlN nanowire *p-i-n* structure

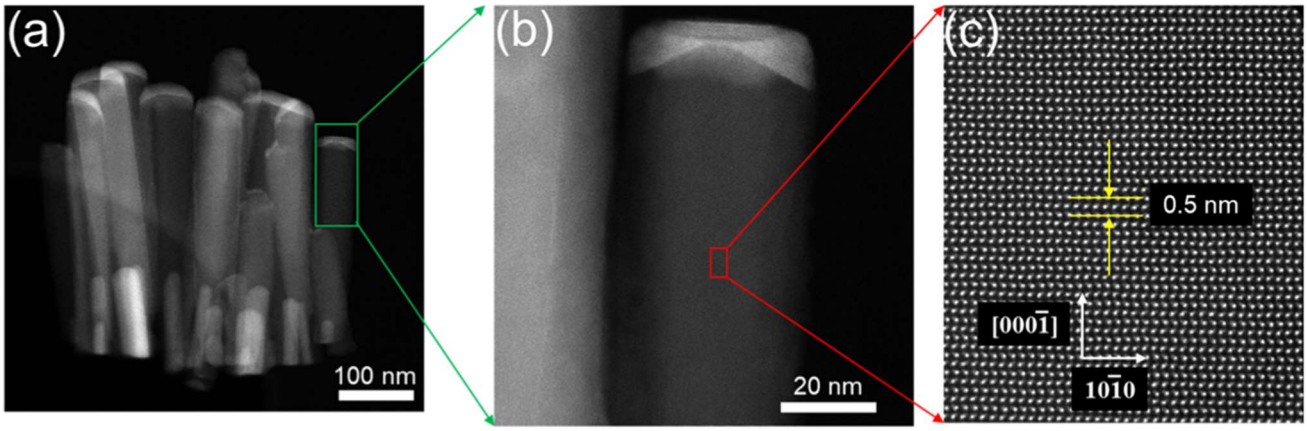

Figure A2. Microstructures of AlN nanowires: (a) Low-magnification STEM-HAADF image showing several GaN/AlN nanowires; (b) Magnified STEM-HAADF image shows that the top end of the nanowire outlined in (a) has a thin AlGaN as contact layer; (c) High-resolution STEM-HAADF image taken from the outlined i-AlN active region in (b) showing crystal structure free from dislocations and SFs.

Section 4. Configuration-coordinate diagram illustrating optical processes related to Mg dopant and Al vacancy in AlN

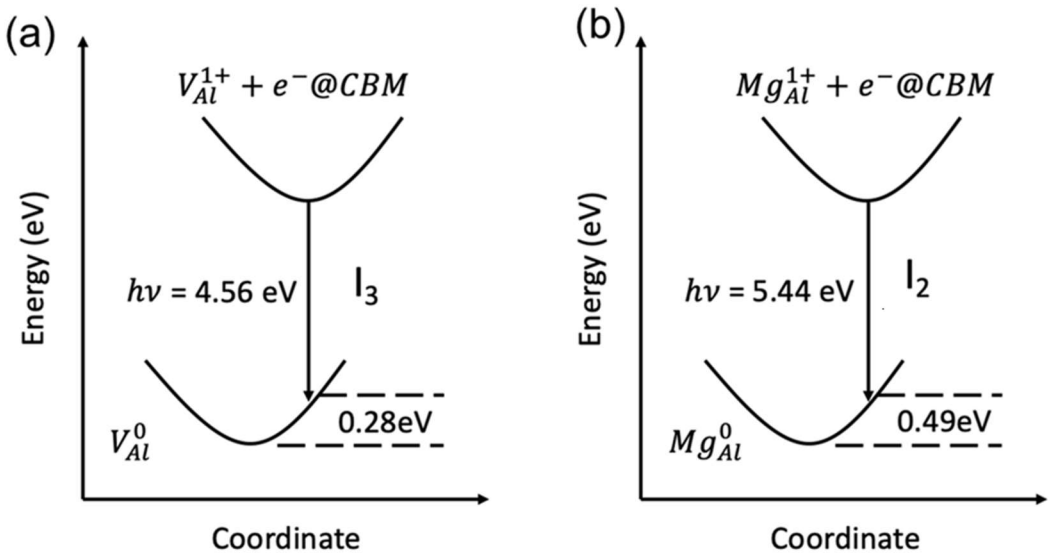

Figure A3. Configuration-coordinate diagram illustrating optical processes related to Mg dopant and Al vacancy in AlN. (a) Recombination of an electron at the CBM with V_{Al}^{1+} to form V_{Al}^{0} leads to an emission peak at 4.56 eV, explaining origin of I_3. (b) Recombination of an electron at the CBM with Mg_{Al}^{1+} to form Mg_{Al}^{0} leads to an emission peak at 5.44 eV, explaining origin of I_2.

Section 5. Non-normalized PL spectra and intensity ratio of I_2 to I_3 versus the N_2 flow rate

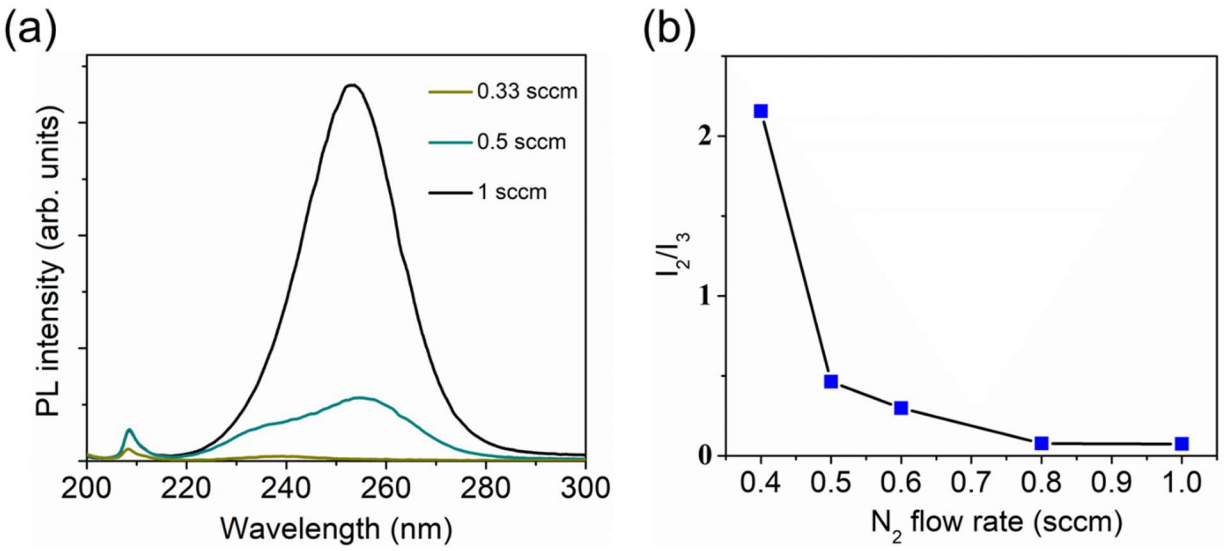

Figure A4. (a) Non-normalized PL spectra of samples from Group B. All samples were grown at substrate temperature of 810 °C and Mg BEP of 3×10^{-9} Torr while the nitrogen flow rate was varied among different samples. (b) Intensity ratio of I_2 to I_3 versus the N_2 flow rate derived from Figure 2c.

Section 6. Eurofins EAG Materials Science Secondary ion mass spectrometry (SIMS) depth profile of Mg-doped AlN nanowires grown on Si substrate

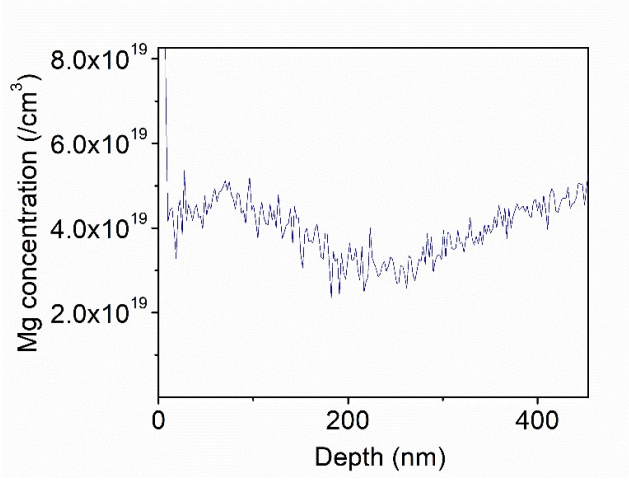

Figure A5. SIMS depth profile of Mg-doped AlN nanowires grown on Si substrate at 865 °C substrate temperature, 1 sccm N_2 flow rate and 7×10^{-9} Torr Mg BEP. A fill factor of 30% for the nanowires was used to derive the average Mg concentration.

Section 7. PL spectrum and Gaussian profile analysis of Mg-doped AlN nanowires

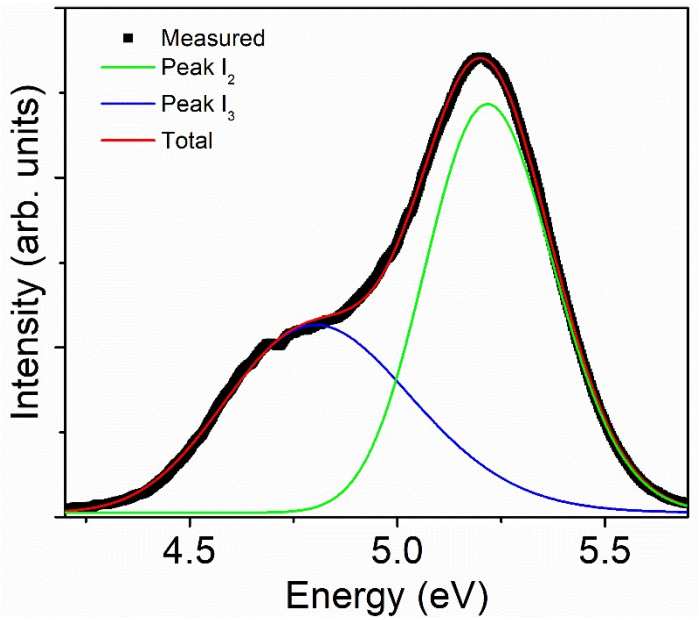

Figure A6. PL spectrum and Gaussian profile analysis of Mg-doped AlN nanowires measured under 0.78 W/cm^2 excitation powers. The sample was grown under a substrate temperature of 865 ºC, N_2 flow rate of 1 sccm and Mg BEP of 7×10^{-9} Torr.

Section 8. Epitaxy and fabrication of AlN nanowire-based LED

Si-doped GaN nanowires (~100 nm) were grown at substrate temperature of 780 ºC. Si-doped AlN nanowires (~110 nm) were grown at a substrate temperature of 875 ºC. Then unintentionally doped AlN nanowires of ~40 nm were grown at the same substrate temperature of 875 ºC. The growth was performed under N-rich conditions with the N_2 flow rate of 0.33 sccm during the active region growth. Subsequently, the substrate temperature was reduced to 810 ºC and the nitrogen flow rate increases to 0.5 sccm to grow a ~40 nm Mg-doped *p*-AlN layer and ~5

nm *p*-$Al_{0.2}Ga_{0.8}N$ contact layer. *p*-$Al_{0.2}Ga_{0.8}N$ contact layer and *p*-AlN layer were grown at same Mg BEPs. The schematic of the as-grown structure is shown in Figure A7a. The estimated Si concentration in *n*-AlN was ~$1.5\times10^{19}/cm^3$ and Mg concentration in *p*-AlN ranges from 1×10^{19}-$6\times10^{19}/cm^3$, depending on the Mg flux during the growth.

The AlN *p-i-n* LEDs were fabricated using standard optical lithography and contact metallization techniques. Ti (80 nm)/Au (20 nm) was deposited on the backside of Si substrate to serve as the *n*-metal contact. *p*-Metal contact consisting of Ni (10 nm)/Au (10 nm) was deposited using a tilting angle deposition technique, which also defines the device area in the range of 300 µm × 300 µm to 1 mm × 1 mm.

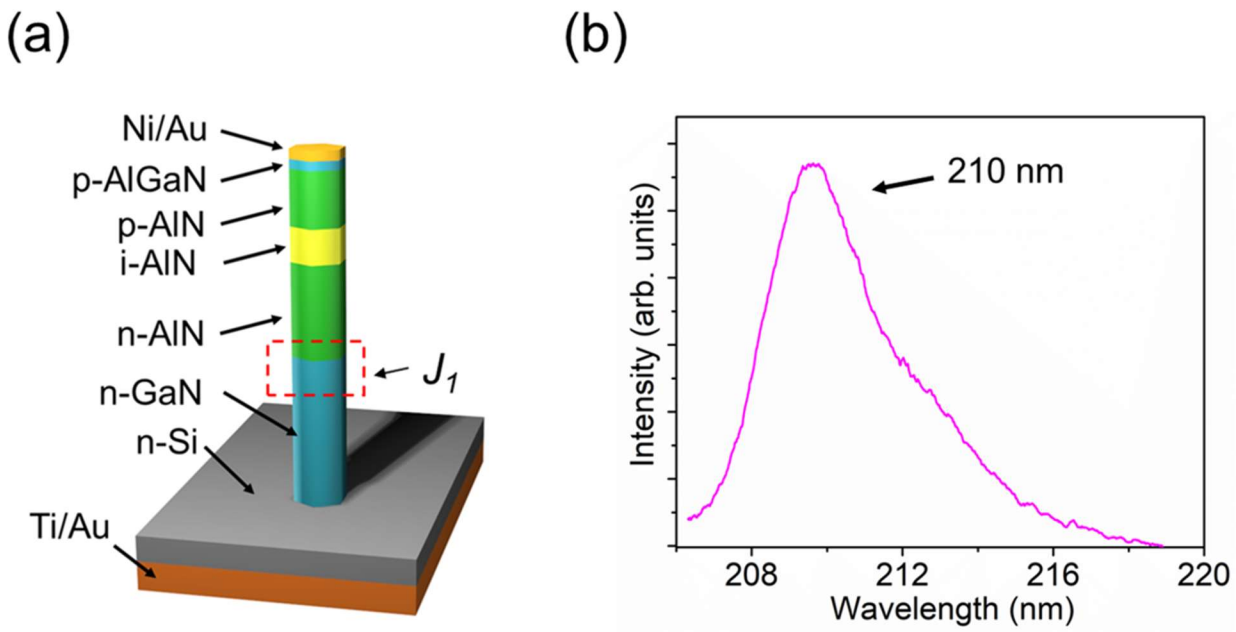

Figure A7. (a) Schematic of AlN nanowire based LED on Si(111) substrate. J_1 points to the heterojunction between *n*-GaN and *n*-AlN. (b) Room-temperature EL spectrum measured under 30 mA current injection from as-fabricated AlN LEDs.

Section 9. Current-voltage characteristics of *n*-GaN/*n*-AlN unipolar heterojunction

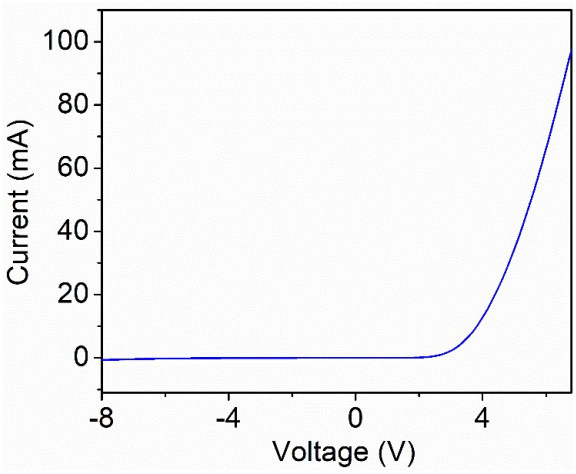

Figure A8. *I-V* characteristics of *n*-type doped unipolar GaN/AlN heterojunction. 80 nm Ti/20 nm Au was used for metal contact with the nanowires.

Table A1: Minimum ideality factor and corresponding voltages of AlN nanowire LEDs with different Mg concentrations in the *p*-AlN layer.

	Sample I	Sample II	Sample III
Mg concentration (cm^{-3})	1×10^{19}	2×10^{19}	6×10^{19}
Minimum ideality factor	14.9	4.6	3.58
Corresponding voltage (V)	3.6	2.4	2.4

Section 10: Analysis of the charge carrier (hole) tunneling process

The hole tunneling process was further explained by calculating the energy band diagram of the AlN *p-i-n* homojunction using two different Mg concentrations as shown in Figure A9. For Mg concentration of $1\times10^{19}/cm^3$, the calculated depletion width into the *p*-AlN region is ~27 nm.

Under equilibrium, despite the Fermi-level is flat throughout the *p-i-n* structure, the built-in potential in the *p*-AlN region causes the band structure as well as the impurity band to bend downwards, wherein the deep level energy states below the Femi-level will be filled by electrons. Under forward bias, these captured electrons can tunnel from one state to adjacent empty states in the valence band, contributing to the tunneling component in Eq. 1 and increasing the ideality factor. When N_A increases to $6\times10^{19}/cm^3$, hole carrier concentration in the valence band increases due to higher Mg concentration and broadened Mg impurity band, leading to a significantly reduced depletion width into *p*-AlN of ~8 nm and a suppressed band bending of *p*-AlN as shown in Figure A9b. As the number of available electrons inside the impurity band reduces, the electron tunneling process is significantly suppressed. It's worth noting that the deep-level assisted tunneling process will also be suppressed at higher measurement temperature as shown in Figure 3.4c, wherein hole concentration increases due to a larger portion of ionized Mg-impurities.

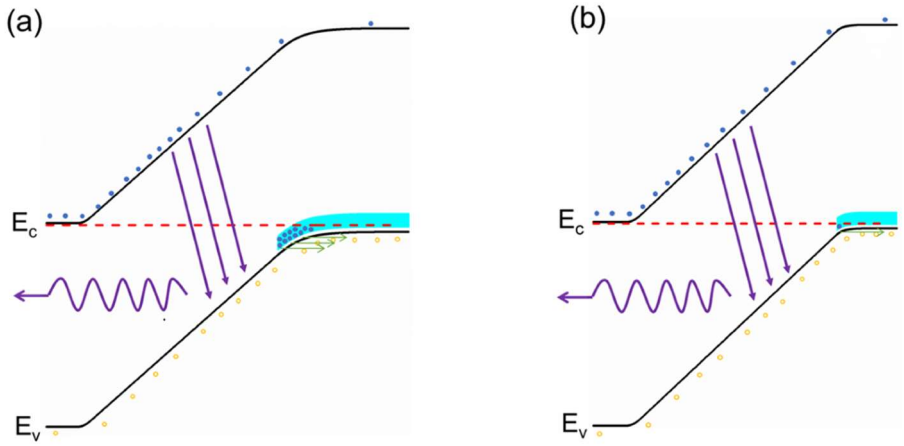

Figure A9. Schematic illustration of the energy band diagram of AlN nanowire *p-i-n* junction with Mg concentration of (a) $1\times10^{19}/cm^3$ and (b) $6\times10^{19}/cm^3$. Mg impurity band bending and deep level assisted electron tunneling process are also illustrate.

Bibliography

[1] "Incandescent light bulb." [Online]. Available:https://en.wikipedia.org/wiki/Incandescent_light_bulb.

[2] "Fluorescent lamp." [Online]. Available:https://en.wikipedia.org/wiki/Fluorescent_lamp.

[3] E. Schubert, "Light-Emitting Diodes (3rd Edition)," 2018.

[4] Shizuo Fujita, "Wide-bandgap semiconductor materials: For their full bloom," *Japanese Journal of Applied Physics*, vol. 54, no. 3, 2015.

[5] Shuji Nakamura, Takashi Mukai, and Masayuki Senoh, "Candela - class high - brightness InGaN/AlGaN double - heterostructure blue - light - emitting diodes," *Applied Physics Letters*, vol. 64, no. 13, pp. 1687, 1994.

[6] M. Auf der Maur, A. Pecchia, G. Penazzi, W. Rodrigues, and A. Di Carlo, "Efficiency Drop in Green InGaN/GaN Light Emitting Diodes: The Role of Random Alloy Fluctuations," *Phys Rev Lett*, vol. 116, no. 2, pp. 027401, 2016.

[7] Aurélien David, Michael J. Grundmann, John F. Kaeding, Nathan F. Gardner, Theodoros G. Mihopoulos, and Michael R. Krames, "Carrier distribution in (0001)InGaN / GaN multiple quantum well light-emitting diodes," *Applied Physics Letters*, vol. 92, no. 5, 2008.

[8] Ansgar Laubsch, Matthias Sabathil, Werner Bergbauer, Martin Strassburg, Hans Lugauer, Matthias Peter, Stephan Lutgen, Norbert Linder, Klaus Streubel, Jörg Hader, Jerome V. Moloney, Bernhard Pasenow, and Stephan W. Koch, "On the origin of IQE-'droop' in InGaN LEDs," *physica status solidi (c)*, vol. 6, no. S2, pp. S913, 2009.

[9] I. V. Rozhansky and D. A. Zakheim, "Analysis of processes limiting quantum efficiency of AlGaInN LEDs at high pumping," *physica status solidi (a)*, vol. 204, no. 1, pp. 227, 2007.

[10] Z. Mi, S. Zhao, S. Y. Woo, M. Bugnet, M. Djavid, X. Liu, J. Kang, X. Kong, W. Ji, H. Guo, Z. Liu, and G. A. Botton, "Molecular beam epitaxial growth and characterization of Al(Ga)N nanowire deep ultraviolet light emitting diodes and lasers," *Journal of Physics D: Applied Physics*, vol. 49, no. 36, pp. 364006, 2016.

[11] Dabing Li, Ke Jiang, Xiaojuan Sun, and Chunlei Guo, "AlGaN photonics: recent advances in materials and ultraviolet devices," *Advances in Optics and Photonics*, vol. 10, no. 1, pp. 43, 2018.

[12] S. M. Islam, Kevin Lee, Jai Verma, Vladimir Protasenko, Sergei Rouvimov, Shyam Bharadwaj, Huili Xing, and Debdeep Jena, "MBE-grown 232–270 nm deep-UV LEDs using monolayer thin binary GaN/AlN quantum heterostructures," *Applied Physics Letters*, vol. 110, no. 4, pp. 041108, 2017.

[13] Hideki Hirayama, Noritoshi Maeda, Sachie Fujikawa, Shiro Toyoda, and Norihiko Kamata, "Recent progress and future prospects of AlGaN-based high-efficiency deep-ultraviolet light-emitting diodes," *Japanese Journal of Applied Physics*, vol. 53, no. 10, pp. 100209, 2014.

[14] Max Shatalov, Wenhong Sun, Alex Lunev, Xuhong Hu, Alex Dobrinsky, Yuri Bilenko, Jinwei Yang, Michael Shur, Remis Gaska, Craig Moe, Gregory Garrett, and Michael Wraback, "AlGaN Deep-Ultraviolet Light-Emitting Diodes with External Quantum Efficiency above 10%," *Applied Physics Express*, vol. 5, no. 8, pp. 082101, 2012.

[15] Hideki Hirayama, Sachie Fujikawa, Norimichi Noguchi, Jun Norimatsu, Takayoshi Takano, Kenji Tsubaki, and Norihiko Kamata, "222-282 nm AlGaN and InAlGaN-based deep-UV LEDs fabricated on high-quality AlN on sapphire," *physica status solidi (a)*, vol. 206, no. 6, pp. 1176, 2009.
[16] Takuya Mino, Hideki Hirayama, Takayoshi Takano, Kenji Tsubaki, and Masakazu Sugiyama, "Realization of 256–278 nm AlGaN-Based Deep-Ultraviolet Light-Emitting Diodes on Si Substrates Using Epitaxial Lateral Overgrowth AlN Templates," *Applied Physics Express*, vol. 4, no. 9, pp. 092104, 2011.
[17] Songrui Zhao, Hieu P. T. Nguyen, Md G. Kibria, and Zetian Mi, "III-Nitride nanowire optoelectronics," *Progress in Quantum Electronics*, vol. 44, pp. 14, 2015.
[18] R. Bhartia, W. F. Hug, E. C. Salas, R. D. Reid, K. K. Sijapati, A. Tsapin, W. Abbey, K. H. Nealson, A. L. Lane, and P. G. Conrad, "Classification of organic and biological materials with deep ultraviolet excitation," *Appl Spectrosc*, vol. 62, no. 10, pp. 1070, 2008.
[19] G. W. Faris and R. A. Copeland, "Wavelength dependence of the Raman cross section for liquid water," *Appl Opt*, vol. 36, no. 12, pp. 2686, 1997.
[20] S. D. Christesen, J. Pendell Jones, J. M. Lochner, and A. M. Hyre, "Ultraviolet Raman spectra and cross-sections of the G-series nerve agents," *Appl Spectrosc*, vol. 62, no. 10, pp. 1078, 2008.
[21] D. Welch, M. Buonanno, V. Grilj, I. Shuryak, C. Crickmore, A. W. Bigelow, G. Randers-Pehrson, G. W. Johnson, and D. J. Brenner, "Far-UVC light: A new tool to control the spread of airborne-mediated microbial diseases," *Sci Rep*, vol. 8, no. 1, pp. 2752, 2018.
[22] Klaus P. Streubel, Hideki Hirayama, Heonsu Jeon, Li-Wei Tu, and Norbert Linder, "Recent progress of 220-280 nm-band AlGaN based deep-UV LEDs," vol. 7617, pp. 76171G, 2010.
[23] C. Mion, J. F. Muth, E. A. Preble, and D. Hanser, "Accurate dependence of gallium nitride thermal conductivity on dislocation density," *Applied Physics Letters*, vol. 89, no. 9, pp. 092123, 2006.
[24] W. Sun, M. Shatalov, J. Deng, X. Hu, J. Yang, A. Lunev, Y. Bilenko, M. Shur, and R. Gaska, "Efficiency droop in 245–247 nm AlGaN light-emitting diodes with continuous wave 2 mW output power," *Applied Physics Letters*, vol. 96, no. 6, 2010.
[25] B. T. Tran and H. Hirayama, "Growth and Fabrication of High External Quantum Efficiency AlGaN-Based Deep Ultraviolet Light-Emitting Diode Grown on Pattern Si Substrate," *Sci Rep*, vol. 7, no. 1, pp. 12176, 2017.
[26] Isaac Bryan, Zachary Bryan, Shun Washiyama, Pramod Reddy, Benjamin Gaddy, Biplab Sarkar, M. Hayden Breckenridge, Qiang Guo, Milena Bobea, James Tweedie, Seiji Mita, Douglas Irving, Ramon Collazo, and Zlatko Sitar, "Doping and compensation in Al-rich AlGaN grown on single crystal AlN and sapphire by MOCVD," *Applied Physics Letters*, vol. 112, no. 6, 2018.
[27] M. Kneissl and J. Rass, *III-Nitride Ultraviolet Emitters-Technology and Applications*. (Springer, New York, NY, USA, 2015).
[28] Cyril Pernot, Myunghee Kim, Shinya Fukahori, Tetsuhiko Inazu, Takehiko Fujita, Yosuke Nagasawa, Akira Hirano, Masamichi Ippommatsu, Motoaki Iwaya, Satoshi Kamiyama, Isamu Akasaki, and Hiroshi Amano, "Improved Efficiency of 255–280 nm AlGaN-Based Light-Emitting Diodes," *Applied Physics Express*, vol. 3, no. 6, pp. 061004, 2010.
[29] James R. Grandusky, Shawn R. Gibb, Mark C. Mendrick, Craig Moe, Michael Wraback, and Leo J. Schowalter, "High Output Power from 260 nm Pseudomorphic Ultraviolet Light-

Emitting Diodes with Improved Thermal Performance," *Applied Physics Express*, vol. 4, no. 8, pp. 082101, 2011.
[30] A. Pandey, W. J. Shin, J. Gim, R. Hovden, and Z. Mi, "High-efficiency AlGaN/GaN/AlGaN tunnel junction ultraviolet light-emitting diodes," *Photonics Research*, vol. 8, no. 3, 2020.
[31] Zengcheng Li, Legong Liu, Yingnan Huang, Qian Sun, Meixin Feng, Yu Zhou, Hanmin Zhao, and Hui Yang, "High-power AlGaN-based near-ultraviolet light-emitting diodes grown on Si(111)," *Applied Physics Express*, vol. 10, no. 7, 2017.
[32] Kai Ding, Vitaliy Avrutin, Ümit Özgür, and Hadis Morkoç, "Status of Growth of Group III-Nitride Heterostructures for Deep Ultraviolet Light-Emitting Diodes," *Crystals*, vol. 7, no. 10, pp. 300, 2017.
[33] Y. Taniyasu, M. Kasu, and T. Makimoto, "An aluminium nitride light-emitting diode with a wavelength of 210 nanometres," *Nature*, vol. 441, no. 7091, pp. 325, 2006.
[34] Takayoshi Takano, Takuya Mino, Jun Sakai, Norimichi Noguchi, Kenji Tsubaki, and Hideki Hirayama, "Deep-ultraviolet light-emitting diodes with external quantum efficiency higher than 20% at 275 nm achieved by improving light-extraction efficiency," *Applied Physics Express*, vol. 10, no. 3, pp. 031002, 2017.
[35] Shin-ichiro Inoue, Naoki Tamari, and Manabu Taniguchi, "150 mW deep-ultraviolet light-emitting diodes with large-area AlN nanophotonic light-extraction structure emitting at 265 nm," *Applied Physics Letters*, vol. 110, no. 14, pp. 141106, 2017.
[36] Yuewei Zhang, Sriram Krishnamoorthy, Fatih Akyol, Jared M. Johnson, Andrew A. Allerman, Michael W. Moseley, Andrew M. Armstrong, Jinwoo Hwang, and Siddharth Rajan, "Reflective metal/semiconductor tunnel junctions for hole injection in AlGaN UV LEDs," *Applied Physics Letters*, vol. 111, no. 5, pp. 051104, 2017.
[37] J. Li, K. B. Nam, M. L. Nakarmi, J. Y. Lin, H. X. Jiang, Pierre Carrier, and Su-Huai Wei, "Band structure and fundamental optical transitions in wurtzite AlN," *Applied Physics Letters*, vol. 83, no. 25, pp. 5163, 2003.
[38] Xianhe Liu, Songrui Zhao, Binh Huy Le, and Zetian Mi, "Molecular beam epitaxial growth and characterization of AlN nanowall deep UV light emitting diodes," *Applied Physics Letters*, vol. 111, no. 10, 2017.
[39] S. Zhao, S. Y. Woo, S. M. Sadaf, Y. Wu, A. Pofelski, D. A. Laleyan, R. T. Rashid, Y. Wang, G. A. Botton, and Z. Mi, "Molecular beam epitaxy growth of Al-rich AlGaN nanowires for deep ultraviolet optoelectronics," *APL Materials*, vol. 4, no. 8, pp. 086115, 2016.
[40] S. M. Sadaf, S. Zhao, Y. Wu, Y. H. Ra, X. Liu, S. Vanka, and Z. Mi, "An AlGaN Core-Shell Tunnel Junction Nanowire Light-Emitting Diode Operating in the Ultraviolet-C Band," *Nano Lett*, vol. 17, no. 2, pp. 1212, 2017.
[41] K. Hestroffer, R. Mata, D. Camacho, C. Leclere, G. Tourbot, Y. M. Niquet, A. Cros, C. Bougerol, H. Renevier, and B. Daudin, "The structural properties of GaN/AlN core-shell nanocolumn heterostructures," *Nanotechnology*, vol. 21, no. 41, pp. 415702, 2010.
[42] Q. Wang, H. P. T. Nguyen, K. Cui, and Z. Mi, "High efficiency ultraviolet emission from AlxGa1−xN core-shell nanowire heterostructures grown on Si (111) by molecular beam epitaxy," *Applied Physics Letters*, vol. 101, no. 4, pp. 043115, 2012.
[43] A. Pierret, C. Bougerol, S. Murcia-Mascaros, A. Cros, H. Renevier, B. Gayral, and B. Daudin, "Growth, structural and optical properties of AlGaN nanowires in the whole composition range," *Nanotechnology*, vol. 24, no. 11, pp. 115704, 2013.

[44] Q. Wang, A. T. Connie, H. P. Nguyen, M. G. Kibria, S. Zhao, S. Sharif, I. Shih, and Z. Mi, "Highly efficient, spectrally pure 340 nm ultraviolet emission from AlxGa(1)-xN nanowire based light emitting diodes," *Nanotechnology*, vol. 24, no. 34, pp. 345201, 2013.
[45] T. Frost, S. Jahangir, E. Stark, S. Deshpande, A. Hazari, C. Zhao, B. S. Ooi, and P. Bhattacharya, "Monolithic electrically injected nanowire array edge-emitting laser on (001) silicon," *Nano Lett*, vol. 14, no. 8, pp. 4535, 2014.
[46] S. Zhao, S. Y. Woo, M. Bugnet, X. Liu, J. Kang, G. A. Botton, and Z. Mi, "Three-Dimensional Quantum Confinement of Charge Carriers in Self-Organized AlGaN Nanowires: A Viable Route to Electrically Injected Deep Ultraviolet Lasers," *Nano Lett*, vol. 15, no. 12, pp. 7801, 2015.
[47] Stephen D. Hersee, Ashwin K. Rishinaramangalam, Michael N. Fairchild, Lei Zhang, and Petros Varangis, "Threading defect elimination in GaN nanowires," *Journal of Materials Research*, vol. 26, no. 17, pp. 2293, 2011.
[48] Nhung Hong Tran, Binh Huy Le, Songrui Zhao, and Zetian Mi, "On the mechanism of highly efficient p-type conduction of Mg-doped ultra-wide-bandgap AlN nanostructures," *Applied Physics Letters*, vol. 110, no. 3, 2017.
[49] Ashfiqua Tahseen Connie, Songrui Zhao, Sharif Md Sadaf, Ishiang Shih, Zetian Mi, Xiaozhang Du, Jingyu Lin, and Hongxing Jiang, "Optical and electrical properties of Mg-doped AlN nanowires grown by molecular beam epitaxy," *Applied Physics Letters*, vol. 106, no. 21, 2015.
[50] S. Zhao, A. T. Connie, M. H. Dastjerdi, X. H. Kong, Q. Wang, M. Djavid, S. Sadaf, X. D. Liu, I. Shih, H. Guo, and Z. Mi, "Aluminum nitride nanowire light emitting diodes: Breaking the fundamental bottleneck of deep ultraviolet light sources," *Sci Rep*, vol. 5, pp. 8332, 2015.
[51] Nhung Hong Tran, Binh Huy Le, Songrui Zhao, and Zetian Mi, "On the mechanism of highly efficient p-type conduction of Mg-doped ultra-wide-bandgap AlN nanostructures," *Applied Physics Letters*, vol. 110, no. 3, pp. 032102, 2017.
[52] S. Zhao, M. Djavid, and Z. Mi, "Surface Emitting, High Efficiency Near-Vacuum Ultraviolet Light Source with Aluminum Nitride Nanowires Monolithically Grown on Silicon," *Nano Lett*, vol. 15, no. 10, pp. 7006, 2015.
[53] Cheng Liu, Yu Kee Ooi, S. M. Islam, Jai Verma, Huili Xing, Debdeep Jena, and Jing Zhang, "Physics and polarization characteristics of 298 nm AlN-delta-GaN quantum well ultraviolet light-emitting diodes," *Applied Physics Letters*, vol. 110, no. 7, 2017.
[54] Cheng Liu, Yu Kee Ooi, S. M. Islam, Huili Xing, Debdeep Jena, and Jing Zhang, "234 nm and 246 nm AlN-Delta-GaN quantum well deep ultraviolet light-emitting diodes," *Applied Physics Letters*, vol. 112, no. 1, 2018.
[55] W. Guo, M. Zhang, A. Banerjee, and P. Bhattacharya, "Catalyst-free InGaN/GaN nanowire light emitting diodes grown on (001) silicon by molecular beam epitaxy," *Nano Lett*, vol. 10, no. 9, pp. 3355, 2010.
[56] H. P. Nguyen, K. Cui, S. Zhang, M. Djavid, A. Korinek, G. A. Botton, and Z. Mi, "Controlling electron overflow in phosphor-free InGaN/GaN nanowire white light-emitting diodes," *Nano Lett*, vol. 12, no. 3, pp. 1317, 2012.
[57] Y. H. Ra, R. Wang, S. Y. Woo, M. Djavid, S. M. Sadaf, J. Lee, G. A. Botton, and Z. Mi, "Full-Color Single Nanowire Pixels for Projection Displays," *Nano Lett*, vol. 16, no. 7, pp. 4608, 2016.

[58] Y. H. Ra, R. T. Rashid, X. Liu, S. M. Sadaf, K. Mashooq, and Z. Mi, "An electrically pumped surface-emitting semiconductor green laser," *Sci Adv*, vol. 6, no. 1, pp. eaav7523, 2020.
[59] K. H. Li, X. Liu, Q. Wang, S. Zhao, and Z. Mi, "Ultralow-threshold electrically injected AlGaN nanowire ultraviolet lasers on Si operating at low temperature," *Nat Nanotechnol*, vol. 10, no. 2, pp. 140, 2015.
[60] S. Zhao, X. Liu, Y. Wu, and Z. Mi, "An electrically pumped 239 nm AlGaN nanowire laser operating at room temperature," *Applied Physics Letters*, vol. 109, no. 19, 2016.
[61] S. Zhao, X. Liu, S. Y. Woo, J. Kang, G. A. Botton, and Z. Mi, "An electrically injected AlGaN nanowire laser operating in the ultraviolet-C band," *Applied Physics Letters*, vol. 107, no. 4, pp. 043101, 2015.
[62] B. H. Le, X. Liu, N. H. Tran, S. Zhao, and Z. Mi, "An electrically injected AlGaN nanowire defect-free photonic crystal ultraviolet laser," *Opt Express*, vol. 27, no. 4, pp. 5843, 2019.
[63] Morteza Monavarian, Arman Rashidi, and Daniel Feezell, "A Decade of Nonpolar and Semipolar III-Nitrides: A Review of Successes and Challenges," *physica status solidi (a)*, 2018.
[64] Suresh Vishwanath, Xinyu Liu, Sergei Rouvimov, Leonardo Basile, Ning Lu, Angelica Azcatl, Katrina Magno, Robert M. Wallace, Moon Kim, Juan-Carlos Idrobo, Jacek K. Furdyna, Debdeep Jena, and Huili Grace Xing, "Controllable growth of layered selenide and telluride heterostructures and superlattices using molecular beam epitaxy," *Journal of Materials Research*, vol. 31, no. 7, pp. 900, 2016.
[65] K. A. Bertness, A. Roshko, N. A. Sanford, J. M. Barker, and A. V. Davydov, "Spontaneously grown GaN and AlGaN nanowires," *Journal of Crystal Growth*, vol. 287, no. 2, pp. 522, 2006.
[66] R. Songmuang, O. Landré, and B. Daudin, "From nucleation to growth of catalyst-free GaN nanowires on thin AlN buffer layer," *Applied Physics Letters*, vol. 91, no. 25, pp. 251902, 2007.
[67] K. A. Bertness, A. Roshko, L. M. Mansfield, T. E. Harvey, and N. A. Sanford, "Mechanism for spontaneous growth of GaN nanowires with molecular beam epitaxy," *Journal of Crystal Growth*, vol. 310, no. 13, pp. 3154, 2008.
[68] Jelena Ristić, Enrique Calleja, Sergio Fernández-Garrido, Laurent Cerutti, Achim Trampert, Uwe Jahn, and Klaus H. Ploog, "On the mechanisms of spontaneous growth of III-nitride nanocolumns by plasma-assisted molecular beam epitaxy," *Journal of Crystal Growth*, vol. 310, no. 18, pp. 4035, 2008.
[69] S. Fernández-Garrido, J. Grandal, E. Calleja, M. A. Sánchez-García, and D. López-Romero, "A growth diagram for plasma-assisted molecular beam epitaxy of GaN nanocolumns on Si(111)," *Journal of Applied Physics*, vol. 106, no. 12, pp. 126102, 2009.
[70] S. Fernandez-Garrido, J. K. Zettler, L. Geelhaar, and O. Brandt, "Monitoring the formation of nanowires by line-of-sight quadrupole mass spectrometry: a comprehensive description of the temporal evolution of GaN nanowire ensembles," *Nano Lett*, vol. 15, no. 3, pp. 1930, 2015.
[71] S. Zhao, M. G. Kibria, Q. Wang, H. P. Nguyen, and Z. Mi, "Growth of large-scale vertically aligned GaN nanowires and their heterostructures with high uniformity on SiO(x) by catalyst-free molecular beam epitaxy," *Nanoscale*, vol. 5, no. 12, pp. 5283, 2013.

[72] S. Fernandez-Garrido, V. M. Kaganer, K. K. Sabelfeld, T. Gotschke, J. Grandal, E. Calleja, L. Geelhaar, and O. Brandt, "Self-regulated radius of spontaneously formed GaN nanowires in molecular beam epitaxy," *Nano Lett*, vol. 13, no. 7, pp. 3274, 2013.
[73] K. A. Grossklaus, A. Banerjee, S. Jahangir, P. Bhattacharya, and J. M. Millunchick, "Misorientation defects in coalesced self-catalyzed GaN nanowires," *Journal of Crystal Growth*, vol. 371, pp. 142, 2013.
[74] Matt D. Brubaker, Shannon M. Duff, Todd E. Harvey, Paul T. Blanchard, Alexana Roshko, Aric W. Sanders, Norman A. Sanford, and Kris A. Bertness, "Polarity-Controlled GaN/AlN Nucleation Layers for Selective-Area Growth of GaN Nanowire Arrays on Si(111) Substrates by Molecular Beam Epitaxy," *Crystal Growth & Design*, vol. 16, no. 2, pp. 596, 2015.
[75] J. E. Kruse, L. Lymperakis, S. Eftychis, A. Adikimenakis, G. Doundoulakis, K. Tsagaraki, M. Androulidaki, A. Olziersky, P. Dimitrakis, V. Ioannou-Sougleridis, P. Normand, T. Koukoula, Th Kehagias, Ph Komninou, G. Konstantinidis, and A. Georgakilas, "Selective-area growth of GaN nanowires on SiO2-masked Si (111) substrates by molecular beam epitaxy," *Journal of Applied Physics*, vol. 119, no. 22, 2016.
[76] I. Vurgaftman and J. R. Meyer, "Band parameters for nitrogen-containing semiconductors," *Journal of Applied Physics*, vol. 94, no. 6, pp. 3675, 2003.
[77] R. R. Pelá, C. Caetano, M. Marques, L. G. Ferreira, J. Furthmüller, and L. K. Teles, "Accurate band gaps of AlGaN, InGaN, and AlInN alloys calculations based on LDA-1/2 approach," *Applied Physics Letters*, vol. 98, no. 15, 2011.
[78] A. Bogner, P. H. Jouneau, G. Thollet, D. Basset, and C. Gauthier, "A history of scanning electron microscopy developments: towards "wet-STEM" imaging," *Micron*, vol. 38, no. 4, pp. 390, 2007.
[79] Y. Wu, X. Liu, P. Wang, D. A. Laleyan, K. Sun, Y. Sun, C. Ahn, M. Kira, E. Kioupakis, and Z. Mi, "Monolayer GaN excitonic deep ultraviolet light emitting diodes," *Applied Physics Letters*, vol. 116, no. 1, 2020.
[80] D. A. Laleyan, S. Zhao, S. Y. Woo, H. N. Tran, H. B. Le, T. Szkopek, H. Guo, G. A. Botton, and Z. Mi, "AlN/h-BN Heterostructures for Mg Dopant-Free Deep Ultraviolet Photonics," *Nano Lett*, vol. 17, no. 6, pp. 3738, 2017.
[81] Joshua D. Caldwell, Igor Aharonovich, Guillaume Cassabois, James H. Edgar, Bernard Gil, and D. N. Basov, "Photonics with hexagonal boron nitride," *Nature Reviews Materials*, vol. 4, no. 8, pp. 552, 2019.
[82] S. J. Pearton, Fan Ren, Marko Tadjer, and Jihyun Kim, "Perspective: Ga2O3for ultra-high power rectifiers and MOSFETS," *Journal of Applied Physics*, vol. 124, no. 22, 2018.
[83] Hitoshi Umezawa, "Recent advances in diamond power semiconductor devices," *Materials Science in Semiconductor Processing*, vol. 78, pp. 147, 2018.
[84] Seongmo Hwang, Monirul Islam, Bin Zhang, Mohamed Lachab, Joe Dion, Ahmad Heidari, Haseeb Nazir, Vinod Adivarahan, and Asif Khan, "A Hybrid Micro-Pixel Based Deep Ultraviolet Light-Emitting Diode Lamp," *Applied Physics Express*, vol. 4, no. 1, 2011.
[85] Vinod Adivarahan, Ahmad Heidari, Bin Zhang, Qhalid Fareed, Seongmo Hwang, Monirul Islam, and Asif Khan, "280 nm Deep Ultraviolet Light Emitting Diode Lamp with an AlGaN Multiple Quantum Well Active Region," *Applied Physics Express*, vol. 2, no. 10, 2009.
[86] Mohsen Nami, Arman Rashidi, Morteza Monavarian, Saadat Mishkat-Ul-Masabih, Ashwin K. Rishinaramangalam, Steven R. J. Brueck, and Daniel Feezell, "Electrically Injected GHz-

Class GaN/InGaN Core–Shell Nanowire-Based μLEDs: Carrier Dynamics and Nanoscale Homogeneity," *ACS Photonics*, vol. 6, no. 7, pp. 1618, 2019.
[87] Yuanpeng Wu, Yongjie Wang, Kai Sun, and Zetian Mi, "Molecular beam epitaxy and characterization of AlGaN nanowire ultraviolet light emitting diodes on Al coated Si (0 0 1) substrate," *Journal of Crystal Growth*, vol. 507, pp. 65, 2019.
[88] K. B. Nam, M. L. Nakarmi, J. Li, J. Y. Lin, and H. X. Jiang, "Mg acceptor level in AlN probed by deep ultraviolet photoluminescence," *Applied Physics Letters*, vol. 83, no. 5, pp. 878, 2003.
[89] M. L. Nakarmi, N. Nepal, C. Ugolini, T. M. Altahtamouni, J. Y. Lin, and H. X. Jiang, "Correlation between optical and electrical properties of Mg-doped AlN epilayers," *Applied Physics Letters*, vol. 89, no. 15, 2006.
[90] M. L. Nakarmi, N. Nepal, J. Y. Lin, and H. X. Jiang, "Photoluminescence studies of impurity transitions in Mg-doped AlGaN alloys," *Applied Physics Letters*, vol. 94, no. 9, 2009.
[91] A. Pandey, X. Liu, Z. Deng, W. J. Shin, D. A. Laleyan, K. Mashooq, E. T. Reid, E. Kioupakis, P. Bhattacharya, and Z. Mi, "Enhanced doping efficiency of ultrawide band gap semiconductors by metal-semiconductor junction assisted epitaxy," *Physical Review Materials*, vol. 3, no. 5, 2019.
[92] Qimin Yan, Anderson Janotti, Matthias Scheffler, and Chris G. Van de Walle, "Origins of optical absorption and emission lines in AlN," *Applied Physics Letters*, vol. 105, no. 11, 2014.
[93] Tristan Koppe, Hans Hofsäss, and Ulrich Vetter, "Overview of band-edge and defect related luminescence in aluminum nitride," *Journal of Luminescence*, vol. 178, pp. 267, 2016.
[94] A. M. Siladie, G. Jacopin, A. Cros, N. Garro, E. Robin, D. Caliste, P. Pochet, F. Donatini, J. Pernot, and B. Daudin, "Mg and In Codoped p-type AlN Nanowires for pn Junction Realization," *Nano Lett*, vol. 19, no. 12, pp. 8357, 2019.
[95] S. Zhao, B. H. Le, D. P. Liu, X. D. Liu, M. G. Kibria, T. Szkopek, H. Guo, and Z. Mi, "p-Type InN nanowires," *Nano Lett*, vol. 13, no. 11, pp. 5509, 2013.
[96] N. Sanders, D. Bayerl, G. Shi, K. A. Mengle, and E. Kioupakis, "Electronic and Optical Properties of Two-Dimensional GaN from First-Principles," *Nano Lett*, vol. 17, no. 12, pp. 7345, 2017.
[97] A. Das, J. Heo, M. Jankowski, W. Guo, L. Zhang, H. Deng, and P. Bhattacharya, "Room temperature ultralow threshold GaN nanowire polariton laser," *Phys Rev Lett*, vol. 107, no. 6, pp. 066405, 2011.
[98] Samuel Matta, Julien Brault, Maxim Korytov, Thi Quynh Phuong Vuong, Catherine Chaix, Mohamed Al Khalfioui, Philippe Vennéguès, Jean Massies, and Bernard Gil, "Properties of AlN layers grown on c-sapphire substrate using ammonia assisted MBE," *Journal of Crystal Growth*, vol. 499, pp. 40, 2018.
[99] K. B. Nam, M. L. Nakarmi, J. Li, J. Y. Lin, and H. X. Jiang, "Photoluminescence studies of Si-doped AlN epilayers," *Applied Physics Letters*, vol. 83, no. 14, pp. 2787, 2003.
[100] R. Boger, M. Fiederle, L. Kirste, M. Maier, and J. Wagner, "Molecular beam epitaxy and doping of AlN at high growth temperatures," *Journal of Physics D: Applied Physics*, vol. 39, no. 21, pp. 4616, 2006.

[101] Q. Wang, S. Zhao, A. T. Connie, I. Shih, Z. Mi, T. Gonzalez, M. P. Andrews, X. Z. Du, J. Y. Lin, and H. X. Jiang, "Optical properties of strain-free AlN nanowires grown by molecular beam epitaxy on Si substrates," *Applied Physics Letters*, vol. 104, no. 22, 2014.
[102] Tosja Zywietz, Jörg Neugebauer, and Matthias Scheffler, "Adatom diffusion at GaN (0001) and (000$\bar{1}$) surfaces," *Applied Physics Letters*, vol. 73, no. 4, pp. 487, 1998.
[103] K. Kishino and S. Ishizawa, "Selective-area growth of GaN nanocolumns on Si(111) substrates for application to nanocolumn emitters with systematic analysis of dislocation filtering effect of nanocolumns," *Nanotechnology*, vol. 26, no. 22, pp. 225602, 2015.
[104] Koji Yamano and Katsumi Kishino, "Selective area growth of InGaN-based nanocolumn LED crystals on AlN/Si substrates useful for integrated μ-LED fabrication," *Applied Physics Letters*, vol. 112, no. 9, 2018.
[105] Y. H. Liang and E. Towe, "Progress in efficient doping of high aluminum-containing group III-nitrides," *Applied Physics Reviews*, vol. 5, no. 1, 2018.
[106] M. Kira and S. W. Koch, "Semiconductor Quantum Optics," 2012.
[107] Ivan Aleksandrov and Konstantin Zhuravlev, "Photoluminescence of GaN/AlN quantum dots at high excitation powers," *physica status solidi (c)*, vol. 7, no. 7-8, pp. 2230, 2010.
[108] A. B. Slimane, A. Najar, R. Elafandy, D. P. San-Roman-Alerigi, D. Anjum, T. K. Ng, and B. S. Ooi, "On the phenomenon of large photoluminescence red shift in GaN nanoparticles," *Nanoscale Res Lett*, vol. 8, no. 1, pp. 342, 2013.
[109] Jay M. Shah, Y. L. Li, Th Gessmann, and E. F. Schubert, "Experimental analysis and theoretical model for anomalously high ideality factors (n≫2.0) in AlGaN/GaNp-njunction diodes," *Journal of Applied Physics*, vol. 94, no. 4, pp. 2627, 2003.
[110] Piotr Perlin, Marek Osiński, Petr G. Eliseev, Vladimir A. Smagley, Jian Mu, Michael Banas, and Philippe Sartori, "Low‐temperature study of current and electroluminescence in InGaN/AlGaN/GaN double‐heterostructure blue light‐emitting diodes," *Applied Physics Letters*, vol. 69, no. 12, pp. 1680, 1996.
[111] H. C. Casey, J. Muth, S. Krishnankutty, and J. M. Zavada, "Dominance of tunneling current and band filling in InGaN/AlGaN double heterostructure blue light‐emitting diodes," *Applied Physics Letters*, vol. 68, no. 20, pp. 2867, 1996.
[112] K. B. Lee, P. J. Parbrook, T. Wang, J. Bai, F. Ranalli, R. J. Airey, and G. Hill, "The origin of the high ideality factor in AlGaN-based quantum well ultraviolet light emitting diodes," *physica status solidi (b)*, vol. 247, no. 7, pp. 1761, 2010.
[113] M. Lee, H. Lee, K. M. Song, and J. Kim, "Investigation of Forward Tunneling Characteristics of InGaN/GaN Blue Light-Emitting Diodes on Freestanding GaN Detached from a Si Substrate," *Nanomaterials (Basel)*, vol. 8, no. 7, 2018.
[114] Jinmin Li, Junxi Wang, Yun Zhang, Jianchang Yan, and Yanan Guo, "Enhancing the light extraction of AlGaN-based ultraviolet light-emitting diodes in the nanoscale," *Journal of Nanophotonics*, vol. 12, no. 04, pp. 1, 2018.
[115] X. Rong, X. Wang, S. V. Ivanov, X. Jiang, G. Chen, P. Wang, W. Wang, C. He, T. Wang, T. Schulz, M. Albrecht, V. N. Jmerik, A. A. Toropov, V. V. Ratnikov, V. I. Kozlovsky, V. P. Martovitsky, P. Jin, F. Xu, X. Yang, Z. Qin, W. Ge, J. Shi, and B. Shen, "High-Output-Power Ultraviolet Light Source from Quasi-2D GaN Quantum Structure," *Adv Mater*, vol. 28, no. 36, pp. 7978, 2016.
[116] Dingyu Ma, Xin Rong, Xiantong Zheng, Weiying Wang, Ping Wang, Tobias Schulz, Martin Albrecht, Sebastian Metzner, Mathias Müller, Olga August, Frank Bertram, Jürgen Christen, Peng Jin, Mo Li, Jian Zhang, Xuelin Yang, Fujun Xu, Zhixin Qin, Weikun Ge, Bo

Shen, and Xinqiang Wang, "Exciton emission of quasi-2D InGaN in GaN matrix grown by molecular beam epitaxy," *Scientific Reports*, vol. 7, no. 1, pp. 46420, 2017.
[117] Yixin Wang, Xin Rong, Sergey Ivanov, Valentin Jmerik, Zhaoying Chen, Hui Wang, Tao Wang, Ping Wang, Peng Jin, Yanan Chen, Vladimir Kozlovsky, Dmitry Sviridov, Michail Zverev, Elena Zhdanova, Nikita Gamov, Valentin Studenov, Hideto Miyake, Hongwei Li, Shiping Guo, Xuelin Yang, Fujun Xu, Tongjun Yu, Zhixin Qin, Weikun Ge, Bo Shen, and Xinqiang Wang, "Deep Ultraviolet Light Source from Ultrathin GaN/AlN MQW Structures with Output Power Over 2 Watt," *Advanced Optical Materials*, vol. 7, no. 10, 2019.
[118] Y. Wu, T. Hasan, X. Li, P. Xu, Y. Wang, X. Shen, X. Liu, and Q. Yang, "High efficiency single Ag nanowire/p-GaN substrate Schottky junction-based ultraviolet light emitting diodes," *Applied Physics Letters*, vol. 106, no. 5, pp. 051108, 2015.
[119] Yuewei Zhang, Sriram Krishnamoorthy, Fatih Akyol, Sanyam Bajaj, Andrew A. Allerman, Michael W. Moseley, Andrew M. Armstrong, and Siddharth Rajan, "Tunnel-injected sub-260 nm ultraviolet light emitting diodes," *Applied Physics Letters*, vol. 110, no. 20, 2017.
[120] Yuewei Zhang, Zane Jamal-Eddine, and Siddharth Rajan, "Recent progress of tunnel junction-based ultra-violet light emitting diodes," *Japanese Journal of Applied Physics*, vol. 58, no. SC, 2019.
[121] Jai Verma, S. M. Islam, Vladimir Protasenko, Prem Kumar Kandaswamy, Huili Xing, and Debdeep Jena, "Tunnel-injection quantum dot deep-ultraviolet light-emitting diodes with polarization-induced doping in III-nitride heterostructures," *Applied Physics Letters*, vol. 104, no. 2, 2014.
[122] R. Dalmau, B. Moody, R. Schlesser, S. Mita, J. Xie, M. Feneberg, B. Neuschl, K. Thonke, R. Collazo, A. Rice, J. Tweedie, and Z. Sitar, "Growth and Characterization of AlN and AlGaN Epitaxial Films on AlN Single Crystal Substrates," *Journal of The Electrochemical Society*, vol. 158, no. 5, 2011.
[123] Sylvia Hagedorn, Arne Knauer, Anna Mogilatenko, Eberhard Richter, and Markus Weyers, "AlN growth on nano-patterned sapphire: A route for cost efficient pseudo substrates for deep UV LEDs," *physica status solidi (a)*, vol. 213, no. 12, pp. 3178, 2016.
[124] Zhaoying Chen, Jason Hoo, Yao Chen, Vincent Wang, and Shiping Guo, "Study of AlN based materials grown on nano-patterned sapphire substrates for deep ultraviolet LED applications," *Japanese Journal of Applied Physics*, vol. 58, no. SC, 2019.
[125] Hideto Miyake, Chia-Hung Lin, Kenta Tokoro, and Kazumasa Hiramatsu, "Preparation of high-quality AlN on sapphire by high-temperature face-to-face annealing," *Journal of Crystal Growth*, vol. 456, pp. 155, 2016.
[126] Sebastian Walde, Sylvia Hagedorn, and Markus Weyers, "Impact of intermediate high temperature annealing on the properties of AlN/sapphire templates grown by metalorganic vapor phase epitaxy," *Japanese Journal of Applied Physics*, vol. 58, no. SC, 2019.
[127] S. M. Islam, Kevin Lee, Jai Verma, Vladimir Protasenko, Sergei Rouvimov, Shyam Bharadwaj, Huili Xing, and Debdeep Jena, "MBE-grown 232–270 nm deep-UV LEDs using monolayer thin binary GaN/AlN quantum heterostructures," *Applied Physics Letters*, vol. 110, no. 4, 2017.
[128] S. M. Islam, Vladimir Protasenko, Kevin Lee, Sergei Rouvimov, Jai Verma, Huili Xing, and Debdeep Jena, "Deep-UV emission at 219 nm from ultrathin MBE GaN/AlN quantum heterostructures," *Applied Physics Letters*, vol. 111, no. 9, 2017.

[129] Dylan Bayerl, S. M. Islam, Christina M. Jones, Vladimir Protasenko, Debdeep Jena, and Emmanouil Kioupakis, "Deep ultraviolet emission from ultra-thin GaN/AlN heterostructures," *Applied Physics Letters*, vol. 109, no. 24, 2016.
[130] Yoshiji Horikoshi, Minoru Kawashima, and Hiroshi Yamaguchi, "Migration-Enhanced Epitaxy of GaAs and AlGaAs," *Japanese Journal of Applied Physics*, vol. 27, no. Part 1, No. 2, pp. 169, 1988.
[131] B. Janjua, H. Sun, C. Zhao, D. H. Anjum, F. Wu, A. A. Alhamoud, X. Li, A. M. Albadri, A. Y. Alyamani, M. M. El-Desouki, T. K. Ng, and B. S. Ooi, "Self-planarized quantum-disks-in-nanowires ultraviolet-B emitters utilizing pendeo-epitaxy," *Nanoscale*, vol. 9, no. 23, pp. 7805, 2017.
[132] X. Liu, B. H. Le, S. Y. Woo, S. Zhao, A. Pofelski, G. A. Botton, and Z. Mi, "Selective area epitaxy of AlGaN nanowire arrays across nearly the entire compositional range for deep ultraviolet photonics," *Opt Express*, vol. 25, no. 24, pp. 30494, 2017.
[133] S. Chatterjee, C. Ell, S. Mosor, G. Khitrova, H. M. Gibbs, W. Hoyer, M. Kira, S. W. Koch, J. P. Prineas, and H. Stolz, "Excitonic photoluminescence in semiconductor quantum wells: plasma versus excitons," *Phys Rev Lett*, vol. 92, no. 6, pp. 067402, 2004.
[134] Dylan Bayerl and Emmanouil Kioupakis," 2019.
[135] B. Mazumder, M. H. Wong, C. A. Hurni, J. Y. Zhang, U. K. Mishra, and J. S. Speck, "Asymmetric interfacial abruptness in N-polar and Ga-polar GaN/AlN/GaN heterostructures," *Applied Physics Letters*, vol. 101, no. 9, 2012.
[136] Karine Hestroffer, Cédric Leclere, Catherine Bougerol, Hubert Renevier, and Bruno Daudin, "Polarity of GaN nanowires grown by plasma-assisted molecular beam epitaxy on Si(111)," *Physical Review B*, vol. 84, no. 24, 2011.
[137] Kunook Chung, Ayush Pandey, Tuba Sarwar, Anthony Aiello, Zetian Mi, Pallab Bhattacharya, and Pei-Cheng Ku, "Wavelength tuning in the purple wavelengths using strain-controlled AlxGa1–xN/GaN disk-in-wire structures," *Applied Physics Letters*, vol. 116, no. 4, 2020.
[138] R. P. Smith, J. K. Wahlstrand, A. C. Funk, R. P. Mirin, S. T. Cundiff, J. T. Steiner, M. Schafer, M. Kira, and S. W. Koch, "Extraction of many-body configurations from nonlinear absorption in semiconductor quantum wells," *Phys Rev Lett*, vol. 104, no. 24, pp. 247401, 2010.
[139] T. F. Kent, S. D. Carnevale, A. T. Sarwar, P. J. Phillips, R. F. Klie, and R. C. Myers, "Deep ultraviolet emitting polarization induced nanowire light emitting diodes with AlxGa(1)-xN active regions," *Nanotechnology*, vol. 25, no. 45, pp. 455201, 2014.
[140] A. T. Sarwar, B. J. May, M. F. Chisholm, G. J. Duscher, and R. C. Myers, "Ultrathin GaN quantum disk nanowire LEDs with sub-250 nm electroluminescence," *Nanoscale*, vol. 8, no. 15, pp. 8024, 2016.
[141] Yuta Aoki, Masakazu Kuwabara, Yoji Yamashita, Yasufumi Takagi, Atsushi Sugiyama, and Harumasa Yoshida, "A 350-nm-band GaN/AlGaN multiple-quantum-well laser diode on bulk GaN," *Applied Physics Letters*, vol. 107, no. 15, pp. 151103, 2015.
[142] Harumasa Yoshida, Yoji Yamashita, Masakazu Kuwabara, and Hirofumi Kan, "Demonstration of an ultraviolet 336 nm AlGaN multiple-quantum-well laser diode," *Applied Physics Letters*, vol. 93, no. 24, pp. 241106, 2008.
[143] Masafumi Jo, Noritoshi Maeda, and Hideki Hirayama, "Enhanced light extraction in 260 nm light-emitting diode with a highly transparent p-AlGaN layer," *Applied Physics Express*, vol. 9, no. 1, pp. 012102, 2016.

[144] Masatsugu Ichikawa, Akira Fujioka, Takao Kosugi, Shinya Endo, Harunobu Sagawa, Hiroto Tamaki, Takashi Mukai, Miyuki Uomoto, and Takehito Shimatsu, "High-output-power deep ultraviolet light-emitting diode assembly using direct bonding," *Applied Physics Express*, vol. 9, no. 7, pp. 072101, 2016.
[145] Shin-ichiro Inoue, Tamari Naoki, Toru Kinoshita, Toshiyuki Obata, and Hiroyuki Yanagi, "Light extraction enhancement of 265 nm deep-ultraviolet light-emitting diodes with over 90 mW output power via an AlN hybrid nanostructure," *Applied Physics Letters*, vol. 106, no. 13, pp. 131104, 2015.
[146] James R. Grandusky, Jianfeng Chen, Shawn R. Gibb, Mark C. Mendrick, Craig G. Moe, Lee Rodak, Gregory A. Garrett, Michael Wraback, and Leo J. Schowalter, "270 nm Pseudomorphic Ultraviolet Light-Emitting Diodes with Over 60 mW Continuous Wave Output Power," *Applied Physics Express*, vol. 6, no. 3, pp. 032101, 2013.
[147] Peng Dong, Jianchang Yan, Junxi Wang, Yun Zhang, Chong Geng, Tongbo Wei, Peipei Cong, Yiyun Zhang, Jianping Zeng, Yingdong Tian, Lili Sun, Qingfeng Yan, Jinmin Li, Shunfei Fan, and Zhixin Qin, "282-nm AlGaN-based deep ultraviolet light-emitting diodes with improved performance on nano-patterned sapphire substrates," *Applied Physics Letters*, vol. 102, no. 24, pp. 241113, 2013.
[148] J. Shakya, K. Knabe, K. H. Kim, J. Li, J. Y. Lin, and H. X. Jiang, "Polarization of III-nitride blue and ultraviolet light-emitting diodes," *Applied Physics Letters*, vol. 86, no. 9, pp. 091107, 2005.
[149] Tim Kolbe, Arne Knauer, Chris Chua, Zhihong Yang, Sven Einfeldt, Patrick Vogt, Noble M. Johnson, Markus Weyers, and Michael Kneissl, "Optical polarization characteristics of ultraviolet (In)(Al)GaN multiple quantum well light emitting diodes," *Applied Physics Letters*, vol. 97, no. 17, pp. 171105, 2010.
[150] Mehrdad Djavid and Zetian Mi, "Enhancing the light extraction efficiency of AlGaN deep ultraviolet light emitting diodes by using nanowire structures," *Applied Physics Letters*, vol. 108, no. 5, pp. 051102, 2016.
[151] A. T. M. Golam Sarwar, Brelon J. May, Julia I. Deitz, Tyler J. Grassman, David W. McComb, and Roberto C. Myers, "Tunnel junction enhanced nanowire ultraviolet light emitting diodes," *Applied Physics Letters*, vol. 107, no. 10, pp. 101103, 2015.
[152] Z. Gu, M. P. Paranthaman, J. Xu, and Z. W. Pan, "Aligned ZnO nanorod arrays grown directly on zinc foils and zinc spheres by a low-temperature oxidization method," *ACS Nano*, vol. 3, no. 2, pp. 273, 2009.
[153] Brelon J. May, A. T. M. Golam Sarwar, and Roberto C. Myers, "Nanowire LEDs grown directly on flexible metal foil," *Applied Physics Letters*, vol. 108, no. 14, pp. 141103, 2016.
[154] C. Zhao, T. K. Ng, N. Wei, A. Prabaswara, M. S. Alias, B. Janjua, C. Shen, and B. S. Ooi, "Facile Formation of High-Quality InGaN/GaN Quantum-Disks-in-Nanowires on Bulk-Metal Substrates for High-Power Light-Emitters," *Nano Lett*, vol. 16, no. 2, pp. 1056, 2016.
[155] Xianhe Liu, Kishwar Mashooq, Thomas Szkopek, and Zetian Mi, "Improving the Efficiency of Transverse Magnetic Polarized Emission from AlGaN Based LEDs by Using Nanowire Photonic Crystal," *IEEE Photonics Journal*, vol. 10, no. 4, pp. 1, 2018.
[156] M. Wolz, C. Hauswald, T. Flissikowski, T. Gotschke, S. Fernandez-Garrido, O. Brandt, H. T. Grahn, L. Geelhaar, and H. Riechert, "Epitaxial Growth of GaN Nanowires with High Structural Perfection on a Metallic TiN Film," *Nano Lett*, vol. 15, no. 6, pp. 3743, 2015.
[157] B. Janjua, H. Sun, C. Zhao, D. H. Anjum, D. Priante, A. A. Alhamoud, F. Wu, X. Li, A. M. Albadri, A. Y. Alyamani, M. M. El-Desouki, T. K. Ng, and B. S. Ooi, "Droop-free

Al_xGa_{1-x}N/Al_yGa_{1-y}N quantum-disks-in-nanowires ultraviolet LED emitting at 337 nm on metal/silicon substrates," *Opt Express*, vol. 25, no. 2, pp. 1381, 2017.

[158] Davide Priante, Rami T. Elafandy, Aditya Prabaswara, Bilal Janjua, Chao Zhao, Mohd Sharizal Alias, Malleswararao Tangi, Yazeed Alaskar, Abdulrahman M. Albadri, Ahmed Y. Alyamani, Tien Khee Ng, and Boon S. Ooi, "Diode junction temperature in ultraviolet AlGaN quantum-disks-in-nanowires," *Journal of Applied Physics*, vol. 124, no. 1, pp. 015702, 2018.

[159] S. Zhao, S. M. Sadaf, S. Vanka, Y. Wang, R. Rashid, and Z. Mi, "Sub-milliwatt AlGaN nanowire tunnel junction deep ultraviolet light emitting diodes on silicon operating at 242 nm," *Applied Physics Letters*, vol. 109, no. 20, pp. 201106, 2016.

[160] Yuanpeng Wu, Yongjie Wang, Kai Sun, Anthony Aiello, Pallab Bhattacharya, and Zetian Mi, "Molecular beam epitaxy and characterization of Mg-doped GaN epilayers grown on Si (0 0 1) substrate through controlled nanowire coalescence," *Journal of Crystal Growth*, vol. 498, pp. 109, 2018.

[161] V. Consonni, M. Knelangen, A. Trampert, L. Geelhaar, and H. Riechert, "Nucleation and coalescence effects on the density of self-induced GaN nanowires grown by molecular beam epitaxy," *Applied Physics Letters*, vol. 98, no. 7, pp. 071913, 2011.

[162] B. Heying, R. Averbeck, L. F. Chen, E. Haus, H. Riechert, and J. S. Speck, "Control of GaN surface morphologies using plasma-assisted molecular beam epitaxy," *Journal of Applied Physics*, vol. 88, no. 4, pp. 1855, 2000.

[163] A. Dadgar, F. Schulze, M. Wienecke, A. Gadanecz, J. Bläsing, P. Veit, T. Hempel, A. Diez, J. Christen, and A. Krost, "Epitaxy of GaN on silicon—impact of symmetry and surface reconstruction," *New Journal of Physics*, vol. 9, no. 10, pp. 389, 2007.

[164] D. Zhu, D. J. Wallis, and C. J. Humphreys, "Prospects of III-nitride optoelectronics grown on Si," *Rep Prog Phys*, vol. 76, no. 10, pp. 106501, 2013.

[165] F. Semond, "Epitaxial challenges of GaN on silicon," *Mrs Bulletin*, vol. 40, no. 5, pp. 412, 2015.

[166] W. Wang, H. Wang, W. Yang, Y. Zhu, and G. Li, "A new approach to epitaxially grow high-quality GaN films on Si substrates: the combination of MBE and PLD," *Sci Rep*, vol. 6, pp. 24448, 2016.

[167] T. S. Zheleva, S. A. Smith, D. B. Thomson, K. J. Linthicum, P. Rajagopal, and R. F. Davis, "Pendeo-epitaxy: A new approach for lateral growth of gallium nitride films," *Journal of Electronic Materials*, vol. 28, no. 4, pp. L5, 1999.

[168] R. F. Davis, T. Gehrke, K. J. Linthicum, P. Rajagopal, A. M. Roskowski, T. Zheleva, E. A. Preble, C. A. Zorman, M. Mehregany, U. Schwarz, J. Schuck, and R. Grober, "Review of pendeo-epitaxial growth and characterization of thin films of GaN and AlGaN alloys on 6H-SiC(0001) and Si(111) substrates," *Mrs Internet Journal of Nitride Semiconductor Research*, vol. 6, no. 14, pp. 1, 2001.

[169] K. Kusakabe, A. Kikuchi, and K. Kishino, "Characterization of overgrown GaN layers on nano-columns grown by RF-molecular beam epitaxy," *Japanese Journal of Applied Physics Part 2-Letters*, vol. 40, no. 3a, pp. L192, 2001.

[170] K. Kusakabe, A. Kikuchi, and K. Kishino, "Overgrowth of GaN layer on GaN nano-columns by RF-molecular beam epitaxy," *Journal of Crystal Growth*, vol. 237, pp. 988, 2002.

[171] K. L. Averett, J. E. Van Nostrand, J. D. Albrecht, Y. S. Chen, and C. C. Yang, "Epitaxial overgrowth of GaN nanocolumns," *Journal of Vacuum Science & Technology B: Microelectronics and Nanometer Structures*, vol. 25, no. 3, pp. 964, 2007.
[172] Qiming Li, Yong Lin, J. Randall Creighton, Jeffrey J. Figiel, and George T. Wang, "Nanowire-Templated Lateral Epitaxial Growth of Low-Dislocation Density Nonpolara-Plane GaN onr-Plane Sapphire," *Advanced Materials*, vol. 21, no. 23, pp. 2416, 2009.
[173] Bo-Ra Yeom, R. Navamathavan, Ji-Hyeon Park, Yong-Ho Ra, and Cheul-Ro Lee, "Growth behavior of GaN epilayers on Si(111) grown by GaN nanowires assisted epitaxial lateral overgrowth," *CrystEngComm*, vol. 14, no. 17, pp. 5558, 2012.
[174] Pinar Dogan, Oliver Brandt, Carsten Pfüller, Anne-Kathrin Bluhm, Lutz Geelhaar, and Henning Riechert, "GaN nanowire templates for the pendeoepitaxial coalescence overgrowth on Si(111) by molecular beam epitaxy," *Journal of Crystal Growth*, vol. 323, no. 1, pp. 418, 2011.
[175] Pinar Dogan, Oliver Brandt, Carsten Pfüller, Jonas Lähnemann, Uwe Jahn, Claudia Roder, Achim Trampert, Lutz Geelhaar, and Henning Riechert, "Formation of High-Quality GaN Microcrystals by Pendeoepitaxial Overgrowth of GaN Nanowires on Si(111) by Molecular Beam Epitaxy," *Crystal Growth & Design*, vol. 11, no. 10, pp. 4257, 2011.
[176] Hiroto Sekiguchi, Kei Kato, Akihiko Kikuchi, and Katsumi Kishino, "Effect of Be-doping on InGaN/GaN nanocolumn light-emitting diode structures by rf-plasma-assisted molecular-beam epitaxy," *physica status solidi (c)*, vol. 5, no. 9, pp. 3069, 2008.
[177] B. H. Le, S. Zhao, X. Liu, S. Y. Woo, G. A. Botton, and Z. Mi, "Controlled Coalescence of AlGaN Nanowire Arrays: An Architecture for Nearly Dislocation-Free Planar Ultraviolet Photonic Device Applications," *Adv Mater*, vol. 28, no. 38, pp. 8446, 2016.
[178] K. K. Sabelfeld, V. M. Kaganer, F. Limbach, P. Dogan, O. Brandt, L. Geelhaar, and H. Riechert, "Height self-equilibration during the growth of dense nanowire ensembles: Order emerging from disorder," *Applied Physics Letters*, vol. 103, no. 13, pp. 133105, 2013.
[179] R. Songmuang, T. Ben, B. Daudin, D. Gonzalez, and E. Monroy, "Identification of III-N nanowire growth kinetics via a marker technique," *Nanotechnology*, vol. 21, no. 29, pp. 295605, 2010.
[180] Vladimir G. Dubrovskii, Vincent Consonni, Lutz Geelhaar, Achim Trampert, and Henning Riechert, "Scaling growth kinetics of self-induced GaN nanowires," *Applied Physics Letters*, vol. 100, no. 15, pp. 153101, 2012.
[181] Johannes K. Zettler, Christian Hauswald, Pierre Corfdir, Mattia Musolino, Lutz Geelhaar, Henning Riechert, Oliver Brandt, and Sergio Fernández-Garrido, "High-Temperature Growth of GaN Nanowires by Molecular Beam Epitaxy: Toward the Material Quality of Bulk GaN," *Crystal Growth & Design*, vol. 15, no. 8, pp. 4104, 2015.
[182] A. Y. Polyakov, N. B. Smirnov, A. V. Govorkov, G. Dang, A. P. Zhang, F. Ren, X. A. Cao, S. J. Pearton, and R. G. Wilson, "Electrical properties and defect states in undoped high-resistivity GaN films used in high-power rectifiers," *Journal of Vacuum Science & Technology B: Microelectronics and Nanometer Structures*, vol. 18, no. 3, pp. 1237, 2000.
[183] A. E. Wickenden, D. D. Koleske, R. L. Henry, M. E. Twigg, and M. Fatemi, "Resistivity control in unintentionally doped GaN films grown by MOCVD," *Journal of Crystal Growth*, vol. 260, no. 1-2, pp. 54, 2004.
[184] Meng Zhang, Pallab Bhattacharya, Wei Guo, and Animesh Banerjee, "Mg doping of GaN grown by plasma-assisted molecular beam epitaxy under nitrogen-rich conditions," *Applied Physics Letters*, vol. 96, no. 13, pp. 132103, 2010.

[185] Peter Kozodoy, Huili Xing, Steven P. DenBaars, Umesh K. Mishra, A. Saxler, R. Perrin, S. Elhamri, and W. C. Mitchel, "Heavy doping effects in Mg-doped GaN," *Journal of Applied Physics*, vol. 87, no. 4, pp. 1832, 2000.
[186] U. Kaufmann, M. Kunzer, M. Maier, H. Obloh, A. Ramakrishnan, B. Santic, and P. Schlotter, "Nature of the 2.8 eV photoluminescence band in Mg doped GaN," *Applied Physics Letters*, vol. 72, no. 11, pp. 1326, 1998.
[187] J. M. Myoung, K. H. Shim, C. Kim, O. Gluschenkov, K. Kim, S. Kim, D. A. Turnbull, and S. G. Bishop, "Optical characteristics of p‐type GaN films grown by plasma‐assisted molecular beam epitaxy," *Applied Physics Letters*, vol. 69, no. 18, pp. 2722, 1996.
[188] P. T. N. Hieu, S. F. Zhang, K. Cui, A. Korinek, G. A. Botton, and Z. T. Mi, "High-Efficiency InGaN/GaN Dot-in-a-Wire Red Light-Emitting Diodes," *Ieee Photonics Technology Letters*, vol. 24, no. 4, pp. 321, 2012.
[189] H. P. Nguyen, K. Cui, S. Zhang, S. Fathololoumi, and Z. Mi, "Full-color InGaN/GaN dot-in-a-wire light emitting diodes on silicon," *Nanotechnology*, vol. 22, no. 44, pp. 445202, 2011.
[190] A. C. Chia and R. R. LaPierre, "Contact planarization of ensemble nanowires," *Nanotechnology*, vol. 22, no. 24, pp. 245304, 2011.
[191] F. Limbach, C. Hauswald, J. Lahnemann, M. Wolz, O. Brandt, A. Trampert, M. Hanke, U. Jahn, R. Calarco, L. Geelhaar, and H. Riechert, "Current path in light emitting diodes based on nanowire ensembles," *Nanotechnology*, vol. 23, no. 46, pp. 465301, 2012.
[192] S. Jahangir, M. Mandl, M. Strassburg, and P. Bhattacharya, "Molecular beam epitaxial growth and optical properties of red-emitting ($\lambda = 650$ nm) InGaN/GaN disks-in-nanowires on silicon," *Applied Physics Letters*, vol. 102, no. 7, pp. 071101, 2013.
[193] H. X. Jiang and J. Y. Lin, "Nitride micro-LEDs and beyond - a decade progress review," *Optics Express*, vol. 21, no. S3, pp. A475, 2013.
[194] Tingzhu Wu, Chin-Wei Sher, Yue Lin, Chun-Fu Lee, Shijie Liang, Yijun Lu, Sung-Wen Huang Chen, Weijie Guo, Hao-Chung Kuo, and Zhong Chen, "Mini-LED and Micro-LED: Promising Candidates for the Next Generation Display Technology," *Applied Sciences*, vol. 8, no. 9, pp. 1557, 2018.
[195] H. Xu, J. Zhang, K. M. Davitt, Y. K. Song, and A. V. Nurmikko, "Application of blue–green and ultraviolet micro-LEDs to biological imaging and detection," *Journal of Physics D: Applied Physics*, vol. 41, no. 9, pp. 094013, 2008.
[196] David Hwang, Asad Mughal, Christopher D. Pynn, Shuji Nakamura, and Steven P. DenBaars, "Sustained high external quantum efficiency in ultrasmall blue III–nitride micro-LEDs," *Applied Physics Express*, vol. 10, no. 3, pp. 032101, 2017.
[197] Yong-Ho Ra, Renjie Wang, Steffi Y. Woo, Mehrdad Djavid, Sharif Md Sadaf, Jaesoong Lee, Gianluigi A. Botton, and Zetian Mi, "Full-Color Single Nanowire Pixels for Projection Displays," *Nano Letters*, vol. 16, no. 7, pp. 4608, 2016.
[198] Zhaojun Liu, Wing Cheung Chong, Ka Ming Wong, and Kei May Lau, "GaN-based LED micro-displays for wearable applications," *Microelectronic Engineering*, vol. 148, pp. 98, 2015.
[199] Deng Peng, Ke Zhang, Victor Shin-Deh Chao, Weijing Mo, Kei May Lau, and Zhaojun Liu, "Full-Color Pixelated-Addressable Light Emitting Diode on Transparent Substrate (LEDoTS) Micro-Displays by CoB," *Journal of Display Technology*, vol. 12, no. 7, pp. 742, 2016.

[200] X. Zhang, P. Li, X. Zou, J. Jiang, S. H. Yuen, C. W. Tang, and K. M. Lau, "Active Matrix Monolithic LED Micro-Display Using GaN-on-Si Epilayers," *IEEE Photonics Technology Letters*, vol. 31, no. 11, pp. 865, 2019.
[201] Niall McAlinden, Yunzhou Cheng, Robert Scharf, Enyuan Xie, Erdan Gu, Christopher Reiche, Rohit Sharma, Prashant Tathireddy, Prashant Tathireddy, Loren Rieth, Steve Blair, and Keith Mathieson, "Multisite microLED optrode array for neural interfacing," *Neurophotonics*, vol. 6, no. 3, pp. 035010, 2019.
[202] D. Tsonev, H. Chun, S. Rajbhandari, J. J. D. McKendry, S. Videv, E. Gu, M. Haji, S. Watson, A. E. Kelly, G. Faulkner, M. D. Dawson, H. Haas, and D. O' Brien, "A 3-Gb/s Single-LED OFDM-Based Wireless VLC Link Using a Gallium Nitride $\mu{\rm LED}$," *IEEE Photonics Technology Letters*, vol. 26, no. 7, pp. 637, 2014.
[203] Matthew S. Wong, Shuji Nakamura, and Steven P. DenBaars, "Review—Progress in High Performance III-Nitride Micro-Light-Emitting Diodes," *ECS Journal of Solid State Science and Technology*, vol. 9, no. 1, 2020.
[204] Hongjian Li, Matthew S. Wong, Michel Khoury, Bastien Bonef, Haojun Zhang, YiChao Chow, Panpan Li, Jared Kearns, Aidan A. Taylor, Philippe De Mierry, Zainuriah Hassan, Shuji Nakamura, and Steven P. DenBaars, "Study of efficient semipolar (11-22) InGaN green micro-light-emitting diodes on high-quality (11-22) GaN/sapphire template," *Optics Express*, vol. 27, no. 17, pp. 24154, 2019.
[205] François Olivier, Sauveur Tirano, Ludovic Dupré, Bernard Aventurier, Christophe Largeron, and François Templier, "Influence of size-reduction on the performances of GaN-based micro-LEDs for display application," *Journal of Luminescence*, vol. 191, pp. 112, 2017.
[206] Masaki Minami, Shigetaka Tomiya, Kenji Ishikawa, Ryosuke Matsumoto, Shang Chen, Masanaga Fukasawa, Fumikatsu Uesawa, Makoto Sekine, Masaru Hori, and Tetsuya Tatsumi, "Analysis of GaN Damage Induced by Cl$_{2}$/SiCl$_{4}$/Ar Plasma," *Japanese Journal of Applied Physics*, vol. 50, no. 8, pp. 08JE03, 2011.
[207] R. J. Shul, L. Zhang, A. G. Baca, C. G. Willison, J. Han, S. J. Pearton, and F. Ren, "Inductively coupled plasma-induced etch damage of GaN p-n junctions," *Journal of Vacuum Science & Technology A*, vol. 18, no. 4, pp. 1139, 2000.
[208] Matthias Auf der Maur, Alessandro Pecchia, Gabriele Penazzi, Walter Rodrigues, and Aldo Di Carlo, "Efficiency Drop in Green $\mathrm{InGaN}/\mathrm{GaN}$ Light Emitting Diodes: The Role of Random Alloy Fluctuations," *Physical Review Letters*, vol. 116, no. 2, pp. 027401, 2016.
[209] R. Singh, D. Doppalapudi, T. D. Moustakas, and L. T. Romano, "Phase separation in InGaN thick films and formation of InGaN/GaN double heterostructures in the entire alloy composition," *Applied Physics Letters*, vol. 70, no. 9, pp. 1089, 1997.
[210] F. C.-P. Massabuau, M. J. Davies, F. Oehler, S. K. Pamenter, E. J. Thrush, M. J. Kappers, A. Kovács, T. Williams, M. A. Hopkins, C. J. Humphreys, P. Dawson, R. E. Dunin-Borkowski, J. Etheridge, D. W. E. Allsopp, and R. A. Oliver, "The impact of trench defects in InGaN/GaN light emitting diodes and implications for the “green gap” problem," *Applied Physics Letters*, vol. 105, no. 11, pp. 112110, 2014.
[211] Takashi Mukai, Motokazu Yamada, and Shuji Nakamura, "Current and Temperature Dependences of Electroluminescence of InGaN-Based UV/Blue/Green Light-Emitting Diodes," *Japanese Journal of Applied Physics*, vol. 37, no. Part 2, No. 11B, pp. L1358, 1998.

[212] S. J. Chang, W. C. Lai, Y. K. Su, J. F. Chen, C. H. Liu, and U. H. Liaw, "InGaN-GaN multiquantum-well blue and green light-emitting diodes," *IEEE Journal of Selected Topics in Quantum Electronics*, vol. 8, no. 2, pp. 278, 2002.
[213] Jacob Day, J. Li, D. Y. C. Lie, Charles Bradford, J. Y. Lin, and H. X. Jiang, "III-Nitride full-scale high-resolution microdisplays," *Applied Physics Letters*, vol. 99, no. 3, pp. 031116, 2011.
[214] Yong-Ho Ra, Roksana Tonny Rashid, Xianhe Liu, Sharif Md. Sadaf, Kishwar Mashooq, and Zetian Mi, "An electrically pumped surface-emitting semiconductor green laser," *Science Advances*, vol. 6, no. 1, pp. eaav7523, 2020.
[215] Žarko Gačević, Mark Holmes, Ekaterina Chernysheva, Marcus Müller, Almudena Torres-Pardo, Peter Veit, Frank Bertram, Jürgen Christen, José María González Calbet, Yasuhiko Arakawa, Enrique Calleja, and Snežana Lazić, "Emission of Linearly Polarized Single Photons from Quantum Dots Contained in Nonpolar, Semipolar, and Polar Sections of Pencil-Like InGaN/GaN Nanowires," *ACS Photonics*, vol. 4, no. 3, pp. 657, 2017.
[216] Lars Nicolai, Žarko Gačević, Enrique Calleja, and Achim Trampert, "Electron Tomography of Pencil-Shaped GaN/(In,Ga)N Core-Shell Nanowires," *Nanoscale Research Letters*, vol. 14, no. 1, pp. 232, 2019.
[217] Francesca Barbagini, Ana Bengoechea-Encabo, Steven Albert, Pierre Lefebvre, Javier Martinez, Miguel Angel Sanchez-Garcia, Achim Trampert, and Enrique Calleja, "E-beam nano-patterning for the ordered growth of GaN/InGaN nanorods," *Microelectronic Engineering*, vol. 98, pp. 374, 2012.
[218] Katsumi Kishino, Naoki Sakakibara, Kazuki Narita, and Takao Oto, "Two-dimensional multicolor (RGBY) integrated nanocolumn micro-LEDs as a fundamental technology of micro-LED display," *Applied Physics Express*, vol. 13, no. 1, pp. 014003, 2019.
[219] K. Kishino, T. Hoshino, S. Ishizawa, and A. Kikuchi, "Selective-area growth of GaN nanocolumns on titanium-mask-patterned silicon (111) substrates by RF-plasma-assisted molecular-beam epitaxy," *Electronics Letters*, vol. 44, no. 13, pp. 819, 2008.
[220] Hieu Pham Trung Nguyen, Kai Cui, Shaofei Zhang, Saeed Fathololoumi, and Zetian Mi, "Full-color InGaN/GaN dot-in-a-wire light emitting diodes on silicon," *Nanotechnology*, vol. 22, no. 44, pp. 445202, 2011.
[221] Yi-Lu Chang, Feng Li, Arya Fatehi, and Zetian Mi, "Molecular beam epitaxial growth and characterization of non-tapered InN nanowires on Si(111)," *Nanotechnology*, vol. 20, no. 34, pp. 345203, 2009.
[222] Frank Glas, "Critical dimensions for the plastic relaxation of strained axial heterostructures in free-standing nanowires," *Physical Review B*, vol. 74, no. 12, pp. 121302, 2006.
[223] Ashwin K. Rishinaramangalam, Mohsen Nami, Michael N. Fairchild, Darryl M. Shima, Ganesh Balakrishnan, S. R. J. Brueck, and Daniel F. Feezell, "Semipolar InGaN/GaN nanostructure light-emitting diodes onc-plane sapphire," *Applied Physics Express*, vol. 9, no. 3, pp. 032101, 2016.
[224] Y. Wu, X. Liu, P. Wang, D. A. Laleyan, K. Sun, Y. Sun, C. Ahn, M. Kira, E. Kioupakis, and Z. Mi, "Monolayer GaN excitonic deep ultraviolet light emitting diodes," *Applied Physics Letters*, vol. 116, no. 1, pp. 013101, 2020.
[225] Akanksha Kapoor, Nan Guan, Martin Vallo, Agnes Messanvi, Lorenzo Mancini, Eric Gautier, Catherine Bougerol, Bruno Gayral, Francois H. Julien, François Vurpillot, Lorenzo Rigutti, Maria Tchernycheva, Joël Eymery, and Christophe Durand, "Green

Electroluminescence from Radial m-Plane InGaN Quantum Wells Grown on GaN Wire Sidewalls by Metal–Organic Vapor Phase Epitaxy," *ACS Photonics*, vol. 5, no. 11, pp. 4330, 2018.

[226] Mohsen Nami, Isaac E. Stricklin, Kenneth M. DaVico, Saadat Mishkat-Ul-Masabih, Ashwin K. Rishinaramangalam, S. R. J. Brueck, Igal Brener, and Daniel F. Feezell, "Carrier Dynamics and Electro-Optical Characterization of High-Performance GaN/InGaN Core-Shell Nanowire Light-Emitting Diodes," *Scientific Reports*, vol. 8, no. 1, pp. 501, 2018.

[227] Y. El Gmili, P. L. Bonanno, S. Sundaram, X. Li, R. Puybaret, G. Patriarche, C. Pradalier, J. Decobert, P. L. Voss, J. P. Salvestrini, and A. Ougazzaden, "Mask effect in nano-selective- area-growth by MOCVD on thickness enhancement, indium incorporation, and emission of InGaN nanostructures on AlN-buffered Si(111) substrates," *Optical Materials Express*, vol. 7, no. 2, pp. 376, 2017.

[228] Jie Song, Benjamin Leung, Yu Zhang, and Jung Han, "Growth, structural and optical properties of ternary InGaN nanorods prepared by selective-area metalorganic chemical vapor deposition," *Nanotechnology*, vol. 25, no. 22, pp. 225602, 2014.

[229] Yadong Wang, Keyan Zang, Soojin Chua, Melissa S. Sander, Sudhiranjan Tripathy, and Clifton G. Fonstad, "High-Density Arrays of InGaN Nanorings, Nanodots, and Nanoarrows Fabricated by a Template-Assisted Approach," *The Journal of Physical Chemistry B*, vol. 110, no. 23, pp. 11081, 2006.

[230] S. Sundaram, R. Puybaret, Y. El Gmili, X. Li, P. L. Bonanno, K. Pantzas, G. Orsal, D. Troadec, Z.-H. Cai, G. Patriarche, P. L. Voss, J. P. Salvestrini, and A. Ougazzaden, "Nanoscale selective area growth of thick, dense, uniform, In-rich, InGaN nanostructure arrays on GaN/sapphire template," *Journal of Applied Physics*, vol. 116, no. 16, pp. 163105, 2014.

[231] Zhaoxia Bi, Anders Gustafsson, Filip Lenrick, David Lindgren, Olof Hultin, L. Reine Wallenberg, B. Jonas Ohlsson, Bo Monemar, and Lars Samuelson, "High In-content InGaN nano-pyramids: Tuning crystal homogeneity by optimized nucleation of GaN seeds," *Journal of Applied Physics*, vol. 123, no. 2, pp. 025102, 2018.

[232] Tilman Schimpke, Adrian Avramescu, Andreas Koller, Amalia Fernando-Saavedra, Jana Hartmann, Johannes Ledig, Andreas Waag, Martin Strassburg, and Hans-Jürgen Lugauer, "The influence of MOVPE growth conditions on the shell of core-shell GaN microrod structures," *Journal of Crystal Growth*, vol. 465, pp. 34, 2017.

[233] Koji Yamano and Katsumi Kishino, "Selective area growth of InGaN-based nanocolumn LED crystals on AlN/Si substrates useful for integrated μ-LED fabrication," *Applied Physics Letters*, vol. 112, no. 9, pp. 091105, 2018.

[234] Y.-L. Chang, J. L. Wang, F. Li, and Z. Mi, "High efficiency green, yellow, and amber emission from InGaN/GaN dot-in-a-wire heterostructures on Si(111)," *Applied Physics Letters*, vol. 96, no. 1, pp. 013106, 2010.

[235] Hieu Pham Trung Nguyen, Shaofei Zhang, Ashfiqua T. Connie, Md Golam Kibria, Qi Wang, Ishiang Shih, and Zetian Mi, "Breaking the Carrier Injection Bottleneck of Phosphor-Free Nanowire White Light-Emitting Diodes," *Nano Letters*, vol. 13, no. 11, pp. 5437, 2013.

[236] Hieu Pham Trung Nguyen, Mehrdad Djavid, Steffi Y. Woo, Xianhe Liu, Ashfiqua T. Connie, Sharif Sadaf, Qi Wang, Gianluigi A. Botton, Ishiang Shih, and Zetian Mi, "Engineering the Carrier Dynamics of InGaN Nanowire White Light-Emitting Diodes by Distributed p-AlGaN Electron Blocking Layers," *Scientific Reports*, vol. 5, no. 1, pp. 7744, 2015.

[237] Yong-Ho Ra, Roksana Tonny Rashid, Xianhe Liu, Jaesoong Lee, and Zetian Mi, "Scalable Nanowire Photonic Crystals: Molding the Light Emission of InGaN," *Advanced Functional Materials*, vol. 27, no. 38, pp. 1702364, 2017.
[238] "Ultraviolet germicidal irradiation." [Online]. Available:http://en.wikipedia.org/wiki/Ultraviolet_germicidal_irradiation.
[239] "Ultraviolet light therapy." [Online]. Available:http://en.wikipedia.org/wiki/Ultraviolet_light_therapy.
[240] "Ultraviolet photography." [Online]. Available:http://en.wikipedia.org/wiki/Ultraviolet_photography.
[241] "Fluorescence." [Online]. Available:http://en.wikipedia.org/wiki/Fluorescence.
[242] "UV curing." [Online]. Available:http://en.wikipedia.org/wiki/UV_curing.
[243] N. Parashurama, T. D. O'Sullivan, A. De La Zerda, P. El Kalassi, S. Cho, H. Liu, R. Teed, H. Levy, J. Rosenberg, Z. Cheng, O. Levi, J. S. Harris, and S. S. Gambhir, "Continuous sensing of tumor-targeted molecular probes with a vertical cavity surface emitting laser-based biosensor," *J Biomed Opt*, vol. 17, no. 11, pp. 117004, 2012.
[244] Valery Khalilov, John Shannon, Richard Timmerman, and Dale Geshell, "Improved deep UV fiber for medical and spectroscopy applications," 2015.
[245] Casey Holder, James S. Speck, Steven P. DenBaars, Shuji Nakamura, and Daniel Feezell, "Demonstration of Nonpolar GaN-Based Vertical-Cavity Surface-Emitting Lasers," *Applied Physics Express*, vol. 5, no. 9, 2012.
[246] Hsin-chieh Yu, Zhi-wei Zheng, Yang Mei, Rong-bin Xu, Jian-ping Liu, Hui Yang, Bao-ping Zhang, Tien-chang Lu, and Hao-chung Kuo, "Progress and prospects of GaN-based VCSEL from near UV to green emission," *Progress in Quantum Electronics*, vol. 57, pp. 1, 2018.
[247] M. Arita, F. Le Roux, M. J. Holmes, S. Kako, and Y. Arakawa, "Ultraclean Single Photon Emission from a GaN Quantum Dot," *Nano Lett*, vol. 17, no. 5, pp. 2902, 2017.
[248] S. Deshpande, J. Heo, A. Das, and P. Bhattacharya, "Electrically driven polarized single-photon emission from an InGaN quantum dot in a GaN nanowire," *Nat Commun*, vol. 4, pp. 1675, 2013.
[249] S. Deshpande, T. Frost, L. Yan, S. Jahangir, A. Hazari, X. Liu, J. Mirecki-Millunchick, Z. Mi, and P. Bhattacharya, "Formation and nature of InGaN quantum dots in GaN nanowires," *Nano Lett*, vol. 15, no. 3, pp. 1647, 2015.
[250] P. E. Blochl, "Projector augmented-wave method," *Phys Rev B Condens Matter*, vol. 50, no. 24, pp. 17953, 1994.
[251] G. Kresse and D. Joubert, "From ultrasoft pseudopotentials to the projector augmented-wave method," *Physical Review B*, vol. 59, no. 3, pp. 1758, 1999.
[252] G. Kresse and J. Furthmuller, "Efficient iterative schemes for ab initio total-energy calculations using a plane-wave basis set," *Phys Rev B Condens Matter*, vol. 54, no. 16, pp. 11169, 1996.
[253] J. P. Perdew, K. Burke, and M. Ernzerhof, "Generalized Gradient Approximation Made Simple," *Phys Rev Lett*, vol. 77, no. 18, pp. 3865, 1996.
[254] Jochen Heyd, Gustavo E. Scuseria, and Matthias Ernzerhof, "Hybrid functionals based on a screened Coulomb potential," *The Journal of Chemical Physics*, vol. 118, no. 18, pp. 8207, 2003.

[255] H. Yamashita, K. Fukui, S. Misawa, and S. Yoshida, "Optical properties of AlN epitaxial thin films in the vacuum ultraviolet region," *Journal of Applied Physics*, vol. 50, no. 2, pp. 896, 1979.
[256] Chris G. Van de Walle, Sukit Limpijumnong, and Jörg Neugebauer, "First-principles studies of beryllium doping of GaN," *Physical Review B*, vol. 63, no. 24, 2001.
[257] Christoph Freysoldt, Jörg Neugebauer, and Chris G. Van de Walle, "Electrostatic interactions between charged defects in supercells," *physica status solidi (b)*, vol. 248, no. 5, pp. 1067, 2011.
[258] J. L. Lyons, A. Janotti, and C. G. Van de Walle, "Shallow versus deep nature of Mg acceptors in nitride semiconductors," *Phys Rev Lett*, vol. 108, no. 15, pp. 156403, 2012.